

BTBD11 INTERACTS WITH PLZF AND MODULATES THE EFFECTOR
FUNCTIONS OF VARIOUS INNATE LYMPHOCYTE POPULATIONS

BY

ANDREW R. CHAVKIN

A thesis submitted to the
Graduate School-New Brunswick
Rutgers, The State University of New Jersey
and

The Graduate School of Biomedical Sciences

In partial fulfillment of the requirements

For the degree of

Masters of Science

Graduate Program in Biomedical Engineering

Written under the direction of

Derek Sant' Angelo

And approved by

New Brunswick, New Jersey

October 2015

ABSTRACT OF THE THESIS

BTBD11 INTERACTS WITH PLZF AND MODULATES THE EFFECTOR FUNCTIONS OF VARIOUS INNATE LYMPHOCYTE POPULATIONS

BY ANDREW CHAVKIN

THESIS DIRECTOR:
DEREK SANT'ANGELO

The BTB-ZF transcriptional regulator, promyelocytic leukemia zinc finger (PLZF), is known to control the innate phenotype and effector functions of NKT cells and $\gamma\delta$ T cells. The unstudied protein, Btbd11, has been shown to be transcriptionally controlled by PLZF and directly interact with PLZF via the shared BTB protein-interaction domain. In order to determine if Btbd11 plays a role in modulating the function of PLZF, we have generated a mouse exhibiting induced overexpression of Btbd11 in all T cells. In conjunction with existing mice ectopically expressing PLZF in all T cells, we investigated the impact that these factors had upon the phenotype and function of T cells. Concurrently, we utilized another mouse line with reduced Btbd11 expression (Btbd11^{GT} mice) to determine the role that Btbd11 alone plays in controlling various characteristics of T cell populations. Significantly, mice with overexpression of both Btbd11 and PLZF (dTG mice) exhibited ~11% of CD8⁺ T cells capable of producing IL-17a upon in vitro activation. This population of IL-17a producing CD8⁺ T cells is almost

non-existent in wild type mice and represents a significant proinflammatory phenotype. Total liver $\gamma\delta$ T cell populations were also found to be dependent on levels of Btbd11, as dTG mice had a two-fold expansion while Btbd11 GT mice showed a three-fold contraction of $\gamma\delta$ T cells compared to wild type. In vivo studies of Concanavalin A induced liver damage determined that Btbd11 GT mice exhibited a four-fold reduction versus wild type in serum ALT activity, an enzyme released via liver damage. Overexpression of Btbd11 and PLZF results in the expansion of proinflammatory effector cells while reduced expression of Btbd11 results in a protection from innate T cell-mediated liver damage, indicating the correlation between Btbd11 and the characteristic proinflammatory phenotype seen in these innate T cell subsets. We conclude that Btbd11 and PLZF interact differently with each other and other co-factors depending upon their setting within different immune cells. These studies indicate a potential role for Btbd11 in modifying the phenotype and effector function of various T cell subsets by regulating PLZF's ability to exert transcriptional control.

Table of Contents

Abstract	ii
Introduction	1
The Immune System	1
Innate Immunity	2
Cell Types	4
Pathogen Recognition	5
Adaptive Immunity	6
Lymphoid Lineage	6
V(D)J Recombination	7
Thymocyte Development	9
Peripheral T-Lymphocyte Activation	11
B-Lymphocyte Activation	12
Innate Lymphocytes	14
$\gamma\delta$ T Cells	14
Tissue Specific Subsets	14
Nonconventional Thymocyte Development	15
Activation and Role in Host Immunity	16
Natural Killer T Cells	21
Nonconventional Thymocyte Development	21
Transcriptional Control	22
Activation	26
Implication in Diseases	29

Role in Liver and Liver Diseases -----	30
PLZF -----	34
Master Regulator of NKT Cells Effector Function -----	34
Specific Expression in $\gamma\delta$ T Cell Subsets -----	37
Ectopic Expression in Conventional T Cells -----	41
Btbd11 -----	46
Interactions with PLZF via Btb-Protein Interaction Domains -----	46
Material and Methods -----	55
Mice -----	55
hCD2-Btbd11 Construct Design -----	56
Generation of hCD2-Btbd11 Construct -----	56
Microinjection of hCD2-Btbd11 Construct -----	60
Btbd11 Gene Trap Mice -----	61
Mouse Tissue Preparation -----	62
Fluorescently Labeled Antibody Staining -----	63
Flow Cytometry -----	65
In Vitro T Cell Stimulation -----	67
Concanavalin A Injection and ALT Assay -----	68
RNA Extraction and Reverse Transcriptase -----	70
Quantitative Real-Time Polymerase Chain Reaction -----	71
Results -----	75
Generation of hCD2-Btbd11 Transgene -----	75
Confirmation of hCD2-Btbd11 Transgene Expression -----	77

Confirmation of Btbd11 Gene-Trap (Btbd11-GT) Transgene Expression -----	78
Btbd11 and PLZF are Differentially Expressed between Experimental Mice ---	79
NKT, CD4 ⁺ , and CD8 ⁺ T Cell Populations are Unchanged between WT, hCD2-Btbd11, lck-PLZF, dTG, and Btbd11-GT Mice -----	81
PLZF and RORγt Expression in CD4 ⁺ , CD8 ⁺ , and NKT Cell Populations is Altered between WT, hCD2-Btbd11, lck-PLZF, dTG, and Btbd11 GT Mice -----	82
Cytokine Production by Splenic CD4 ⁺ , CD8 ⁺ , and NKT Cell Populations is Slightly Altered Following in-vitro Stimulation -----	83
Cytokine Production by Liver CD4 ⁺ , CD8 ⁺ , and NKT Cell Populations is Significantly Altered Following in-vitro Stimulation -----	85
γδ T Cell Populations are Significantly Altered between WT, hCD2-Btbd11, lck- PLZF, dTG, and Btbd11-GT Mice -----	86
ALT Activity is Significantly Different between WT and Btbd11-GT Following Concanavalin A Injection -----	87
T Cell Populations and PLZF Expression are Significantly Different within WT and Btbd11-GT Mice Following Concanavalin A Injections -----	89
Discussion -----	110
References -----	122

Table List

Table 1: Primers and PCR program used for the homologous arm extension -----	58
Table 2: Primers used to sequence the hCD2-Btbd11 transgene construct -----	58
Table 3: Primers used for qRT-PCR of PLZF and Btbd11 gene expression -----	73

Figure List

Fig. 1: The Hematopoietic stem cell compartment -----	3
Fig. 2: Specific $\gamma\delta$ T Cell development during ontogeny -----	19
Fig. 3: $\gamma\delta$ T Cells interact with target cells during all stages of immune response -----	20
Fig. 4: Nonconventional NKT Cell Development via CD1d Selection -----	25
Fig. 5: Invariant NKT Cells interact with various innate and adaptive immune cells ---	28
Fig. 6: Various immunotherapies involve the activation or suppression of iNKT cells -	33
Fig. 7: Restricted PLZF expression within NKT Cells of the thymus and liver -----	36
Fig. 8: $\gamma\delta$ T Cells express PLZF within various immune tissues -----	38
Fig. 9: PLZF expression is restricted to $V\gamma 1.1^+$, $V\delta 6.3^+$ $\gamma\delta$ T cells -----	39
Fig. 10: $V\delta 6.3^+$ $\gamma\delta$ T cells require PLZF to coproduce IFN- γ and IL-4 -----	40
Fig. 11: IFN- γ and IL-4 co-production by conventional T cells is not altered in lck-PLZF mice -----	43
Fig. 12: IL-17a producing $CD8^+$ T Cells are present in activated lck-PLZF mice -----	44
Fig. 13: Various NKT Cell-based cancer therapies currently undergoing clinical trials-	45
Fig. 14: Predicted conserved regions of Btbd11 protein -----	48
Fig. 15: Btbd11 interacts with PLZF via Btb-interaction proteins -----	49
Fig. 16: Btbd11 is expressed in all NKT cell subsets -----	50
Fig. 17: Btbd11 is expressed in certain subsets of $\gamma\delta$ T cells -----	51
Fig. 18: Graphical representation of Btbd11 GT transgene configuration -----	54
Fig. 19: In-Fusion reaction used to generate hCD2-Btbd11 construct -----	58
Fig. 20: Sample qRT-PCR amplification plot with threshold value -----	73
Fig. 21: Graphical representation of hCD2-Btbd11 construct -----	90

Fig. 22: Successful hCD2-Btbd11 clone following PCR and In-Fusion Cloning	91
Fig. 23: Isolation and purification of hCD2-Btbd11 construct prior to microinjection	92
Fig. 24: Genotyping results of the two hCD2-Btbd11 transgene positive founder pups	93
Fig. 25: Overexpression of Btbd11 in hCD2-Btbd11 mice	94
Fig. 26: Reduction in Btbd11 mRNA transcript within Btbd11 GT mice	95
Fig. 27: Validation of Btbd11, PLZF, and GAPDH qRT-PCR primers	96
Fig. 28: Altered PLZF gene expression between lck-PLZF and dTG mice	97
Fig. 29: NKT Cell populations are not altered in experimental mice	98
Fig. 30: ROR γ t protein expression is increased in dTG and lck-PLZF mice	99
Fig. 31: PLZF protein expression is decreased in T cell subsets of dTG mice	100
Fig. 32: Splenic NKT cells do not exhibit altered cytokine production	101
Fig. 33: Splenic CD4 ⁺ T cells do not exhibit altered cytokine production	102
Fig. 34: Splenic CD8 ⁺ T cells do not exhibit altered cytokine production	103
Fig. 35: Btbd11 GT NKT cells do not exhibit altered cytokine production	104
Fig. 36: Significant expansion of IL-17a producing liver CD8 ⁺ T cells in dTG mice	105
Fig. 37: Total $\gamma\delta$ T cells are significantly different in experimental mice	106
Fig. 38: Percentages of $\gamma\delta$ NKT cells are significantly different in experimental mice	107
Fig. 39: Btbd11 GT mice exhibited lower ALT activity following Con A dosage	108
Fig. 40: Btbd11 GT liver samples had altered effector cell populations and PLZF expression following Con A dosage	109

Introduction

The Immune System

The immune system is composed of many different types of cells, tissues, organs, and molecules that prevent and protects the body from infection and disease. Countless unique and highly specialized cells work together to fend off the millions of infectious agents that we come in contact with on a daily basis. The workings of this fantastically complex and intricate system have been studied for as long as humans have been getting sick. How easy it must have been back in the days of ancient Greece when sickness and disease transmission could be blamed on “miasma” or poisonous mist! Progressing from these days, scientists and immunologists specifically have gone down the proverbial rabbit hole; the more we discover about the immune system and the microorganisms it fights, the more we realize how much more there is still undiscovered. Whether it is a virus, bacteria, fungi, or parasite, it is imperative to learn how the body deals with these pathogens so that we can take proper steps in specific prevention and treatment in case the immune system fails to eliminate the threat.

The immune system operates via four general functions in order to defend the body from infection: immunological recognition, immune effector function, immune regulation, and immunological memory. These four pillars are collectively upheld and carried out by the innate and adaptive immune systems. While this delineation seems concrete, we will see that there are many components of the immune system that fall between and serve as bridges between these types of immunity.

Due to the close interaction and overlapping characteristics observed in the innate and adaptive immune system, it is not surprising that every immune cell comprising the two

systems is derived from the same class of pluripotent stem cells known as hematopoietic stem cells (HSCs). Hematopoietic stem cells are responsible for populating all cellular components of the blood. Through the process of hematopoiesis, HSCs in the bone marrow give rise to three cell lineages: erythrocytes or red blood cells, myelocytes or immune cells comprising the innate immune system, and lymphocytes or adaptive immune system cells. The differentiation from HSCs to each of the mature cell types is illustrated in Figure 1.

The various different immune cell types differentiate to perform vastly different functions within the immune system. These cells reside in various body compartments based upon their functions. Primary immune system organs include the bone marrow and thymus, where HSCs proliferate and lymphocytes develop. Secondary immune system organs include the lymph nodes, spleen, liver, and mucosal lymphoid tissues, and provide sites for mature lymphocytes to carry out their adaptive immune system functions.

Innate Immunity

The innate immune system is, as its name suggests, a natural and basic response that occurs within the first moments of contact with an infectious agent. This preventative system is present at all times within the organism and consists of both a physical barrier to incoming pathogens as well as the first immune cells to interact with pathogens.

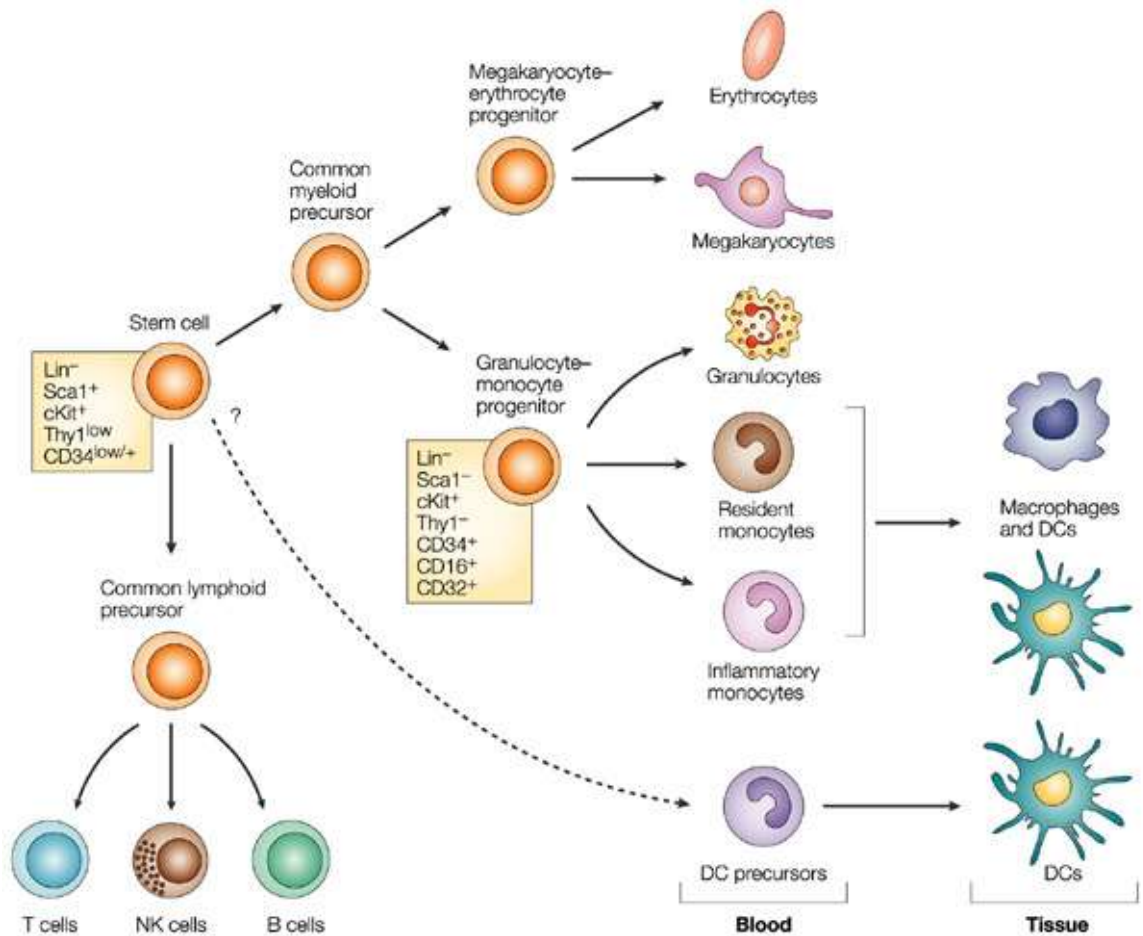


Figure 1. The Hematopoietic stem cell compartment. Hematopoietic stem cell differentiate and populate all components of the blood and immune system. Stem cells differentiate into common lymphoid precursors (CLPs) and common myeloid precursors (CMPs). CLPs proceed to differentiate and produce lymphocytes including T cells, NK cells, and B cells. CMPs differentiate into megakaryocyte-erythrocyte progenitors and granulocyte-monocyte progenitors (GMPs). GMPs further differentiate into monocytes, macrophages, and dendritic cells (DCs) which comprise the innate immune system.

Reprinted by permission from Macmillan Publishers Ltd: [Nature Reviews Immunology] (97), copyright (2004).

These natural barriers include the skin and mucosal membranes that cover the entire surface of the human body that regularly comes in contact with foreign and potentially infectious particles. As long as this barrier remains intact, the pathogen threat level remains low.

Innate Immunity: Cell Types

It is once this physical barrier is breached that the first wave of immune cells are called to arms against the invading pathogen. These first responder immune cells within the infected tissue include neutrophils, monocytes, macrophages, dendritic cells (DCs), and natural killer (NK) cells. Each of these cell types are derived from HSCs and more specifically the common myeloid progenitor with the exception of the lymphoid- derived NK cells as seen above in Figure 1. NK cells release lytic granules in order to destroy cancerous and virally infected host cells. Neutrophils are short lived myeloid cells that migrate to infected tissues and phagocytize and destroy pathogens. Monocytes are granulocytes that travel from the blood into tissues and differentiate into macrophages. Macrophages are responsible for activating bactericidal mechanisms by phagocytizing pathogens, presenting antigens, and releasing chemokines and cytokines. Dendritic cells are phagocytic cells that reside in tissues and serve to present antigens.

The phagocytic ability shared by the members of the innate immune system serves two main purposes. Firstly, through phagocytosis it is possible to completely consume and destroy an entire pathogen. In certain infections, the innate immune system fully eliminates the infection. When the innate immune system fails to completely eliminate

the infection, the second role of phagocytosis becomes apparent. Phagocytic cells such as macrophages and dendritic cells also have the ability to present antigens on their surface.

Innate Immunity: Pathogen Recognition

Innate immune system cells are able to prevent and eliminate early infections by sacrificing specificity for speed. As innate immune system cells do not have the ability to adaptively recognize antigens, they rely upon the ability to recognize generic patterns shared by various classes of pathogens. One example of this is the Toll-like receptor (TLRs) recognition pathway. Innate immune system cells express various types of TLRs that each specifically recognize conserved epitopes on pathogens. These conserved patterns can be ligands such as double stranded RNA, bacterial flagellin, bacterial peptidoglycans, and other pathogen specific macromolecules [1]. Once the TLR recognizes and binds its ligand, the innate cell produces a non-specific effector function such as release of inflammatory cytokines and chemokines [1, 2].

The second example of a recognition pathway unique to innate immunity is the complement system. Consisting of three pathways that are separate but similar, one specific pathway of the complement system is the mannose- binding lectin (MBL) pathway. The MBL pathway is the process of tagging a pathogen with extracellular sentinel molecules specific to the mannose, ficolin, and fucose residues found on pathogen surfaces [3]. Once this complex tags the pathogen, other complement proteins interact with the complex to produce inflammatory mediators that recruit phagocytic innate immune system cells.

Adaptive Immunity

As mammals evolved in complexity, the need for a more complex and robust system of protection arose. As this “Rolls-Royce” organism came about, there was an apparent need for the installation of a state-of-the-art security system to replace the previous simplistic defense of a locked car door. This “adaptive” security system needed to be as cunning and clever as the intruders posing a threat. And thus the adaptive immune system developed within early stage jawed- vertebrates [4, 5].

Following the initial stages of an immune response to infection and disease carried out by the innate immune system, the adaptive immune system mediates the following stages of disease clearance. The cells of the adaptive immune system have the ability to adapt, adjust, and eventually eliminate unique pathogens threatening the organism. T and B lymphocytes work in tandem to carry out the roles of adaptive immunity. T cells account for what is known as the cell-mediated arm of the adaptive immune system. They have the ability to eliminate infected host cells as well as activate other immune cells to destroy foreign pathogenic threats. B cells make up the humoral or antibody-mediated arm of the adaptive immune system. Antibodies are released immunoglobulin molecules that share the same antigen specificity as the B cell that produce them. As we will see, these arms of the adaptive immune system interact with each other as well as members of the innate immune system to effectively eliminate both foreign and self- derived threats to the body.

Adaptive Immunity: Lymphoid Lineage

As depicted in Figure 1, adaptive immune system cells are derived from common lymphoid progenitors (CLPs), which have differentiated from pluripotent hematopoietic

stem cells residing in the bone marrow. B and T cells were historically named based upon the tissue that they gain their functionality within; the bone marrow and the thymus respectively. CLPs differentiate within the bone marrow into either B-cell progenitors or T-cell progenitors. B-cell progenitors remain within the bone marrow while T-cell progenitors travel to the thymus. Within each of these tissues, the adaptive immune system cells develop and eventually relocate to peripheral immune tissues such as the lymph nodes, spleen, and liver.

Mature T and B cells express membrane-bound receptors that recognize and interact with antigens presented by other members of the immune system. This process of antigen recognition, B and T-cell maturation, and effector functionality illustrates how the adaptive immune system trades speed for highly specific and robust elimination of pathogens.

Adaptive Immunity: V(D)J Recombination

In 1973, Susumu Tonegawa discovered and defined V(D)J recombination or somatic recombination [6]. Through the comparison of genomic DNA from mouse embryos and mouse cancerous B-cells, he found that large portions of DNA were missing in the somatic cancer cell genomes. This contradicted the previous theory that recombination within the genome occurred only during the formation of the embryo. Upon further study, Tonegawa concluded that recombination does in fact occur within somatic cells, exclusively in lymphocytes. Tonegawa's discovery unveiled that lymphocyte-specific somatic recombination is responsible for the staggering receptor diversity that T and B-cells possess and rely upon to carry out the functions of the adaptive immune system, and appropriately earned him the Nobel Prize in Physiology or Medicine in 1987.

Specifically, V(D)J recombination is the mechanism by which the V, D, and J segments translate and recombine to code for the B or T-cell receptor (BCR and TCR).

Following B-cell progenitor differentiation from CLPs through interaction with bone marrow stromal cells, B cells pass the early pro-B cell phase to the late pro-B cell phase to the pre-B cell phase and eventually to the immature B cell stage. It is during these stages of B-cell development that V(D)J recombination occurs to recombine various segments of the gene that codes for the B- cell receptor. This recombination occurs at three gene loci that code for the immunoglobulin (Ig) heavy chain, the Ig kappa light chain, and the Ig lambda light chain. Each of these loci contains various exons coding for different versions of V, D, and J segments. Through complex enzymatically-controlled processes, one D and one J segment join together followed by one V segment. After this recombination, the Ig heavy chain pairs with one of the light chains to form the membrane bound BCR. Importantly, this random combination of the V, D, and J segments on the heavy, kappa light, and lambda light loci occurs separately within each B-cell progenitor. This leads to a theoretical yield of approximately 10^{11} B-cells expressing a unique BCR [7, 8]. This astounding repertoire of BCR enables B-cells to recognize antigens, differentiate into effector cells, and carry out their role in the adaptive immune system.

V(D)J recombination similarly occurs during T-cell development along with other T-cell specific mechanisms responsible for proper T-cell functionality.

Adaptive Immunity: Thymocyte Development

As pluripotent hematopoietic stem cells divide and differentiate in the bone marrow, a portion of common lymphoid progenitors travel to the thymus during early gestation. These CLPs receive Notch1 signaling from thymic stromal cells to commit to the T-cell fate and continue to divide in the thymus to generate large quantities of immature thymocytes [9, 10]. The process of thymopoiesis relies upon various signals provided by the thymic environment to generate functional T-cells. Immature thymocytes are classified based upon their expression of the cell surface markers, CD44 and CD25 [11-13]. DN1 thymocytes ($CD44^{+}CD25^{-}$) are the most immature, “double-negative” thymocytes that travel to the thymic cortex and differentiate into DN2 thymocytes. DN2 thymocytes upregulate CD25 to become $CD44^{+}CD25^{+}$ and begin V(D)J recombination. V(D)J recombination in DN2 thymocytes begins with synchronized somatic recombination on the β TCR loci, γ TCR loci, and δ TCR loci. After this gene rearrangement occurs, DN2 thymocytes differentiate into DN3 thymocytes as the rearranged TCR genes are transcribed, translated, and trafficked to the membrane as preliminary TCR protein dimers. DN3 thymocytes express two distinct types of preliminary TCR dimers, the $\gamma\delta$ TCR and the β pre-TCR. At this stage, DN3 thymocytes commit into $\gamma\delta$ T-cells or $\alpha\beta$ T-cells based upon which TCR receives proper signaling [14]. Signaling through the $\gamma\delta$ TCR leads to differentiation into $\gamma\delta$ T-cells whereas signaling through the β pre-TCR leads to further differentiation into $\alpha\beta$ T-cells. This checkpoint is known as β -selection, where $\gamma\delta$ T cells exit the conventional thymocyte development pathway [14].

Following β -selection and the successful, stable signaling through the β pre-TCR, these DN3 thymocytes down regulate cell surface markers, CD44 and CD25, and undergo proliferation and differentiation into DN4 thymocytes [15]. DN4 thymocytes then undergo V(D)J recombination of the α TCR gene loci. Once the α TCR is successfully expressed, it replaces the pre-TCR and complexes with the β TCR subunit, marking the progression of DN4 thymocytes into double-positive (DP) $\alpha\beta$ thymocytes.

DP thymocytes are named such due to the co-expression of the CD4 and CD8 receptors. At this stage, the thymocytes interact with thymic stromal cells and undergo positive selection. Positive selection is the mechanism by which all of the fledgling thymocytes are tested to ensure that they have the ability to interact with MHC class I or class II molecules, presenting self-antigens, expressed on the surrounding thymic stromal cells (TSCs). DP thymocytes that successfully interact with MHC class I molecules down-regulate CD4 and become $CD8^+CD4^-$ thymocytes or cytotoxic killer T -cells. DP thymocytes that successfully interact with MHC class II molecules down-regulate CD8 and become $CD4^+CD8^-$ thymocytes or helper T-cells. All remaining DP thymocytes that do not complex to MHC class I or class II undergo apoptosis, or programmed cell death [16-18].

As the names suggest, thymocytes only expressing CD4 or CD8 co-receptors have successfully navigated through positive selection and reached the single positive (SP) thymocyte stage. After down regulation of the receptor not interacting with the MHC, thymocyte negative selection occurs. As discussed earlier, the MHC molecules on the TSCs present self-peptides originating from host proteins. As members of the host immune system, it is of vital importance that T cells do not interact with self-antigens

with sufficient affinity to activate. Any thymocyte that does bind strongly to MHC molecules presenting self-antigens must be removed from the thymocyte population. Thus, the TSCs expressing self-antigens select the self-reactive thymocytes, leading to their depletion via apoptosis or anergy. Remaining thymocytes, comprising a very small percentage of the original pool of thymocytes, are ready to exit the thymus and become mature naïve $\alpha\beta$ T cells [19, 20].

Adaptive Immunity: Peripheral T-Lymphocyte Activation

T cells leaving the thymus circulate throughout the lymphatic system and “home” to secondary lymphoid tissues via expression of the cell surface marker, CD62L or L-selectin [32]. This lymphatic system serves as the main method of travel for lymphocytes and other members of the immune system. Macrophages and dendritic cells work at infection sites to uptake and present antigens within their MHC class II molecule. These APCs then travel through the lymphatic system to secondary immune organs such as the lymph nodes and spleen.

Once within the lymph nodes or spleen, the APCs survey the population of resident mature, naïve $CD4^+$ T lymphocytes for those with the appropriate TCR capable of binding the antigen peptide-MHC complex. TCR to antigen-MHC complex binding is the first signal to activate T- cells. Following this first signal, the T cell must receive a secondary signal from the APC such as CD28 to CD80/CD86 binding. Without CD28 activation and the subsequent intracellular signaling, T cells do not receive proper activation and survival cues and will undergo anergy [21, 22].

This costimulatory secondary signaling induces intracellular signaling that eventually reaches the nucleus of the T cell where maturation and activation T cell messages are

transcribed. This includes expression of activated T cell surface markers and the production and release of effector cytokines. One such example is when $CD4^+$ T cells produce IL-2 and upregulate IL-2 receptors on their surface which serves to self-induce proliferation [23, 24]. At this stage, clonal expansion of a specific T cell leads to the generation of effector T helper cells and memory T helper cells. The effector T helper cells work in the short term and die once the infection has been eliminated. Memory T cells remain following the elimination of the infection in a “primed” state so that in the future, when APCs present the same antigen, the memory T cells can immediately activate and proliferate without the need for a secondary costimulatory activation.

The induction and activation of mature $CD8^+$ T cells works similarly through interactions with self-antigens being presented through the MHC class I molecule. Naïve $CD8^+$ or cytotoxic T cells also require secondary costimulatory signaling such as CD28 binding to CD80/CD86 before inducing changes into their effector functionality. Cytotoxic T cells differentiate into either effector or memory cells similarly to helper T cells. Effector cytotoxic T cells release enzymes and cytotoxins such as perforin, granulysin, and granzymes, which as the names suggest, serve to enter the infected cell and induce apoptosis and cell death [25].

Adaptive Immunity: B-Lymphocyte Activation

B cells are responsible for the humoral or antibody-mediated arm of the adaptive immune system. As addressed earlier, B cells are generated in the bone marrow to express a unique receptor that allows it to recognize and bind specific antigens. For certain antigens, T cell dependent B cell activation is required for B cells to produce antibodies and eliminate pathogens. These B cells become activated primarily within germinal

centers in secondary lymphoid tissues such as the lymph nodes, spleen, and liver [31].

These germinal centers are regions where APCs arrive via the lymphatic system and present antigens to naïve T and B cells which then activate and mount an immune response towards the pathogenic antigen. Importantly, the BCR also has the ability to recognize antigens without presentation through MHC molecules. It is through this direct B cell to antigen recognition that B cells can activate in a T cell independent fashion.

T cell independent B cell activation occurs when B cells recognize and bind a soluble antigen and then receive the proper secondary activation signal. This secondary signal can be signaling through Toll-like receptors on the B cell surface binding to generic pathogen epitopes or by considerable BCR crosslinking as the various BCRs bind to similar and closely residing antigens on the surface of the pathogen. This T cell independent activation of B cells leads to swift B cell effector function such as the release of restricted antibody classes such as IgG2, IgG3, and IgM [27, 28].

T cell dependent B cell activation begins when the B cell presents a peptide within its MHC class II molecule to helper T cells. Following successful binding of the MHC II-peptide complex with the TCR and CD4 co-receptor, secondary signaling through CD40L-CD40 binding on the B cell confirms B cell activation [29, 30]. Importantly, “primed” or memory T cells can release cytokines to activate B cells instead of signaling through CD40L-CD40. Upon activation, the B cell proliferates and clonally expands into plasma and memory B cells. Plasma B cells are short term effector cells that circulate to infected body tissues, undergo class switching, gain the ability to produce large amounts of antibodies of type IgG, IgA, and IgE, and die once the infection has been eliminated [27, 28]. Each class of antibody has a different efficacy and function as they release and

bind to their target pathogen. Pathogens tagged by antibodies are then eliminated through phagocytosis or the complement system via innate immune cells such as macrophages and dendritic cells. Memory B cells remain within the germinal centers and undergo somatic hypermutation to increase their affinity for the antigens. These memory B cells with increased affinity persist and can activate more quickly and effectively when re-challenged with the same antigen at a later time.

These interactions between the cell-mediated arm and humoral arm of the adaptive immune system evidence the intricacies and complexity of antigen-specific immunity as well as the cross-talk between the innate and adaptive immune system.

Innate Lymphocytes

Residing within the murky delineations between the innate and adaptive immune system, certain lymphocytes share characteristics and functions with immune cells of both systems. These innate lymphocytes are defined by various factors such as their unconventional development, T cell repertoire, antigen specificity, method of activation, cytokine release, and effector function. Gamma-delta ($\gamma\delta$) T cells and natural killer T cells (NKT cells) are two members of this unique class of innate lymphocytes.

$\gamma\delta$ T Cells: Tissue Specific Subsets

$\gamma\delta$ T cells comprise about 1-5% of adult lymphocytes and possess the γ and δ chain TCR heterodimer rather than the more common α chain and β chain TCR heterodimer indicative of $\alpha\beta$ T cells [34, 75]. Due to this difference, we expect $\gamma\delta$ T cells to have different specificity conferred by their different TCR combinations and to thus play a unique role in immunity. $\gamma\delta$ T cells exist in similar tissue to $\alpha\beta$ T cells with the exception of their marked increase in mucosal tissues including the tongue, intestinal, vaginal, and

lung epithelium [34, 75]. Specific combinations of the γ and δ TCR chain define the function and localization of the $\gamma\delta$ T cells. For example, $V\gamma 7^+$ and $V\gamma 5^+$ $\gamma\delta$ T cells are located within the skin and gut epithelial tissues, are able to produce pro-inflammatory molecules such as IL-2 and IFN- γ , and are responsible for tissue tumor surveillance and immunoregulation [75]. $V\gamma 4^+$ $\gamma\delta$ T cells exist in the blood, thymus, spleen, liver, and lymph nodes and are responsible for producing IL-17 and IFN- γ in order to recruit neutrophils to early stage infections [76, 77]. A specific subset of $V\gamma 1.1^+$, $V\delta 6.3^+$ T cells exist in the spleen, thymus, and liver and are able to produce IFN- γ and IL-4 simultaneously. The significance and importance of this ability will be further discussed in sections below.

$\gamma\delta$ T Cells: Nonconventional Thymocyte Development

$\alpha\beta$ and $\gamma\delta$ T cells follow the same developmental pathway within the thymus up until the DN3 stage. At this stage the thymocyte precursor has undergone V(D)J recombination to express a β , γ , and δ chain on their cell surface. If the γ and δ chain successfully complex into a functional $\gamma\delta$ TCR, then the thymocyte will be classified into the $\gamma\delta$ lineage. If the precursor does not form the $\gamma\delta$ TCR, then it has “passed” β -selection and moves into the $\alpha\beta$ T cell lineage.

Importantly, it has been shown that the timing of $\gamma\delta$ T cell production in the thymus controls the specific γ and δ chains of the precursor which then in turn controls the final tissue home of the $\gamma\delta$ T cells. As shown in Figure 2, production of $\gamma\delta$ T cells possessing specific γ variable chain regions occurs in overlapping waves throughout murine embryonic development [78]. Also shown is the final location and thus the functionality of these restricted groups of $\gamma\delta$ T cells. There is some debate as to whether or not $\gamma\delta$ T

cells maturing in the thymus require any sort of selective interaction that confers survival or functional specificity. Unlike $\alpha\beta$ T cells, $\gamma\delta$ T cells do not require MHC interactions for development, as proved by the un-interrupted presence of $\gamma\delta$ T cells in MHC knockout mouse models [79]. There have been reports a certain subset, $V\gamma 5^+$, $V\delta 1^+$ $\gamma\delta$ T cells that require a selecting ligand, Skint-1, in order to become functional in the epidermis [80].

Another important distinction between $\alpha\beta$ and $\gamma\delta$ T cells is the stage at which the developing thymocytes reach functional maturity. As explained earlier, conventional $\alpha\beta$ T cells leave the thymus as mature but naïve cells and do not gain their effector functionality until they undergo activation in the periphery. Significantly, $\gamma\delta$ T cells have been shown to receive specific transcriptional messages that define the migration and function of the $\gamma\delta$ T cells as they reach maturity in the thymus [81, 82].

$\gamma\delta$ T Cells: Activation and Role in Host Immunity

As previously discussed, $\gamma\delta$ T cells mature and travel to their resident tissues in the mucosal regions of the periphery, and possess specificity to antigens through their unique combination of γ and δ variable chain regions of their $\gamma\delta$ TCR. This TCR directly detects and interacts with antigens, dis-similar to conventional T cells that require antigen presentation. It is this ability to directly interact with antigens and the location of $\gamma\delta$ T cells at the “front line” of the body that classifies $\gamma\delta$ T cells as nonconventional “innate-like” T cells.

Further enforcing this definition of “innate-like” T cells, $\gamma\delta$ T cells recognize antigens through various receptors associated with both the adaptive and innate immune system. $\gamma\delta$ T cells have been shown to play a role in almost all phases of a typical immune

response as summarized by Figure 3. Broadly speaking, $\gamma\delta$ T cells interact with infected and damaged target cells that have upregulated stress-induced NKR ligands, stress-induced $\gamma\delta$ TCR ligands, and various TLR ligands. Upon recognition of these stress signals on the target cells, $\gamma\delta$ T cells can then activate, polarize, proliferate, and release cytokines to play a role in inflammation, targeted cytotoxicity, immunoregulation, and disease clearance. At the earliest phase of infection, $\gamma\delta$ cells recognize signs of stress within host cells, and promptly activate and release inflammatory cytokines and chemokines that recruit neutrophils, macrophages, and other cells of the innate immune system. Within the next phase of the immune response, $\gamma\delta$ cells are responsible for interacting with cells of the adaptive immune system. After primary activation, $\gamma\delta$ T cells undergo proliferation and polarization. These polarized $\gamma\delta$ T cells release cytokines leading to dendritic cell maturation, B cell activation, and $\alpha\beta$ T cell proliferation and polarization. In the final stages of the clearance of the infection, $\gamma\delta$ T cells are responsible for releasing immunosuppressive cytokines such as IL-10 in order to “inactivate” the previously activated adaptive immune system cells. $\gamma\delta$ T cells also promote the healing of the previously infected tissues by releasing trophic growth factors such as TGF- β , KGF1, and IGF1 [83]. To underline the role that $\gamma\delta$ T cells play in wound-healing, mice lacking $\gamma\delta$ T cells have a dramatic inability to regenerate and heal wounds within the skin [83].

As discussed earlier, certain subsets of $\gamma\delta$ T cells, as defined by their type of γ and δ TCR subunits, produce a very specific profile of cytokines upon activation. While primarily of the Th1 and Th17 subtype, a few specific subsets of $\gamma\delta$ T cells have the ability to produce Th2 cytokines such as IL-4 [84]. Significantly, a subset of $\gamma\delta$ T cells express a V γ 1.1, V δ 6.3 TCR and are found within the thymus, spleen, and liver [84-86]. Of particular

interest to our laboratory, these $V\gamma 1.1^+$, $V\delta 6.3^+$ T cells can rapidly release both IL-4 and IFN- γ simultaneously following activation [85, 86]. This ability to produce Th1 and Th2 cytokines is a vitally important aspect of the “innate-like” T cell phenotype only elsewhere seen in NKT cells [85, 86, 90]. The significance of this particular subset of $\gamma\delta$ T cells, and their similarities with NKT cells will be addressed later.

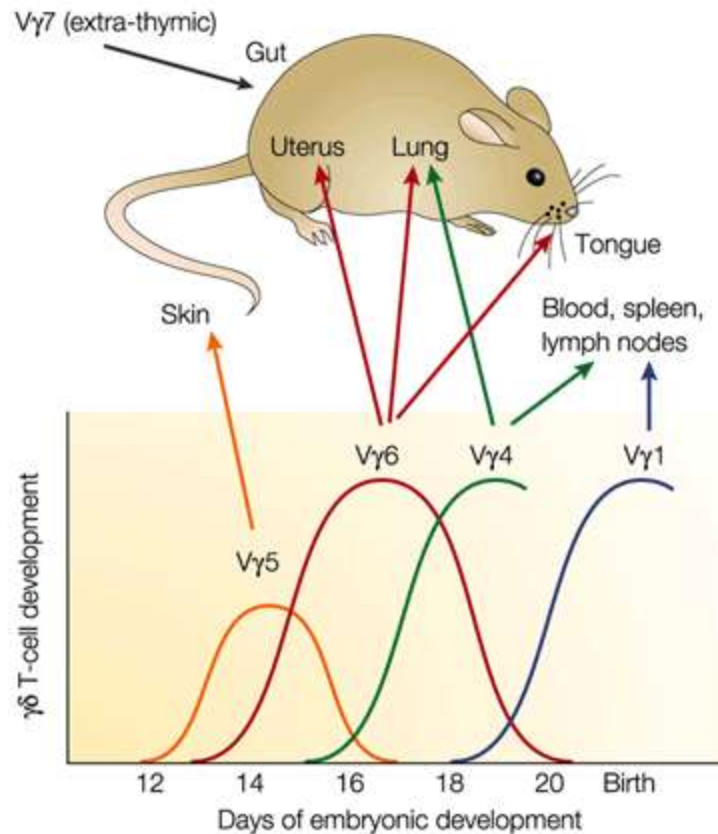


Figure 2. Specific $\gamma\delta$ T cell development during ontogeny. $\gamma\delta$ T cells develop in a cyclical fashion, where each wave consist of a specific subset of $\gamma\delta$ T cells. These specific subsets are defined by their restricted variable chain of the gamma receptor. The specific subsets of $\gamma\delta$ T cells also localize to specific sites within the mammalian body which marks their purpose and effector function within the host immune system.

Reprinted by permission from Macmillan Publishers Ltd: [Nature Reviews Immunology] (78), copyright (2002).

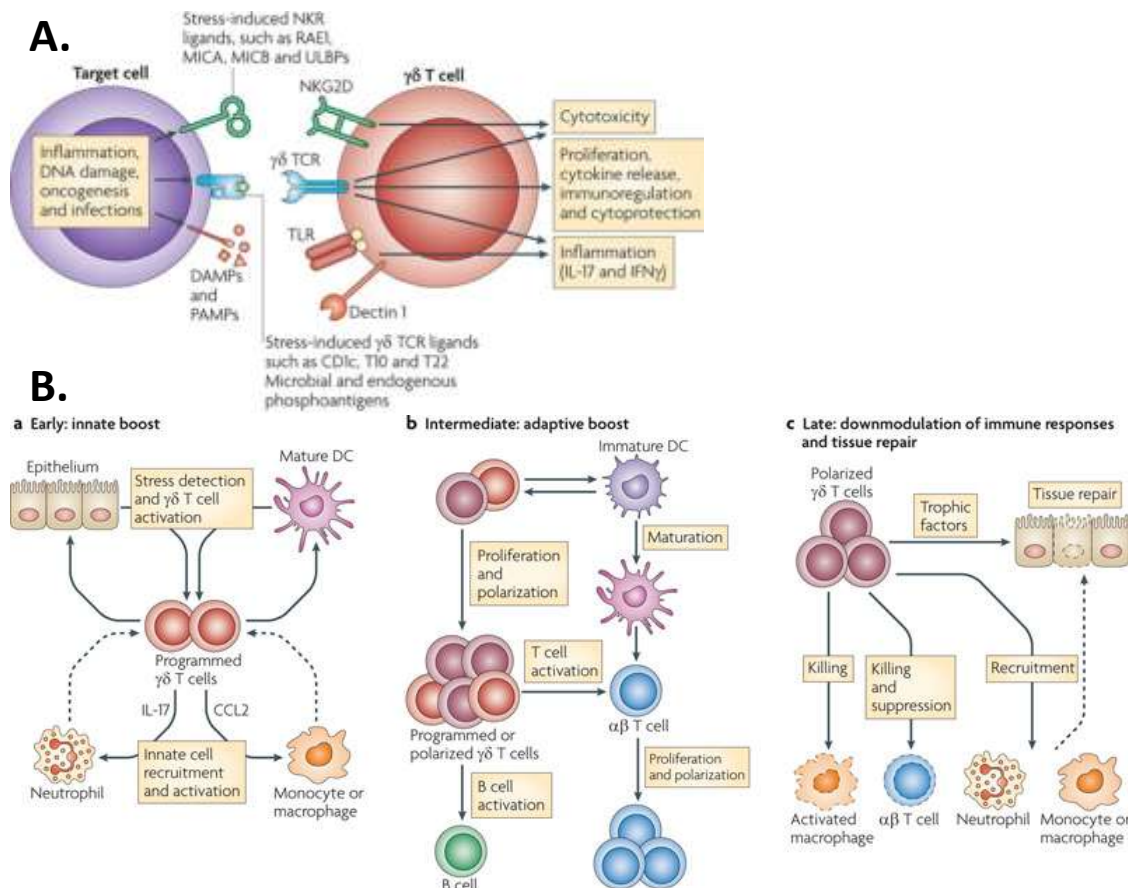


Figure 3. $\gamma\delta$ T Cells interact with various target cells during all stages of immune response . **(A)** $\gamma\delta$ T cells interact with their target cells via multiple recognition pathways, all of which are independent of an antigen-presenting cell. The $\gamma\delta$ TCR interacts with compatible damage markers on the target cell surface. $\gamma\delta$ T cells can also interact with target cells via unspecific receptors such as TLRs, NKG2D, DAMPs, and PAMPs similarly seen in innate cells. Upon recognition by any combination of these receptors, the $\gamma\delta$ T cell activates to proliferate, release cytokines, and begin the immune response to the infected cell. **(B)** $\gamma\delta$ T cells play a role in all three phases of an immune response to infection **(a, b, and c)**. Within the early phase, $\gamma\delta$ T cells interact with the infected cell and recruit innate immune system cells. During the intermediate phase, $\gamma\delta$ T cells can both directly and indirectly activate T and B cells to proliferate and begin the adaptive immune system response. In the late phase, following clearance of the infection, $\gamma\delta$ T cells directly induce tissue repair while also suppressing the previously activated immune cells.

Reprinted by permission from Macmillan Publishers Ltd: [Nature Reviews Immunology] (34), copyright (2010).

Natural Killer T Cells: Nonconventional Thymocyte Development

NK T cells were originally defined as such based on their co-expression of normal T cell surface markers, such as CD3 and an $\alpha\beta$ TCR, as well as the natural killer cell surface marker NK1.1 [36]. NKT cells diverge from conventional thymocyte development at the DP stage in the thymus. Instead of undergoing positive selection by binding its TCR to MHC class I or II expressed on thymic stromal cells, NKT cells are those thymocytes that can bind to CD1d molecule expressed on other DP thymocytes [36]. This non-conventional process is defined as thymocyte-thymocyte selection and is responsible for selecting fledgling NKT cells into the innate NKT cell lineage.

CD1d is a non-classical MHC molecule that is expressed on APCs that presents foreign and self-derived lipid-based antigens. CD1d is a non-polymorphic molecule that presents a very limited variety of lipid antigen ligands. These lipid ligands include α -galactosylceramide (α -GalCer), α -glucuronylceramide, and α -galacturonylceramides which can be found within the cell wall of gram-negative bacteria [33, 38]. Due to the non-polymorphic nature of the presenting molecule and the limited library of ligands it presents, the pool of $\alpha\beta$ TCRs capable of recognizing and binding the ligands are equally limited. This fact leads to NKT cells being defined as having an invariant and conserved T cell receptor repertoire.

NKT cells are further classified as either type 1 or type 2. While both types are CD1d restricted, type 1 Mouse NKT cell TCRs are those with the invariant TCR α chain, V α 14-J α 18 and the semi-variant TCR β chain, V β 8.2, V β 7, or V β 2 [37]. Conversely, type 2 NKT cells have a more diverse T cell repertoire. Type 1 or invariant-NKT cells (iNKT cells) are highly reactive to the lipid α -GalCer and are the most studied and biologically-

relevant group of NKT cells [33]. In fact, CD1d tetramers loaded with α -GalCer are a commonly used tool used to activate, label, and study NKT cells.

Upon NKT cell selection via CD1d interactions on DP thymocytes in the cortex, NKT cells upregulate CCR7 and travel to the medulla as stage 0 cells [39]. There they receive further cues from CCL21⁺ medulla thymic epithelial cells to grow into stage 1 cells (CD44⁺NK1.1⁻) and stage 2 cells (CD44⁺NK1.1⁻). Throughout this development and independent of NK1.1 and CD44 expression, NKT cells can exist as either CD4⁺CD8⁻ or CD4⁻CD8⁻ [41-44]. Immature NKT cells, defined as such by their lack of NK1.1 expression, can be exported to and mature in peripheral lymphoid tissues or remain in the thymus to mature into stage 3 NKT cells (CD44⁺NK1.1⁺) [40]. The development and maturation of iNKT cells is tightly controlled by various transcription factors and the pathways they modulate.

Natural Killer T Cells: Transcriptional Control

Various signaling pathways and transcription factors are responsible for directing the differentiation and maturation of natural killer T cells. These transcriptional pathways are apparent at the earliest stage of NKT cell development, the thymocyte-thymocyte selection at the double negative stage. As the invariant TCR of the double positive thymocyte binds the selecting ligand being presented by the CD1d molecule, there are other important signaling molecules interacting between the DP thymocytes, namely the SLAM family receptors. These SLAM surface receptors begin a signal cascade called the SLAM-SAP-Fyn signaling axis that is vital for the early stages of iNKT cell development [57]. As the SLAM receptors interact, the intracellular tails interact with an adapter molecule SAP and the tyrosine kinase Fyn. Through further interactions with PKC θ and

Bcl10, NF-kappa-B transcription factors are activated and enter the nucleus to direct gene expression towards the NKT cell lineage [45, 47]. This process is outline in Figure 4 shown below.

Concurrently at the DP stage of thymocyte development, the transcription factor ROR γ t is active in NKT precursor cells. Traditionally, ROR γ t has been known as the transcription factor directly associated with a cell's ability to produce IL-17a, a cytokine that induces the activation of neutrophils and release of other proinflammatory cytokines [50]. Specifically within NKT cells, ROR γ t is responsible for facilitating the V(D)J recombination of the distal α and β subunits of the invariant NKT TCR [42, 47, 49]. Recent studies have also found that ROR γ t also plays a role in the differentiation of a distinct subset of NKT cells, iNKT17 cells. These iNKT17 cells are those NKT cells that can quickly produce IL-17a, analogous to the Th17 class of conventional CD4⁺ T helper cells [50].

As precursor NKT cells emerge from the DP thymocyte stage, the transcription factor PLZF is found to be highly expressed [45-48]. More about this transcription factor will be addressed in a following section.

The transcription factor T-bet has also been found to play a role in the development of NKT cells [45, 47, 51]. Although it was originally thought to be exclusively responsible for the induction of the Th1 lineage, it has been proven that T-bet plays a role in almost every immune cell type. Specifically within NKT cells, T-bet is expressed starting at stage 1 and has increasing expression as the NKT cell matures to stage 3 NKT cells [47, 51, 52]. T-bet induces the expression of the IL-2 and IL-15 receptors which are crucial for the proliferation and long term survival of the stage 3 mature NKT cells [51, 52].

Each of these transcription factors and their associated signaling pathways are responsible for the unique differentiation, resting phenotype, activation, and effector function of iNKT cells.

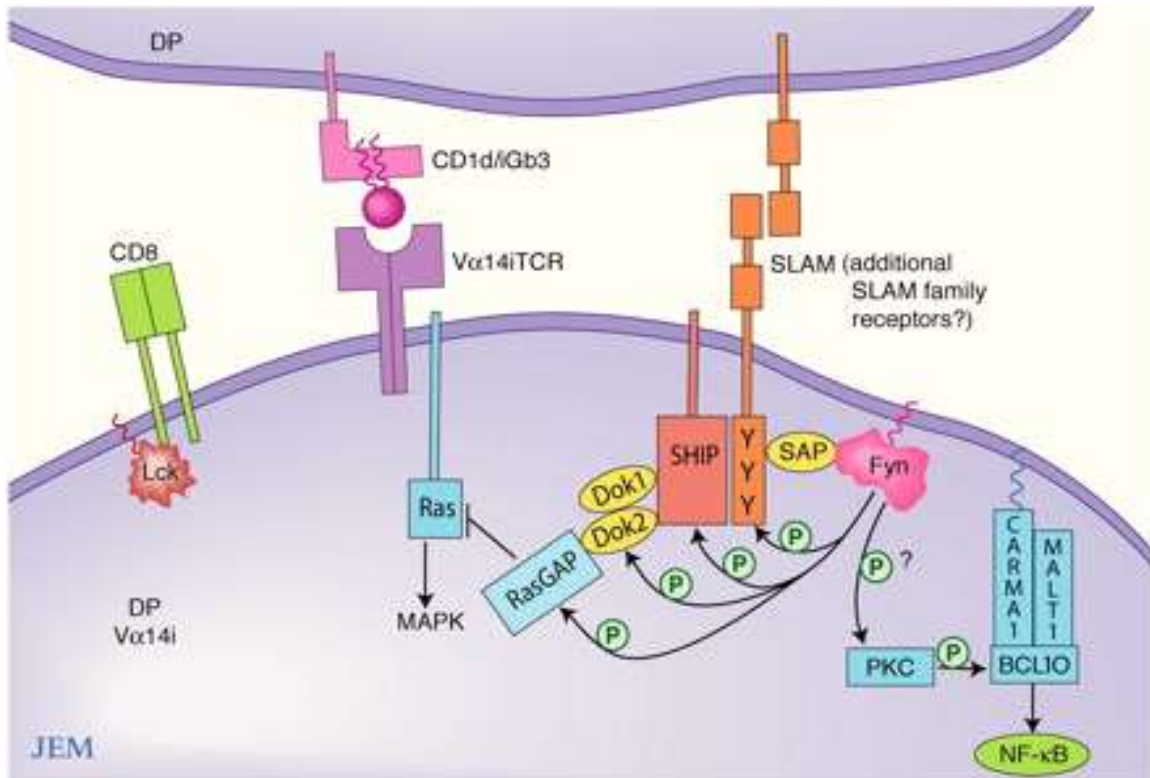


Figure 4. Nonconventional NKT Cell Development via CD1d Selection. As fledgling NKT cells undergo their nonconventional development within the thymus, they select via interactions between their restricted invariant TCR conformation and CD1d presenting molecules on other DP thymocytes. Following binding of TCR to CD1d, there is also interaction between the SLAM family receptors on each of the DP thymocytes. This SLAM receptor interaction leads to intracellular signaling via phosphorylation of various proteins by the tyrosine kinase, Fyn. Phosphorylation of PKC and Bcl10 leads to activation of NF-kappa B transcription factors that then induce the specific gene expression profile of an NKT cell. Adapted from [92].

Natural Killer T Cells: Activation

As address earlier, NKT cell activation occurs through to the specific interaction between the iNKT TCR and glycolipid ligands presented by CD1d molecules. In the periphery, APCs such as macrophages and dendritic cells are responsible for processing and presenting the glycolipids. NKT cells can recognize both endogenous and exogenous glycolipids. Upon sufficient recognition and binding of the TCR to the CD1d presented lipid, NKT cells undergo maturation and exhibit their first stage of activation. This first stage of activation includes the large scale production of Th1 and Th2 cytokines as well as upregulation of CD40L. This CD40L then in turn binds to CD40 on the APCs to induce superactivation. APC superactivation consists of upregulation of CD40, B7.1, B7.2, and IL-12 release, which leads to strong activation of both CD4⁺ and CD8⁺ T cells [33, 53, 54]. The released IL-12 induces the secondary activation of the NKT cell, which consists of IFN- γ cytokine production and subsequent NK cell activation.

The time scale with which this NKT cell activation and cytokine production occurs evidences the role of NKT cells as the bridge between the innate and adaptive immune system. Uniquely and importantly, NKT cells have the ability to almost instantly produce huge amounts of IL-4 and IFN- γ , cytokines that have the ability to activate both members of the cell-mediated and antibody-mediated arms of the adaptive immune system.

Researchers have discovered that this quick release is due to the constitutive transcription of IL-4 and IFN- γ cytokine mRNAs in resting NKT cells [55]. Following the primary NKT cell activation described above, the mRNAs are translated, and the p38 MAP kinase pathway is activated to induce further gene expression of cytokines [55, 56]. The full

gambit of effector functions performed by NKT cells are succinctly illustrated in Figure 5 below.

NKT cells that undergo activation in response to a CD1d-presented antigen and the associated cytokine release, subsequently exhibit anergy and apoptosis. The findings by Uldrich et al. determined that α -GalCer stimulated NKT cells do not in fact die, but actually proliferate up to ten fold by three days following stimulation, and then contract down to normal levels by 6-9 days [58, 59]. The contraction phase of the NKT cell response is due to Bim regulated apoptosis in the same fashion that conventional T cells exhibit [58]. If previously challenged NKT cells are then re-challenged with the same α -GalCer, they exhibit a weakened response. This weakened response consists of a dramatic decrease in cytokine release and the absence of activation and co-stimulatory cell surface marker upregulation [57 -59].

The presence of NKT cells in the early stage of infections and disease support their definition as “innate-like” T cells. However, many studies have also eluded to the role that NKT cells play in long term illnesses. The conclusions summarized above highlight the importance of these rare but powerful members of the immune system, but also illustrate the gaps in knowledge that exist regarding the ability to harness and control the function of NKT cells.

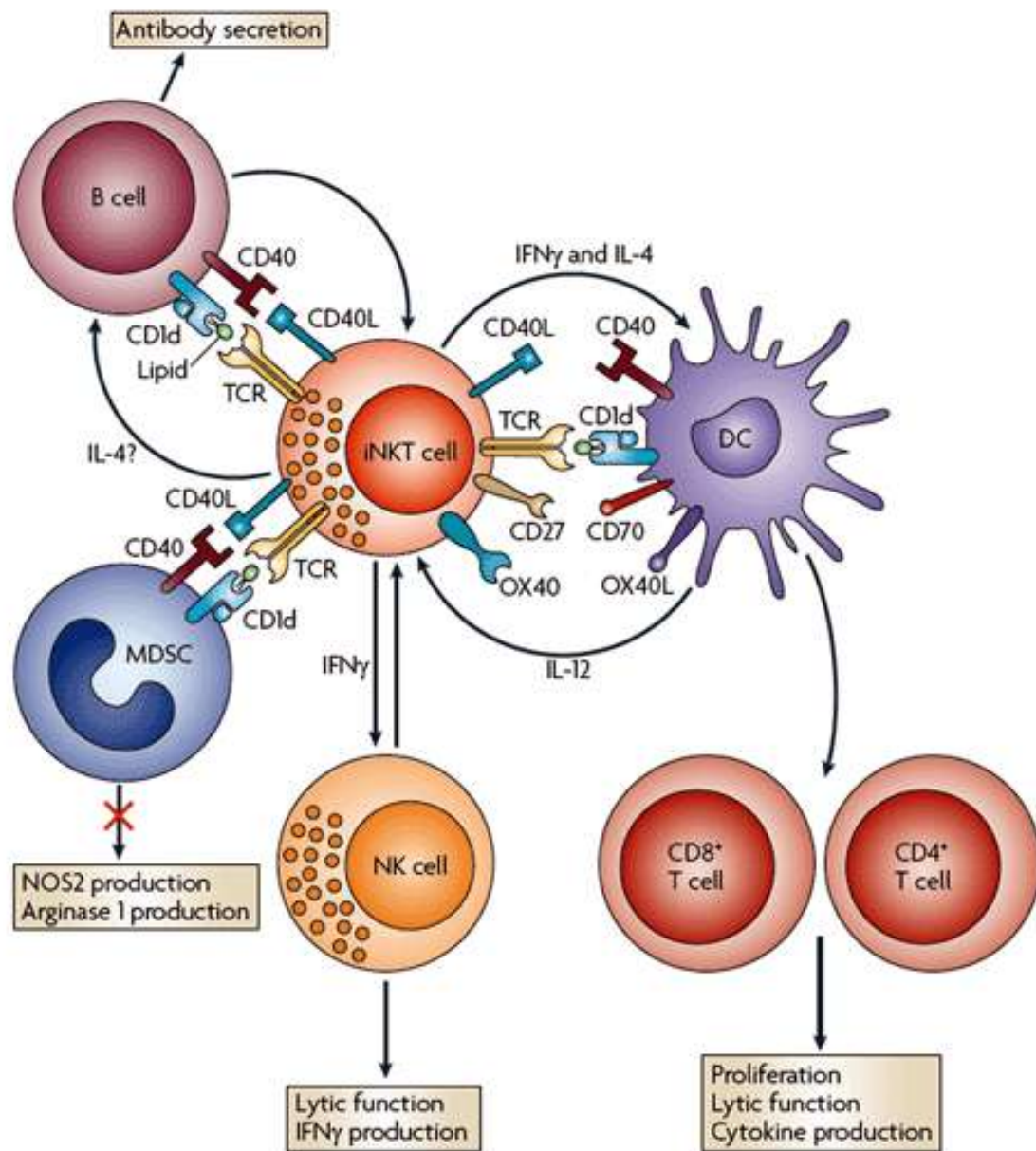


Figure 5. Invariant NKT Cells interact with various innate and adaptive immune system cells. Via activation by interactions between the iNKT TCR and CD1d-presented glycolipids, iNKT cells upregulate co-stimulatory molecules and release cytokines that can directly and indirectly activate B cells, NK cells, DCs, MDSCs, and T cells.

Reprinted by permission from Macmillan Publishers Ltd: [Nature Reviews Immunology] (93), copyright (2009).

Innate Lymphocytes: Implication in Diseases

Keeping in mind the role that they play in the innate immune response to infection, their ability to respond to host and pathogenic antigens, their ability to release cytokines, and their ability to activate most other members of the immune system, it should not at all be surprising that $\gamma\delta$ T cells and NKT cells play a role in a wide array of diseases. Beginning with the brief list of bacterial infections, viral infections, parasitic infections, cancer, type-I diabetes, asthma, and lupus, NKT cells are continuing to be discovered as participants of many common diseases plaguing humans. Similarly, $\gamma\delta$ T cells are implicated in the fields of wound healing, tissue regeneration, liver damage, tumor clearance, and HIV treatment [87]. Clearly defining their roles in these diseases remains a goal of many research laboratories across the world.

The role of innate lymphocytes in tumor immunity is a hot topic for cancer immunologists. Studies show that mice lacking NKT cells have a marked drop in the ability to defend themselves from sarcomas and melanoma tumors [50, 51]. The same lab also found that treatment with functional iNKT cells induced tumor rejection [50, 51]. NKT cells seem to help with tumor rejection based on their ability to release IFN- γ to stimulate cytotoxic killer T cell and NK cell-mediated tumor elimination. These early studies led others to attempt to harness NKT cells as an anti-tumor cell therapy. Figure 6 depicts various possible applications of NKT cells in cancer immunotherapy. These various methodologies rely upon the robust anti-tumor cytokine release by NKT cells and their specific activation by α -GalCer.

$\gamma\delta$ T cells are commonly present at the site of solid tumor growth and have been defined as members of the tumor-infiltrating lymphocytes (TILs) population. In various studies,

$\gamma\delta$ T cells from this TIL population have been cultured *ex vivo* and have the ability to recognize and kill autologous tumors [88, 89]. Finally, mice lacking $\gamma\delta$ T cells experienced a significant increase in the frequency of epithelial tumor growth [88, 89].

Innate Lymphocytes: Role in Liver and Liver Diseases

The liver is an organ that is responsible for many vital body processes. One such process is immune surveillance and filtration of blood coming from the gastrointestinal tract. Antigen presenting cells and their related adaptive immune effector cells reside within liver sinusoids. Importantly, the population of liver lymphocytes is dominated by NKT and NK cells. NKT cells make up 1% of healthy human liver lymphocytes and 30% of mouse liver lymphocytes [64]. This is the highest NKT to conventional T cell ratio found within the body and thus is an intriguing arena to study the effector function of NKT cells.

The majority of liver diseases consist of the destruction of hepatocytes and replacement with extracellular matrix in a process known as fibrosis that ultimately ends in cirrhosis and total failure of the organ. Liver failure is an enormous burden upon human society as there is no cure other than a liver transplant and many patients die before receiving a life-saving transplant. There exists a need to study the pathways by which these liver diseases occur so that treatments can be designed to save patients before they require a transplant.

Unsurprisingly, based upon what we know about NKT cells, and their presence in the liver, they have been found to play a significant role in some liver-based diseases. Upon taking a closer look at liver diseases, we see the perfect illustration of the impressive array of effector functionality that NKT cells possess. In the aptly-named review, “Hepatic NKT cells: friend or foe?” Mark Swain outlines NKT cells in normal and

diseased liver models [62]. NKT cells have been found to support liver regeneration, tumor rejection, and liver infection clearance. Using hepatitis mouse models, researchers have also concluded that NKT cell mediated IFN- γ release arrests hepatitis B viral replication as well as playing a role in the successful hepatitis B vaccination. These seem to be the protective functions that NKT cells perform in a normally functioning, healthy liver.

Conversely, NKT cells have also been implicated in hepatocyte destruction, liver-specific autoimmune diseases, and toxic/metabolic liver disease. NKT cells resident within the liver have been shown to induce destruction of hepatocytes when irregularly activated. The cytokines released by these NKT cells mediate the development of fibrosis and subsequent cirrhosis as immune cells destroy hepatocytes and induce scarring via collagen production. NKT cells in chronically infected livers have a Th2 skewed cytokine profile that have been shown to induce pro-fibrinogenic changes in the liver [62, 63]. Human patients suffering from PBC, a liver autoimmune disease, have a markedly increased population of NKT cells [62, 63].

Mice injected with Concanavalin A are an appropriate model for NKT mediated liver autoimmune disorders [62-65]. Con A injection leads to the specific activation of NKT cells within the liver causing a typical cytokine release which induces a state of liver damage similar to human liver autoimmune diseases. Mice lacking NKT cells exhibit no liver damage upon Con A injections, further evidencing the role that NKT cells play in Con A induced liver damage, and endogenous liver damage in general [62]. Liver damage can be measured by the release of liver proteins into the bloodstream. Proteins levels of ALT and AST are positively correlated with liver damage.

Determining the exact level of NKT cell activation required for normal functionality versus an autoimmune response within the liver remains an important research goal of many immunologists. By defining what factors control the augmented activation of liver NKT cells we will be able to design better treatment protocols for patients exhibiting NKT cell mediated liver damage.

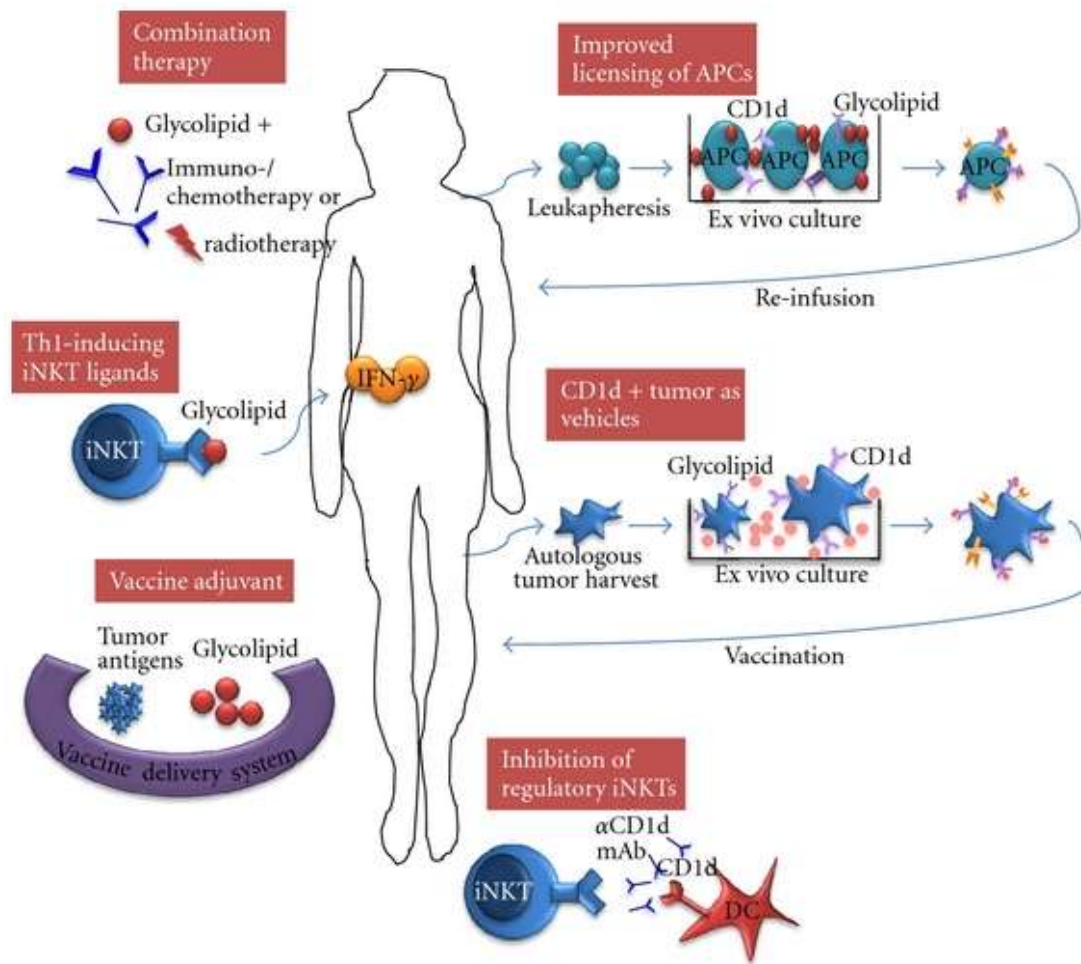


Figure 6. Various immunotherapies involve the activation or suppression of iNKT cells. Due to the fact that CD1d-loaded glycolipids such as alpha-Gal-Cer can specifically activate endogenous NKT cells, dosing of alpha-Gal-Cer is seen as an exciting method of recruiting and activating NKT cells at the site of disease. Adapted from [61].

PLZF

The family of broad complex, tramtrack, bric-a-brac-zinc finger transcription factors (BTB-ZF) are a distinct group of zinc finger transcription factors that control the development of specific subsets of various immune system cells [66]. One member of this family is promyelocytic leukemia zinc finger (PLZF), a transcription factor identified by Dr. Sant'Angelo's laboratory as the master regulator for NKT cell effector functionality [46, 47]. Other important and well known members of this family of transcription factors are ThPOK, Irf, and Bcl-6 [66]. The functionality of these transcription factors is dependent on their ability to interact with DNA through the zinc finger motifs. The zinc finger domains of these transcription factors bind specifically to regions along the DNA of the genes they regulate. Zinc finger transcription factors can act either to activate or repress gene expression. The activity of BTB-ZF transcription factors is also dependent on the interactions that occur at the highly conserved BTB protein interaction domains [70]. This binding of supporting proteins at this region is crucial for the proper functionality of zinc finger transcription factors. In fact, recent data has been published showing that Bcl-6, a BTB-ZF transcription factor vital for the formation of germinal centers, specifically requires BTB-domain interaction with corepressors such as NCOR and BCOR in order to function properly [91].

PLZF: Master Regulator of NKT Cell Effector Function

PLZF is a nuclear transcription factor protein coded by the gene *zbtb16* on the human chromosome 11 and mouse chromosome 9. It was originally identified in promyelocytic leukemia where a chromosomal translocation created the PLZF-RAR- α chimeric oncoprotein that was responsible for uncontrolled cancer cell growth. This oncoprotein negates the normal function of PLZF, the induction of cellular quiescence through

interactions with histone deacetylases [66, 71]. It was not until years later that researchers defined another role for PLZF. Dr. Sant'Angelo and other researchers found that PLZF was expressed specifically in iNKT cells within the immune system [46, 48]. Using a CD1d tetramer loaded with PBS57, a α -Gal-Cer analog conjugated to a fluorophore, to define the iNKT cell TCR in conjunction with an antibody for the PLZF transcription factor, PLZF expression was confirmed within NKT cells. Figure 7 shows that PLZF expression within CD1d tetramer⁺ NKT cells was markedly higher than conventional T cells within the thymus and liver. Through the use of the PLZF antibody, the CD1d tetramer, NK1.1 antibody, and CD44 antibody, they showed that PLZF expression is highest expressed within stage one (CD44⁻NK1.1⁻) and stage two (CD44⁺NK1.1⁻) iNKT cells before dropping to a lower level in stage three iNKT cells. Utilizing a PLZF-KO mouse model, they showed that there are no CD1d tetramer⁺ NKT cells in PLZF-KO mouse thymus and liver. Furthermore, the NKT cells of PLZF-KO mice lose the ability to co-release IFN- γ and IL-4 following stimulation by α -GalCer, the hallmark of normal NKT cell activity. PLZF-KO mice also lose the ability to upregulate activation cell surface markers and do not exhibit an activated phenotype. From these experiments, Dr. Sant'Angelo and his laboratory concluded that the transcription factor PLZF is required for proper effector functionality of iNKT cells [46, 47, 66, 68].

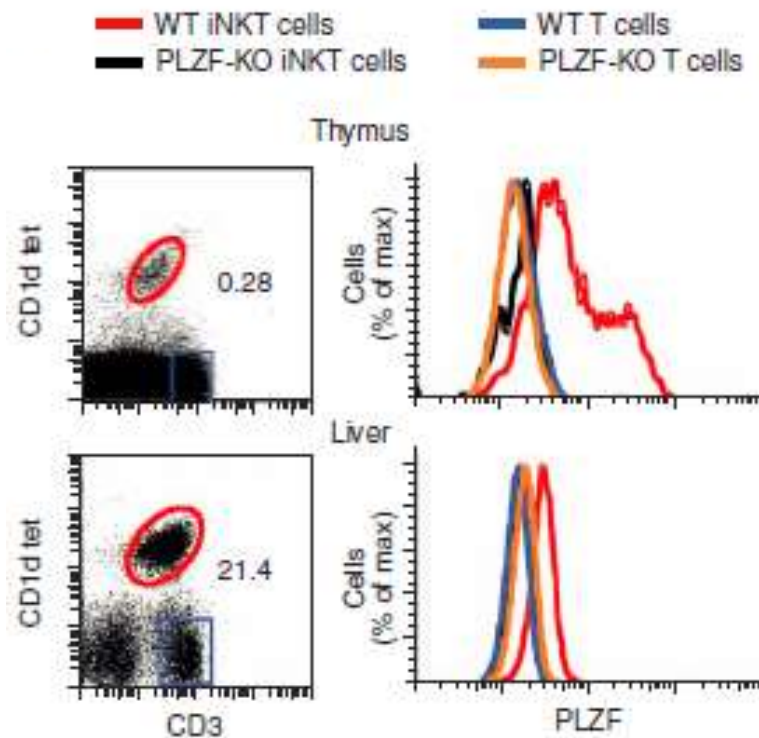


Figure 7. Restricted PLZF expression within NKT Cells of the thymus and liver. The expression of PLZF within CD1d tetramer⁺ cells is displayed as a histogram. Within the top row, the histogram is displaying the PLZF expression of thymic WT iNKT cells compared to the PLZF expression within PLZF-KO iNKT cells and WT conventional T cells. As seen, the PLZF expression within the CD1d tetramer⁺ cells from the PLZF-KO mice is markedly reduced when compared to WT iNKT cells and is comparable to PLZF expression within conventional T cells. The same findings are seen in the liver samples, shown in the bottom row.

Reprinted by permission from Macmillan Publishers Ltd: [Nature Reviews Immunology] (46), copyright (2008).

PLZF: Specific Expression in $\gamma\delta$ T Cell Subsets

As introduced earlier, the specific subset of $V\gamma 1.1^+$, $V\delta 6.3^+$ $\gamma\delta$ T cells are unique amongst all $\gamma\delta$ T cell subsets due to their ability to simultaneously release IL-4 and IFN- γ cytokine. In fact, the only other cell type that can co-release IFN- γ and IL-4 are NKT cells. Due to this, we will refer to $V\gamma 1.1^+$, $V\delta 6.3^+$ $\gamma\delta$ T cells as $\gamma\delta$ NKT cells. Strikingly, research performed in our laboratory defined PLZF as a transcription factor integral to the development and function of these $\gamma\delta$ NKTs. Figures 8, 9, and 10 below are data produced by Dr. Eric Alonzo as part of his doctoral thesis in Dr. Sant'Angelo's laboratory [86]. Figure 8 shows that $\gamma\delta$ T cells from the thymus, spleen, liver, lymph nodes and iIEL all express some level of PLZF. Specifically, Figure 9 shows that PLZF expression is restricted to $V\gamma 1.1^+$ $\gamma\delta$ T cells and $V\delta 6.3^+$ $\gamma\delta$ T cells. Further testing defined the $\gamma\delta$ NKT cells as the main source of PLZF expression. Within the thymus, 74% of $\gamma\delta$ NKT cells express PLZF. The delineation of PLZF-positive and PLZF-negative $\gamma\delta$ NKT cells is apparent when studying their effector functionality. Studies performed by our laboratory show that the PLZF-positive $\gamma\delta$ NKT cells are able to co-produce IFN- γ and IL-4 upon *in vitro* activation as seen below in Figure 10 [86]. They also were found to express NKT cells markers including NK1.1, CD4, CD44, and CD69. The $\gamma\delta$ NKT cells were also found to have similar low levels of CD24, similar to thymic NKT cells.

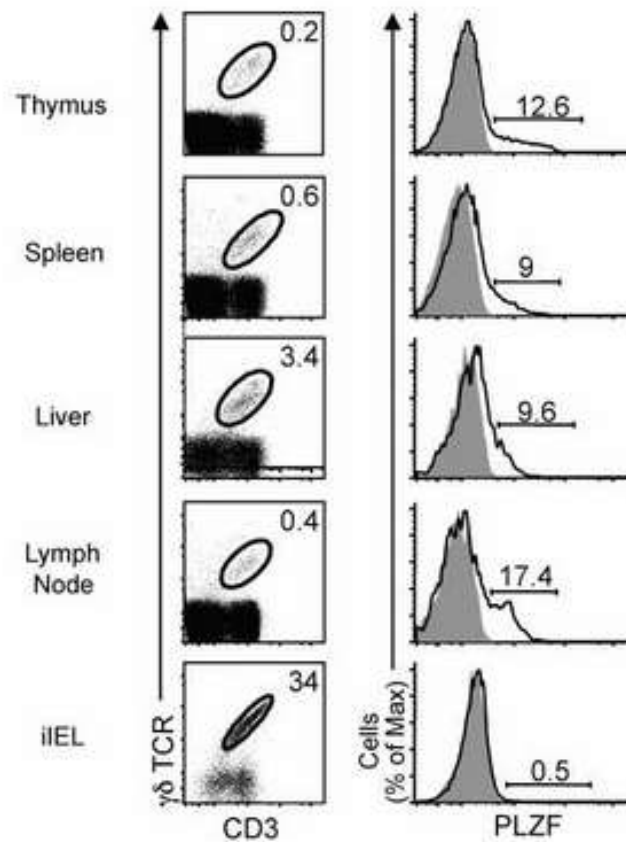


Figure 8. $\gamma\delta$ T Cells express PLZF within various immune tissues. The percentage of $\gamma\delta$ T cells within the specific tissues is displayed in left column. There is a significant population of $\gamma\delta$ T cells within the liver and intestinal epithelium specifically. The right column displays the PLZF expression within all $\gamma\delta$ T cells gated upon within the left column. Each PLZF histogram includes a PLZF-KO samples to serve as a negative control. Adapted from [86].

Copyright 2010. The American Association of Immunologists, Inc.

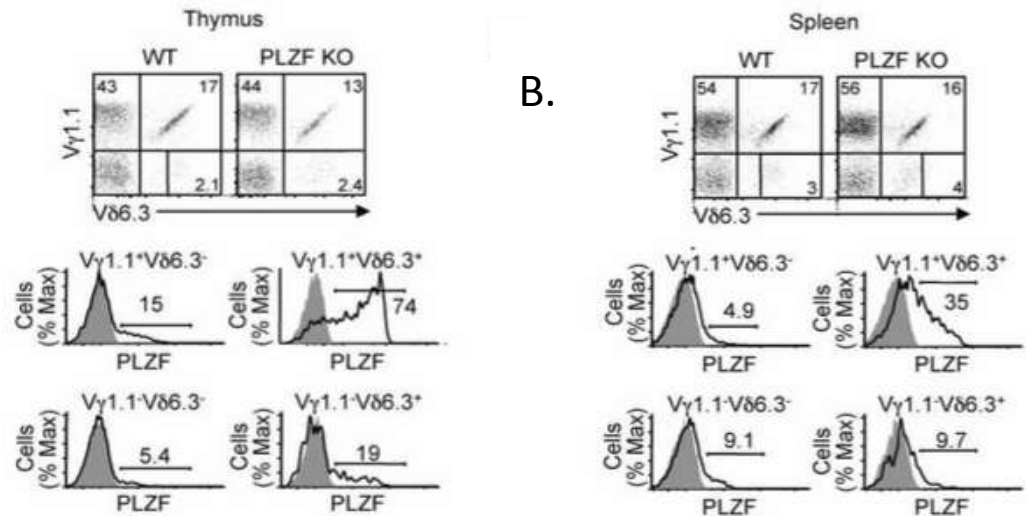


Figure 9. PLZF expression is restricted to $V\gamma 1.1^+$, $V\delta 6.3^+$ $\gamma\delta$ T cells. These cells are not dependent on PLZF for their development. **(A)** Within the thymus, there is moderate expression within all four subpopulations of $\gamma\delta$ T cells, with a significant increase in the $V\gamma 1.1^+$, $V\delta 6.3^+$ subpopulation. **(B)** The same studies were performed in the spleen, where the same $V\gamma 1.1^+$, $V\delta 6.3^+$ subpopulation was found to have highly elevated levels of PLZF expression. Adapted from [86].

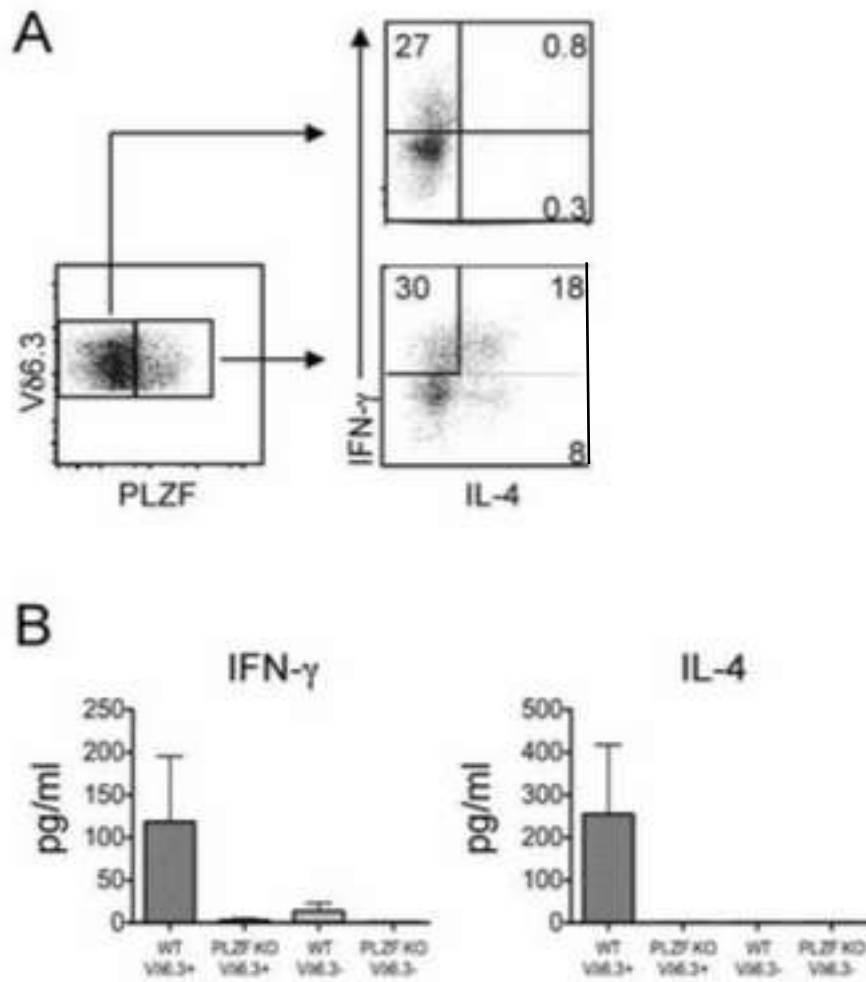


Figure 10. Vδ6.3⁺ γδ T cells require PLZF to coproduce IFN-γ and IL-4. Vδ6.3⁺ γδ T cells are separated into those that express PLZF and those that do not. The PLZF and non-PLZF expressing cells have different functional properties. **(A)** PLZF expression is used to separate the Vδ6.3⁺ γδ T cells. Vδ6.3⁺ T cells that express PLZF have the ability to double produce IFN-γ and IL-4 while the Vδ6.3⁺ γδ T cells that do not express PLZF do not have the ability to co-produce IFN-gamma and IL-4. **(B)** The IFN-γ and IL-4 production by each of sub-groups of WT and PLZF KO, Vδ6.3⁺ and Vδ6.3⁻ γδ T cells was quantified by plate-bound ELISA. The lack of PLZF in turn leads to a dampened or eliminated ability to produce IFN-γ and IL-4. Adapted from [86].

PLZF: Ectopic Expression in Conventional T Cells

Following the findings summarized above, Dr. Sant'Angelo and his laboratory strove to define the limits of the expression of PLZF. They asked the very interesting question: will forced expression of PLZF in all T cells lead to transgenic T cells sharing the iNKT cell activation phenotype and effector functionality? The lck-PLZF mouse line was designed to ectopically express PLZF in all T cells as specified by the lck promoter region [67]. Flow cytometry experiments illustrated that expression of PLZF in transgenic T cells was significantly increased over wild type T cells, evidencing that the transgene was functional. They found that lck-PLZF mice did not have significantly more NKT cells than wild type mice, or variation in the ratio of CD4⁺/CD8⁺ conventional T cells. Upon inspection of the various cell surface markers that iNKT cells express, it was found that transgenic conventional T cells had upregulation of some but not all of these memory and effector markers when compared to wild type conventional T cells. Next they investigated the cytokine secretion profile of the transgenic conventional T cells. Shown in Figure 11, conventional T cells with forced expression of PLZF did not acquire the same degree of ability to co-release IL-4 and IFN- γ as seen in wild type iNKT cells. One significant difference seen in the cytokine release profile of the lck-PLZF mice compared to wild type mice is the marked emergence of a population of CD8⁺ T cells that produce high levels of IL-17a. This significant change is shown in Figure 12.

There was also the need to define whether or not overexpression of PLZF in $\gamma\delta$ T cells would affect the phenotype and function of $\gamma\delta$ T cell subsets. As discussed earlier, the specific subset of $\gamma\delta$ NKT cells have the ability to co-produce IL-4 and IFN- γ due to their relative high levels of PLZF compared to other $\gamma\delta$ T cell subsets. Previously, our

laboratory has shown that the ectopic overexpression of PLZF in $\gamma\delta$ T cell subsets do not induce a different phenotype or function when compared to wild type $\gamma\delta$ NKT cells [66].

The exact pathway by which the endogenous expression of PLZF regulates the unique effector function of $\gamma\delta$ NKT cells independent of the ectopic forced overexpression of PLZF in the lck-PLZF mice remains an interesting and intriguing unanswered question.

The ramifications of this study are significant although they did not achieve the exact intended results. As comprehensively introduced above, iNKT and $\gamma\delta$ T cells are unique and powerful immune cells that have the ability to operate within the gap between the innate and adaptive immune system. This ability to interact and activate almost every immune cell through the quick release of cytokines has made it a very handsome target for possible cellular therapies [61, 72]. As listed in Figure 13, there are many NKT cell based therapies already undergoing phase I/II clinical trials. Each of these methods harnesses the specific activation of iNKT cells by α -GalCer and/or the adoptive transfer of expanded iNKT cells into target sites of diseases.

By attempting to genetically modify conventional T cells into cells with iNKT-like functionality using ectopic expression of PLZF, this study represents an exciting exploratory endeavor; attempting to engineer a more specific, more powerful, longer lasting, and more effective T cell population for adoptive T cell therapy. Imagine being able to withdraw patients' abundant T cells, genetically modify them to act as iNKT cells, and inject them back into the patient at the site of preliminary tumor growth. This personalized process of enhancing the host's own cells to have increases effectiveness represents the holy grail of cellular engineering. It is in this same vein of thought that gave birth to the idea that is my Master's thesis research.

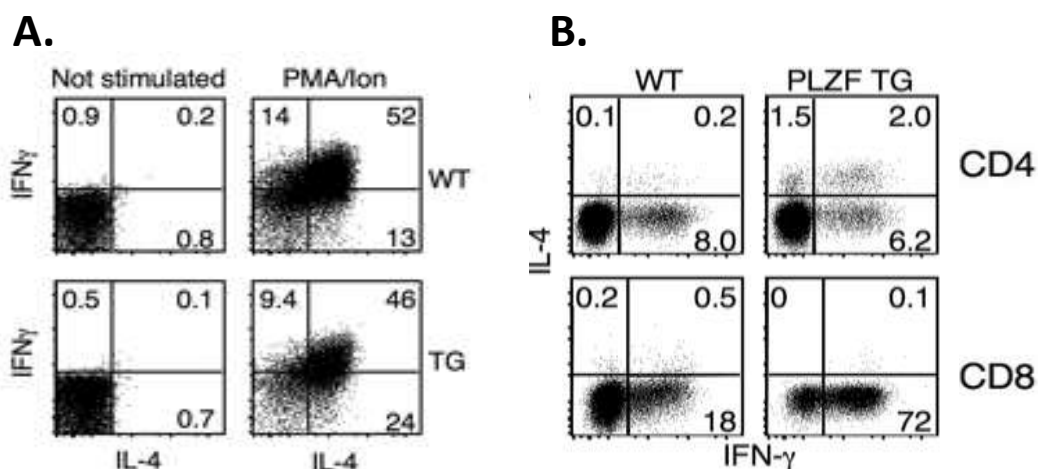


Figure 11. IFN- γ and IL-4 co-production by conventional T cells is not altered in lck-PLZF mice. PMA and ionomycin followed by Brefeldin A were used for in vitro stimulation of various T cell subsets. **(A)** NKT cells have the unique ability to double produce IFN- γ and IL-4 upon in vitro stimulation. Without stimulation, there is no production of either IFN- γ or IL-4. The lck-PLZF TG samples have similar populations of double-producing NKT cells. **(B)** Upon inspection of the CD4 and CD8 T cells, there is a robust increase in IFN- γ production within the CD8 T cells of the lck-PLZF TG mice compared to the WT CD8 T cells. There is a small but non-significant increase in the ability of the CD4 T cells of the lck-PLZF TG mice to co-produce IFN- γ and IL-4. Adapted from [67].

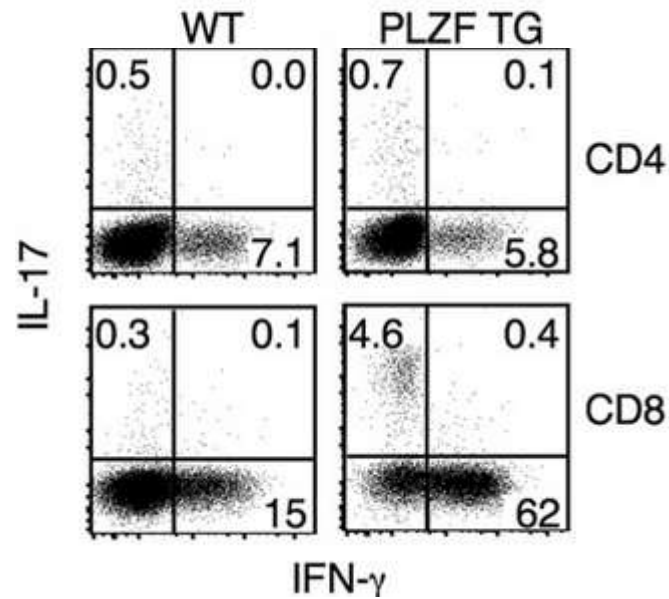


Figure 12. IL-17a producing CD8⁺ T Cells are present in activated lck-PLZF mice. PMA and ionomycin followed by Brefeldin A were used for in vitro stimulation of various T cell subsets. Upon inspection of the CD4⁺ and CD8⁺ T cells, there is a robust increase in IL-17a production within the CD8⁺ T cells of the lck-PLZF TG mice compared to the WT CD8⁺ T cells. Adapted from [67].

Tumor	Number of patients	Treatment regimen	Summary of study results	Reference
(A) Direct α -galactosylceramide injection				
Solid tumors	24	α -Galactosylceramide i.v. (40–4800 μ g/m ²)	(1) No dose-limiting toxicity (2) Increase serum TNF- α and GM-CSF in 5 of 24 patients (3) Response dependent on pre-existing number of NKT cells which were significantly lower in cancer patients	Giaccone et al., 2002 [89]
(B) Infusion of ex vivo expanded NKT cells				
Non-small cell lung cancer	6	V α 24NKT cells restimulated with α -galactosylceramide-pulsed PBMCs	(1) No adverse effects (2) Highest dose induced expansion of NKT cells (in 2 of 3 patients) and IFN- γ producing cells (in 3 of 3 patients)	Motohashi et al., 2006 [90]
(C) Ex vivo generated DC loaded with α -GalCer				
Non-small cell lung cancer	11	α -Galactosylceramide-pulsed dendritic cells	(1) No severe toxicities (2) Increase NKT cells in 1 of 11 patients (3) No partial or complete response seen	Ishikawa et al., 2005 [91]
Head and neck cancer	9	α -Galactosylceramide-pulsed APC	(1) No serious toxicities (2) Increase NKT cells in 4/9 patients (3) Increase NK activity in 8/9 patients	Uchida et al., 2008 [92]
Non-small cell lung cancer	23	α -Galactosylceramide-pulsed PBMC cultured with IL-2/GM-CSF	(1) No severe toxicities (2) Stable disease in 5 (3) Increased IFN response correlated with survival	Motohashi et al., 2009 [93]
Non-small cell lung cancer	4	α -Galactosylceramide-pulsed APC	(1) Increase in NKT cells in lung tumors (2) Highest IFN- γ production following in vitro restimulation of TILs with α -galactosylceramide	Nagato, K et al 2012 [94]
(D) Combination strategies				
Head and neck squamous cell cancer	8	In vitro expanded NKT + α -galactosylceramide-pulsed APC	(1) Transient and mild adverse effects (2) Increased NKT cells and IFN- γ secretion in 7 of 8 patients (3) Partial response in 3 patients, stable disease in 4, progressive disease in 1	Kunii, N et al. 2009 [95]

Figure 13. Various NKT cell-based cancer therapies are currently undergoing clinical trials. Through the use of the NKT cell agonist, α -Gal-Cer, researchers are directly activating endogenous NKT cells, expanding NKT cells ex vivo, and loading dendritic cells ex vivo prior to re-infusion. Adapted from [61].

Btbd11

The protein Btbd11 belongs to a group of proteins that possess the protein-protein binding region, Btb that is previously discussed above. It is through this binding region that Btb family proteins modulate and interact with the activities of other proteins sharing this Btb region. Although no protein crystallography studies have been performed on Btbd11, through the study of conserved protein sequences within the amino acid sequence of Btbd11 we can uncover possible roles and interactions that Btbd11 participates in. In Figure 14, we see the various conserved regions and motifs that exist along the 1103 amino acid long Btbd11 protein. In addition to the Btb protein binding region previously discussed, Btbd11 also consists of five ankyrin repeat motifs. These ankyrin motifs are another common protein-protein binding domain seen within mammalian proteins. Btbd11 is of particular interest to our research due to its linked interactions with PLZF.

Btbd11: Interactions with PLZF via Btb-Protein Interaction Domains

Btbd11 first became a protein of interest to our laboratory following its appearance in the list of differentially expressed genes in a microarray experiment comparing wild type and PLZF knockout mice. Btbd11 was found to exhibit significantly decreased expression in the PLZF KO mice when compared to the wild type mice [Unpublished Data]. Due to the relatively restricted expression of PLZF in NKT cells, this interesting microarray data led us to question the possible role that Btbd11 plays in NKT cells. Upon consulting the literature, it became apparent that no previous work has focused on the specific role or function of Btbd11, in any biological system. This represents a significant challenge and opportunity to gather meaningful data on an unstudied protein.

Interestingly, the only article that mentions Btbd11, linked the protein to studies relevant to immune system and the NKT cell setting. Mass spectrometry data from the Bendelac laboratory, known for their extensive work in characterizing NKT cells and PLZF, listed various proteins that directly interact with PLZF. Significantly, Btbd11 was one of the named proteins listed as interacting with PLZF through the BTB protein-binding region as shown in Figure 15 [73].

Another tool we used to discover more information on Btbd11 was data from the Immunological Genome Project. This database is a collection of information gathered from immunology laboratories commissioned by the NIH in an effort to map gene regulatory pathways that govern immune system functionality by quantifying and collating microarray data from various experiments. The database allows users to search a gene/protein and display its gene expression profile within the various subsets of cells within the immune system. The relative expression levels of Btbd11 are markedly higher in NKT cell subsets than other cells within the $\alpha\beta$ T cell population, as shown in Figure 16. The data found on Btbd11 further enforced the likelihood that Btbd11 is interacting with PLZF in NKT cell populations. Even within the different subsets of NKT cells there is variation in Btbd11 expression, namely a higher level of expression in the spleen and liver versus thymus. Similarly, there is a unique expression profile of Btbd11 within $\gamma\delta$ T cells, shown in Figure 17. Peripheral $\gamma\delta$ T cells, such as those from the spleen, possess a significantly higher level of Btbd11 than thymic $\gamma\delta$ T cells.



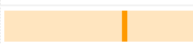
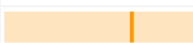
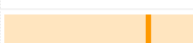


Feature key	Position(s)	Length	Description	Graphical view
Repeat ⁱ	608 – 637	30	ANK 1	
Repeat ⁱ	654 – 683	30	ANK 2	
Repeat ⁱ	692 – 721	30	ANK 3	
Repeat ⁱ	735 – 764	30	ANK 4	
Repeat ⁱ	830 – 859	30	ANK 5	
Domain ⁱ	928 – 994	67	BTB  PROSITE-ProRule annotation ▼	

Figure 14. Predicted conserved regions of the Btbd11 protein. The program from uniprot.org has the ability to predict the various conserved regions of an unstudied protein, such as Btbd11 in this case. By comparing the gene sequence of known proteins to the sequence of Btbd11, they predict that Btbd11 contains the BTB domain as well as 5 Ankyrin repeat features.

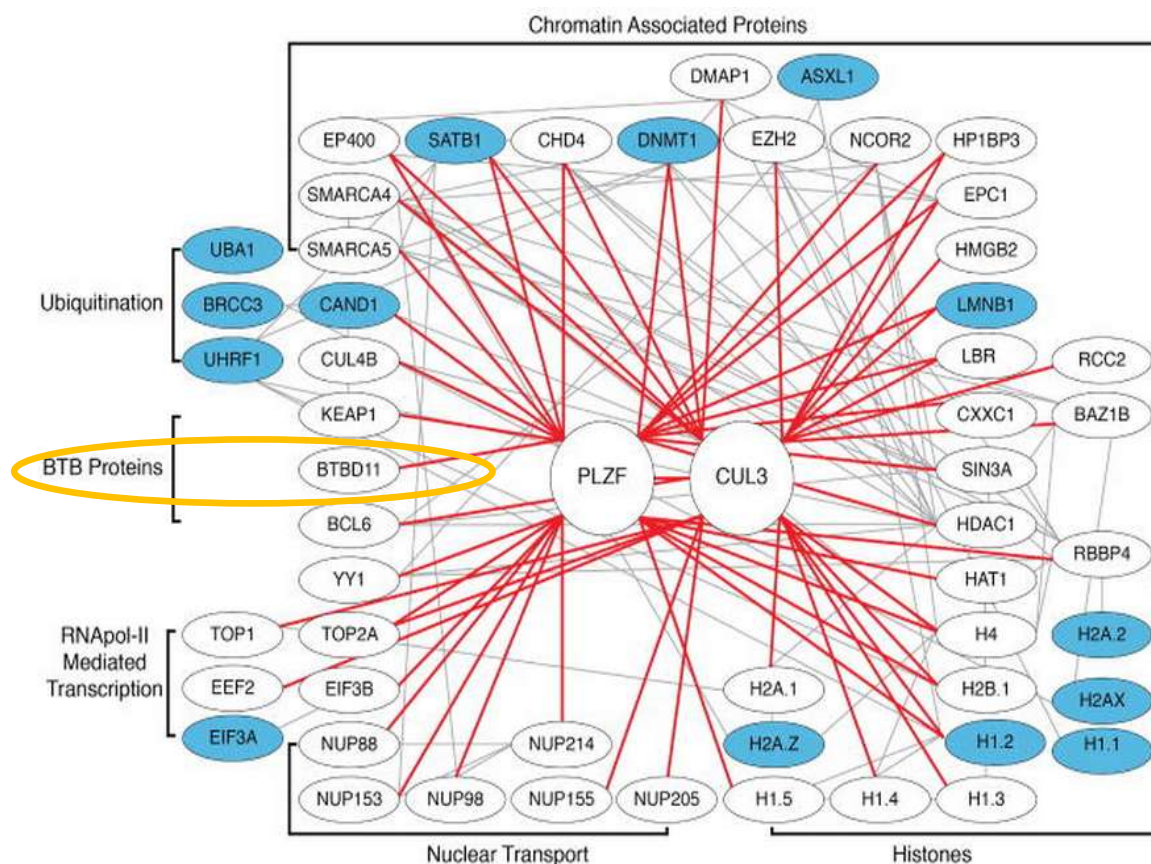


Figure 15. Btbd11 interacts with PLZF via Btb-interaction proteins. Data from the Bendelac laboratory defines Btbd11 as a protein that directly interacts with PLZF via its BTB conserved protein - protein interaction domain. PLZF was pulled down via immunohistochemistry and was then submitted to mass spectrometry analysis. The mass spectrometry was then able to pick up any proteins that directly bound and interacted with PLZF. Adapted from [73].

Reprinted by permission from Macmillan Publishers Ltd: [Nature Reviews Immunology] (73), copyright (2012).

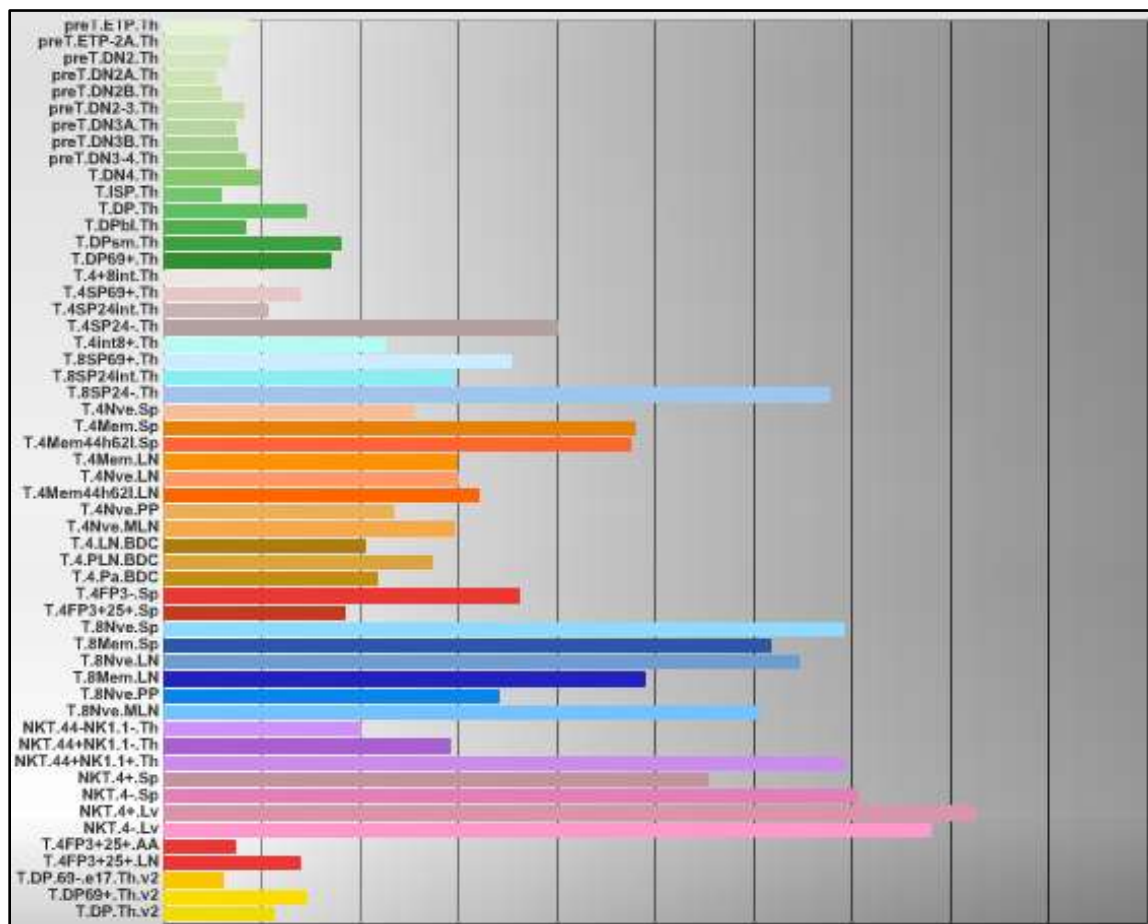


Figure 16. Btbd11 is expressed in all NKT cell subsets. Microarray data collected from various laboratories in collaboration with the ImmGen Project is collated to allow users to display the relative expression levels of a protein within various immune system subsets. This plot displays the expression of Btbd11 within $\alpha\beta$ T cells. There are significant and high levels of Btbd11 expression within NKT cells compared to other $\alpha\beta$ T cells, shown in the pink bar graphs.

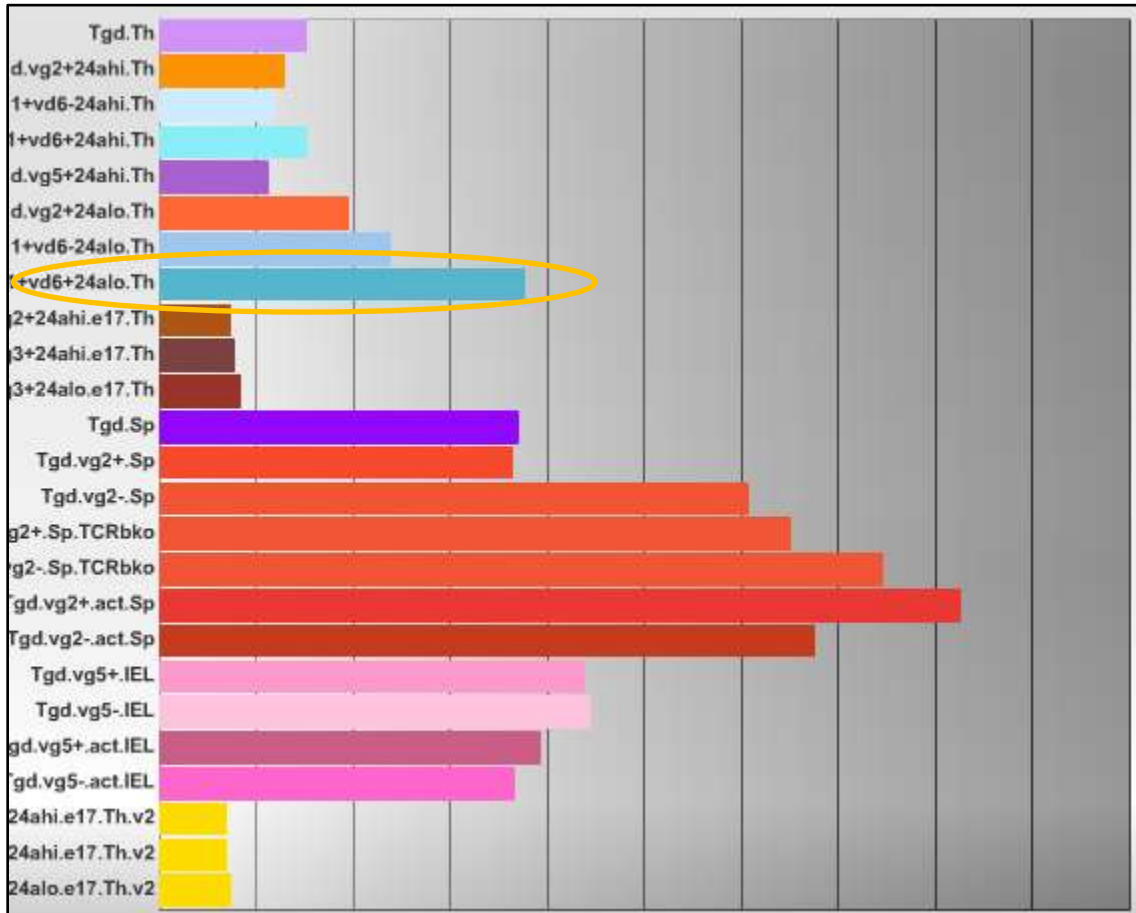


Figure 17. Btbd11 is expressed in certain subsets of $\gamma\delta$ T cells. Microarray data collected from various laboratories in collaboration with the ImmGen Project is collated to allow users to display the relative expression levels of a protein within various immune system subsets. This plot displays the expression of Btbd11 within $\gamma\delta$ T cells. There is significant and high levels of Btbd11 expression within various $\gamma\delta$ T cell subsets including thymic $V\gamma 1.1^+$, $V\delta 6.3^+$ $\gamma\delta$ T cells shown in the circled blue bar graph above.

Due to its reported expression in NKT cells, and interactions with PLZF, we hypothesize that Btbd11 may play a role in modulating the function of the transcription factor, PLZF. Through the BTB protein-binding domain, we further hypothesize that Btbd11 acts as a co-factor to PLZF and could play a role in controlling PLZF protein function within NKT cells. As PLZF is responsible for the effector function of NKT cells, it is not unreasonable to conclude that Btbd11 may support PLZF in the acquisition of NKT cell effector functionality. We also observe a loss of Btbd11 in the NKT cells of PLZF KO mice, mice whom have a severe loss in normally functioning NKT cells, evidencing the need of Btbd11 and PLZF in order to have proper NKT cell functionality. Often, transcription factors are responsible for upregulating expression of proteins that they directly complex with, an idea supported by the loss of Btbd11 expression in PLZF-KO mouse NKT cells. Significantly, transgenic expression of PLZF in all T cells does not fully induce a NKT cell- like phenotype and effector function in the transgenic T cells as summarized above. Finally, we hypothesize that transgenic overexpression of Btbd11 in all T cells, in conjunction with PLZF, may more effectively induce a NKT cell- like phenotype and effector function in the transgenic T cells.

In order to test this hypothesis, we will utilize two separate transgenic mouse lines with altered Btbd11 expression profile. The first mouse line exhibits transgenic expression of Btbd11 in all T cell subsets, known as hCD2-Btbd11 mice. This transgenic line was produced as part of my Master's Thesis research and it's creation and validation is extensively discussed below in the methods and results section. We bred these mice with transgenic expression of PLZF in all subsets in order to define the phenotype of T cells

with expression of both Btbd11 and PLZF. The second mouse line is a Btbd11 “Gene-Trap” (Btbd11 GT) mouse line purchased from EMMA at EUComm. This mouse has a neomycin selection cassette inserted between the fourth and fifth endogenous exons of the native copy of Btbd11. This inserted cassette serves as a “trap” exon due to its splice acceptor site and internal stop codon. This alternative splicing site induces preferential splicing from endogenous Btbd11 exon 4 to the inserted cassette exon so that when mRNA splicing occurs, there is a high likelihood that the native exons will splice to the transgene exon and produce a truncated and dysfunctional copy of the Btbd11 mRNA. The decrease in functional copies of Btbd11 mRNA result in decreased levels of translation and a significant “knock-down” of Btbd11 protein expression. A map of this transgene is illustrated below in Figure 18.

These two mouse models will be utilized to elucidate the role that Btbd11 plays in various immune system cell types, with particular emphasis on the innate-like lymphocytes introduced above.

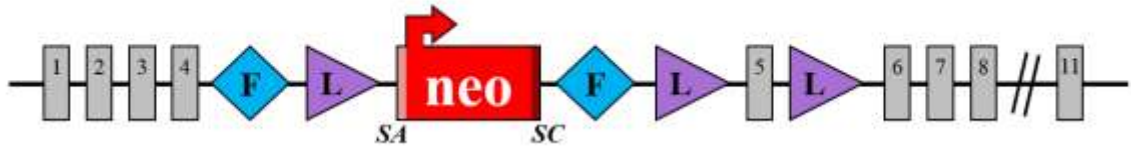


Figure 18. Graphic representation of the Btbd11 GT transgene configuration. adapted from Allele Map on IMPC.org. The endogenous codons are numbered and colored gray while the inserted neomycin selection cassette or “gene trap” exon appears in red. SA site preceding the gene trap represents the preferential splice acceptor site. The purple triangles represent the position of the loxP sites while the blue diamonds represent the flipase recombination sites. The gene trap exon includes a stop codon labeled as SC above and induces preferential splicing to Btbd11 exon 4 during mRNA splicing. This transgenic mRNA splice variant then is unable to translate into a fully functional Btbd11 protein, leading to the drastic lack of Btbd11 expression within the Btbd11 GT mice. Adapted from Allele Map on IMPC.org.

Materials and Methods

Mice

Murine models such as mice and rats are a staple in immunology labs. The ability to manipulate the genetic composition, breeding patterns, nutrition, and activity of these animals provides researchers with just about as many variables as they could possibly want. Extraordinarily, the human and mouse genome only differs by approximately 300 of their 23,000 genes [95]. This highly conserved number of genes between mice and humans enables researchers to use mouse models as in vivo studies of complex immunological systems and disorders with the hopes of applying their findings to future cures for the human condition [96].

The most commonly used mouse line in the lab setting is the C57BL/6 or B6 mouse. By only maintaining and using mice with this specific genetic background, researchers can induce and study specific genetic mutations and alterations to the mouse genome.

Comparing a mutated mouse on a B6 background mouse to a wild-type B6 mouse can illuminate any changes caused exclusively by the mutation. When studying systems as complex as the mammalian immune system it is vitally important to maintain as many aspects of the experiment as constant as possible. Each mouse line discussed in this paper is on the C57BL/6 or B6 background and each wild-type control mouse is a B6 mouse purchased from Jackson Laboratories.

All mice were housed in the Child Health Institute of New Jersey Vivarium. Here the mice were housed under tight temperature, light, and humidity control. Each cage provided up to 5 mice with sufficient food, water, and bedding. Veterinarians and veterinarian technicians provided care for mice in the case of illness or other conditions

as well as performing routine changes and cleaning of cages. All animal studies were performed in compliance with Internal Animal Care and Use Committee and the guidelines of the Federal Office of Laboratory Animal Welfare.

hCD2-Btbd11 Construct Design

Upon determining that we would like to investigate the interactions between Btbd11 and PLZF within T cell subsets, the next step was to design a transgene that will ectopically express Btbd11 in T cells. Btbd11 isoform 1 ORF cDNA clone was purchased from Origene Inc. and mouse hCD2 promoter vector was purified from an existing transgene construct previously created by Dr. Sant'Angelo's laboratory. The mouse hCD2 vector is composed of three main components, the 2.5 kb bacterial vector backbone, the 5 kb hCD2 promoter sequence, and the 5.5 kb hCD2 LCR or locus control region. The standard cloning vector pBluescript SK(-) allows for the expression and replication within bacterial strains. The hCD2 promoter and LCR are responsible for driving expression of the insert in hCD2 specific tissues. The promoter region is positioned at the beginning of the insert while the LCR follows the insert. Studies have shown that the promoter-insert-LCR configuration leads to stable expression of the transgene in the desired cell type proportional to the number of copies of the transgene [100]. Successful cloning of this vector will result in the creation of the hCD2-Btbd11 construct that will be microinjected to generate a transgenic mouse line.

Generation of hCD2-Btbd11 Construct

Insertion of the Btbd11 cDNA clone into the hCD2 promoter vector was accomplished using the In-Fusion® HD Cloning Kit (Clontech® Laboratories, Inc.). An overview of this process is illustrated below in Figure 19. This kit uses enzymatically controlled

homologous recombination between two pieces of DNA that share 22 complementary base pairs. In order to create the 22 complementary base pair overhangs, I designed PCR amplification primers that would amplify the Btbd11 cDNA while concurrently adding the 22 bases to each end of the cDNA. The primers were designed with 22 bases that will bind to the 5' and 3' end of the cDNA as well as 19 bases that are complementary to the sequence of the hCD2 promoter vector. Ensuring that the insert is oriented in the correct direction is vital, as we must have the start of the insert at the end of the hCD2 promoter sequence and the end of the insert at the very beginning of the hCD2 LCR sequence. The sequence of the primers, purchased from Integrated DNA Technologies, as well as the PCR amplification program are listed in Table 1. DNA PCR amplification was performed using 20 ng of Btbd11 cDNA, 10 μ l of Taq Polymerase Master Mix (Life Technologies Inc.), and 1 μ l each of the forward and reverse primers in a total volume of 20 μ l. Following DNA amplification of the Btbd11 cDNA with the additional overhang, I performed gel electrophoresis on a 1% agarose gel followed by Gel Extraction and Purification Kit (Qiagen). The concentration of the resulting PCR product was measured through absorbance measurements on the Nandrop1000 (Thermo Scientific).

Concurrently, the linearized hCD2 vector was prepared using a restriction enzyme digest consisting of the enzymes EcoRI and SalI that cut the vector DNA at the specific site that the insert is to be cloned into. Following the digestion, I purified the 13 kb linearized vector. The In-Fusion cloning reaction consisted of 200 ng of the PCR product, 100 ng of the linearized vector, and 2 μ l of 5X In-Fusion HD Enzyme Premix for a total of 10 μ l. The recombination reaction occurs during incubation for 15 minutes at 50 °C. Following this incubation, we needed to insert the recombined DNA into target bacterial cells.

TABLE 1

Primer Name	Primer Sequence (5' to 3')
hCD2_btbd11_Prom_FWD1	CACCATCACGCGATCGCCATGGCCAGG- AGAGGTAAGAAGCCTG
hCD2_btbd11_Prom_REV1	AACCTCGAGTGCGGGCCGCTCATACCAC- GGAACCCTTGAAG
PCR Extension Program <ul style="list-style-type: none"> • 94° C – 4 minutes • 35 cycles <ul style="list-style-type: none"> ○ 94° C – 30 seconds (Denaturation) ○ 60° C – 1 minute (Primer Annealing) ○ 72° C – 6 minutes (Extension) 	
Primers designed and used to add homologous arms to Btbd11 cDNA insert through the listed PCR extension program.	

TABLE 2

Primer Name	Primer Sequence (5' to 3')
hCD2_btbd11_REV1	ACAGAGACAAGTTGGAGGAG
hCD2_btbd11_FWD2	AGAGTCTCTTCCGGGACATC
hCD2_btbd11_FWD3	TTCAGGACCTACAGAGGACG
hCD2_btbd11_REV4	TCTGGATCTCGTACTTGGTGC
hCD2_btbd11_REV5	TACGATCTCCATGGCACTCTG
hCD2_btbd11_REV6	TCTGGATCTCGTACTTGGTGC
Primers designed and used to sequence the entire transgene.	

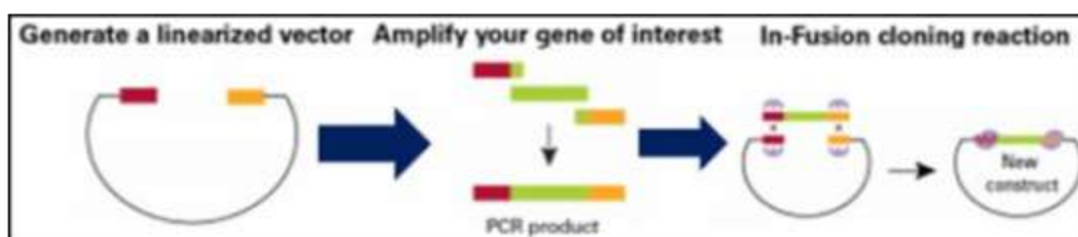


Figure 19. Adapted from Clontech® Laboratories, Inc. In-Fusion® HD Cloning Kit User Manual. PCR amplification is used to add homologous arms to the Btbd11 cDNA insert. These homologous arms are designed to be complementary to the two ends of the linearized vector. Then the In-Fusion reaction is performed which uses an enzyme-mediated process that combines the insert and linearized vector into a complete plasmid via interactions with the complementary homologous arms.

I performed a chemical DNA transformation process that consisted of adding the In-Fusion cloning reaction to 100 µl of Subcloning Efficiency™ DH5α™ E. coli Competent Cells (Life Technologies Inc.), followed by 30 minutes on ice, a 30 second heat shock at 42 °C, incubation on ice for 2 minutes, addition of 300 µl of LB outgrowth media, and incubate/shake at 37 °C for 1 hour.

At this point the bacteria cells are transformed and ready to be plated on ampicillin-resistant agar plates. Plating on ampicillin-resistant agar leads to bacterial colonies that were successfully transformed with an ampicillin-resistant sequence, specifically the sequence contained within the pBluescript SK(-) vector portion of the hCD2 vector. The agar plates are then incubated overnight at 37 °C.

Bacterial colonies from the In-Fusion cloning reaction are picked the following morning and placed into 5 ml of ampicillin LB media. Then after 12 hours of incubating and shaking at 37 °C, I analyzed whether or not the bacteria had taken up the In-Fusion product. This was executed by first extracting the plasmid DNA from the bacteria through the QIAprep® Spin Miniprep Kit (Qiagen). Then the resulting plasmid DNA is screened for the intended hCD2-btbd11 construct using a restriction enzyme digest of EcoRI and SmaI.

Following this first round of screening of the plasmid products from the In-Fusion reaction, I confirmed that the product was correct by sending sample out for sequencing by Genewiz Inc. DNA Sequencing Services. Sequencing of the insert and its location within the hCD2 vector is vital due to the high rates of spontaneous mutagenesis that occur during the initial PCR amplification and the In-Fusion cloning reaction. Mutations such as an insertion, deletion, substitution, frameshift, or nonsense mutations would

compromise the ability of the hCD2-btbd11 transgene to be effectively expressed as a functional protein. In order to fully sequence the insert, I designed primers listed in Table 2. Using the alignment feature of the ApE Plasmid Editor I analyzed the results of the sequencing. Upon confirming that the Btbd11 cDNA had been successfully inserted into the correct site of the hCD2 vector we proceeded to the next step of producing the transgene.

In order to prepare the final transgene for microinjection into the mouse embryos, there a few remaining, vital steps. I needed to cleave the pBluescript SK(-) portion of the vector and linearize the remaining portion of the transgene. The pBluescript SK(-) portion of the vector was vital for the plasmid to be able to grow and replicate within the bacterial cells but would lead to considerable complications if injected into the mouse embryos.

Cleavage of this portion of vector was accomplished with a restriction enzyme digest with NotI and SalI. This digestion would lead to the generation of two DNA fragments, the unwanted pBluescript SK(-) portion of the vector and the desired linearized transgene. Linearization of the transgene is imperative for the successful integration of the transgene into the genome of the mouse embryos. Linearized DNA is far more likely to be successfully integrated within the target genome versus plasmid or circular DNA. Mammalian cells preferentially destroy plasmid DNA found within the cell through endonucleases as part of the anti-bacterial surveillance of the cell [101].

Microinjection of hCD2-Btbd11 Construct

DNA microinjection was performed by the Shared Transgenic/Knock-out Mouse Core Services (TG/KO), of the Cancer Institute of New Jersey and the Child Health Institute of New Jersey. Linearized and purified DNA was delivered to the TG/KO members. Their

method of pronuclear injection strives to successfully integrate one or more copies of the transgene within the zygote genome while preserving the viability. The microinjection was performed on C57BL/6 fertilized zygotes which is the “wild-type” mouse used within our laboratory. After pronuclear microinjection, the injected zygotes underwent oviduct transfer into a foster C57BL/6 female mouse and brought to term. Following birth of the injected mice, we performed targeted PCR to test for the presence of the transgene. By designing primers to amplify a portion of the transgene that spans the hCD2 promotor and beginning of the Btbd11 cDNA we can distinguish between the presence of the transgenic copy of Btbd11 versus the endogenous copy of Btbd11. The primers used are the previously listed “hCD2_btbd11_Prom_FWD1” and “hCD2_btbd11_REV4” from Table 1 and 2 respectively. Genotyping through PCR with this primer pair generates a product size of 432 base pairs. From 40 injected mice living to adolescence, two mice tested positive for at least one copy of the transgene. These two founder mice were both female and were separately expanded into two distinct lines of transgenic mice. These two hCD2-btbd11 lines were eventually crossed to previously generated lck-PLZF mice to create the desired double transgenic mice.

Btbd11 Gene Trap Mice

The mouse line Btbd11[tm1a(EUCOMM)Wtsi] was purchase from the European Mouse Mutant Archive (EMMA) in conjunction with the European Conditional Mouse Mutagenesis Program (EUCOMM), members of the International Knockout Mouse Consortium (IKMC). This mouse line was created on a C57BL/6 background using the EPD0463_1_A11 embryonic stem cell line containing the transgenic copy of Btbd11 and will be referred to as Btbd11 Gene Trap or Btbd11 GT mice throughout this report. The

transgene map for this mouse is illustrated and explained above in the introduction Figure 18. These mice were designed with the option to be crossed to mice expressing Cre-recombinase in order to completely remove exon 5 of the *Btbd11* gene, leading to complete elimination of the *Btbd11* transcript and protein expression. This extra step was not necessary for our experiments as mice homozygous for the *Btbd11* GT allele exhibited an almost complete loss of *Btbd11* mRNA transcript. All of the *Btbd11* GT mice used were homozygous for the transgenic *Btbd11* GT allele as confirmed by genotyping and controlled breeding of homozygous mice to homozygous mice.

Mouse Tissue Preparation

For each flow cytometry experiment, mice were euthanized and sacrificed via CO₂ asphyxiation followed by confirmation via toe pinch and lack of respiration. Approved surgical procedures were performed to remove necessary tissues. All live cell centrifugation was performed on temperature controlled centrifuges set at 4°C and 1500 RPM for 3 minutes. Following homogenization of the tissue into single cell suspension, Red Blood Cell Lysis Buffer (Sigma) was used to remove red blood cells from the sample. Centrifuge-assisted filtration (40 µm BD Falcon Cell Strainer) was then performed to remove non-cellular components of the sample such as cell debris and extracellular matrix components. Special procedures were used to ensure viable lymphocyte isolation from liver samples. This process utilized the reagent Purcoll (BD Falcon) at a 33% concentration to perform a differential density centrifugation that separates the fatty cellular debris from the white blood cell sample. Samples were manually counted via microscopy and a hemocytometer. Trypan blue was used to dilute and dye a small portion of the sample. Live cells are those cells not permeated by the

Trypan blue dye and were counted within various grids within the hemocytometer to determine the concentration of the sample. This concentration is used to determine optimal volumes of antibody staining. Prior to extracellular antibody staining, the sample is incubated in blocking buffer consisting of normal mouse serum (1:200 dilution) Fc-receptor blocking antibody (1:1000 dilution), and unlabeled streptavidin (1:500 dilution) at 4°C for at least 20 minutes.

Fluorescently-Labeled Antibody Staining

Tissue samples are fluorescently labeled in order to determine the different cell types within a tissue or to determine protein expression within individual cells. Cells are fluorescently labeled through monoclonal antibodies (mAb) conjugated to fluorophores. Monoclonal antibodies are antibodies secreted by homogeneous cultures of B cells that are mono-specific to the epitopes of a cellular component. Fluorophores are chemical compounds that are excited by specific wavelengths of light to emit light at a different specific wavelength. While a sample can be stained with many conjugated antibodies, it is important to ensure that each fluorophore used does not overlap in its excitation wavelength and in its emission wavelength.

The following antibody conjugates were purchased from eBioscience (San Diego, Ca): anti-CD3 ϵ (145-2C11), anti-CD4 (L3T4), anti-CD8 (53-6.7), anti-CD44 (IM7), anti-CD25 (PC61.5), anti-NK1.1 (PK136), anti-IFN- γ (XMG1.2), anti-IL-4 (BVD6-24G2), anti-GATA-3 (TWAJ), and anti-ROR γ t (AFKJS-9). The following antibody conjugates were purchased from BD Biosciences (San Jose, CA): anti-CD3 ϵ (500A2), anti- $\gamma\delta$ TCR (GL3), anti-V δ 6.3 TCR (8F4H7B7), anti-CD4 (RM4-5, H129.19), anti-CD8 α (53-6.7), anti-CD8 α (53-5.8), anti-NK1.1 (PK136), and anti-CD69 (H1.2F3).

The following mAb conjugates were purchased from Biolegend (San Diego, CA): anti-V γ 1.1 TCR (2.11), anti-CD24 (M1/69), anti-IL-17a (TC11-18H10.1), anti-T-bet (4B10). In certain instances there was a need to use biotin labeled antibodies and then perform a secondary anti-biotin labeling using the following reagents: streptavidin-PeCy7 (BD Biosciences), -FITC (BD Biosciences), -PE (eBioscience), -APC-eFluor780 (eBioscience), and -Qdot625 (A10196, Invitrogen). In all experiments requiring staining of NKT cells, CD1d:PBS57 CD1d tetramer was used. This tetramer of CD1d molecules is loaded with the CD1d ligand, alpha-Galactosyl Ceramide (α -GalCer), labeled with fluorophores for detection, and were obtained from the National Institutes of Health Tetramer Core Facility. The mouse anti-human PLZF (Mags-21F7) and anti-MHCII (212.A1) were generated by the Monoclonal Antibody Core Facility at MSKCC. Tetramer staining was performed separately from the rest of the antibody cocktail for 30 minutes at room-temperature to allow for non-competitive binding and labeling of NKT cells. Following one wash of the samples with Phosphate-Buffered Saline (PBS) and 10% Fetal Bovine Serum (FBS), the cells are stained with the remaining antibody cocktail for 30 minutes at 4°C. The cells are then washed and either proceed to intracellular staining or dead cell exclusion by the DNA-intercalating dye, DAPI before analysis by flow cytometry.

For experiments including intracellular staining, the Cytofix/Cytoperm kit (BD Biosciences) was used to stain intracellular components such as cytokine production and the FOXP3 kit (eBioscience) was used for intranuclear staining of transcription factors. These kits serve to permeabilize the cell to allow antibodies to enter the cell and fixate the cells to arrest cellular mechanisms and “freeze” the location of cellular components.

Cells that have undergone fixation are spun at 4 °C and 2700 RPM for 3 minutes. All samples are washed at least three times before final re-suspension and analysis by flow cytometry.

Flow Cytometry

Flow cytometry is a highly utilized tool in immunological studies due to its ability to define the many different types of cells present in any given tissue based on its physical properties and fluorescently labeled cellular components following fluorescent labeling with mAb conjugates. All flow cytometry experiments were performed with the LSR II Cytometer (BD Biosciences) housed within the Sant'Angelo Laboratory. The cytometer uses fluid flow to focus the input cell sample into a single-cell stream in a process known as hydrodynamic focusing. This single-cell stream is then exposed to laser light sources while detectors and sensors convert the resulting scattered light into information such as the relative size, shape, internal complexity, and fluorescent intensity of each individual cell within the sample.

Sensors and filters positioned around the cell measure the intensity and wavelength of the light that scatters off of the cell as it passes through the laser light source. The cytometer then uses various algorithms to convert the measured scattered light into a relative quantification of intensity. Each cell/particle measured is known as an event. The various parameters of an event can be used to group cells into their individual subpopulations for further classification and study.

Cell size and shape is measured as the light that scatters around the external surface of the cell and is known as the forward-scattered light or FSC. Conversely, side-scattered light or SSC is the light that reflects off of internal components of the cell. SSC measures the

cellular complexity and wavelengths of light emitted from mAb conjugates bound to cellular components.

Following the sample information acquisition by the flow cytometer, the data is exported and loaded into an analysis program, FloJo v.10 (Tree Star). This program is used to display the information recorded by the cytometer in a visually meaningful fashion. Using two axes, the events are graphically displayed. Each axis can be set to show the intensity of each event as measured by each of the sensors detecting fluorescence from the mAb conjugates. For example, a graph of FSC-height versus FSC-width would show us the sizes of the events collected within our experimental sample. Importantly, the fluorescent intensity measures coming from each of the fluorophore colors used in the experiment are displayed on a logarithmic scale axis. Different combinations of axes can be used to define subpopulations within the sample. It is possible to “gate” upon a portion of the graph that allows the user to further investigate just the group of events being “gated” upon.

For each experiment performed, initial analysis consisted of the same steps. For extracellular staining experiments, exclusion of DAPI positive events eliminates dead cells from the analysis. FSC-height versus SSC-height is used to gate on the events that are cell granularity and size indicative of a lymphocyte. Then we can exclude cell doublets and aggregations by comparing SSC-width versus SSC-height and then FSC-width versus FSC-height. In order to finally gate upon T-cell lymphocytes we gate on MHC-II negative cells, which excludes antigen presenting cells such as B cells, macrophages, and dendritic cells. Within the T-cell population we can further divide into subpopulations such as CD4 versus CD8 to determine if the T-cell is a helper T cell or a

cytotoxic T cell respectively. Similarly, within the T-cell population, we can plot CD3 versus CD1d-tetramer to gate upon NKT cells. Lastly, once each population of interest is gated upon, we can use the histogram function to look at the levels of fluorescent intensity of a single parameter. By calculating the mean fluorescent intensity of a histogram plot, we can compare the relative levels of expression in each sample. This is often used to compare the expression of a transcription factor between various cell types or tissues.

***In-Vitro* T Cell Stimulation**

Certain experiments were designed to study how various T-cell populations behaved in an activated state. One method of studying stimulated T-cell is through the in vitro dosing of PMA (phorbol 12-myristate 13-acetate) and ionomycin followed by Brefeldin A [102]. Tissues are removed and homogenized into a single-cell suspension. The stimulation was performed on various lymphoid tissues, namely the spleen and liver. RBC lysis buffer is used to remove red blood cells from the sample and the cells are filtered. The cells are plated in tissue culture plates with complete media at the normal seeding density. PMA and ionomycin are added to the sample wells at a concentration of 100 ng/ml and 50 ng/ml respectively. The cells are then incubated at 37 °C for 5 hours. After 1 hour of activation, Brefeldin A (eBioscience) was added at a concentration of 3 µg/ml. The cultures are mixed and suspended every hour to prevent adhesion to the plate. Once the activation is completed the samples are spun at 4 °C and 1500 RPM for 3 minutes. Following a washing of the cells, the samples are stained for extracellular markers as well as intracellular production of cytokines including IL-4, IFN- γ , IL-17a, GM-CSF, and IL-2 using the Cytofix/Cytoperm kit (BD Biosciences) to permeabilize and fixate the cells.

Concanavalin A Injection and ALT Assay

In order to study the role that *Btbd11* and PLZF play in the experimental mouse livers, an ALT Assay was performed to measure and quantify the levels of liver damage following systemic immune system activation through ConA injection. The assay was performed on serum purified from the experimental mouse blood samples. Serum purification consists of letting whole blood coagulate at room temperature for 15 minutes, spinning the sample at 2,000 x g for 15 minutes, and then removing the clear serum supernatant. Baseline serum was extracted at least 12 hours prior to ConA (Sigma) dosage via intraocular bleedings. ConA was dosed to mice via intraocular injection at a concentration of 15 µg per gram of mouse weight. Experimental mice had subsequent serum extractions at 6 hours and 24 hours following the ConA injection. Mice were sacrificed at the 24 hour time point and tissues were removed for analysis by flow cytometry.

The ALT assay was performed using the BioVision Alanine Aminotransferase (ALT or SGPT) Activity Colorimetric/Fluorometric Assay Kit following the provided protocol for the colorimetric assay. I performed the assay using the QuantStudio SpectraMax i3 spectrophotometer at the Child Health Institute of New Jersey. Samples included serum extracted from experimental and wild type mice at each of the three time points, pre-activation, 6 hours post activation, and 24 hours post activation. Technical duplicates of each sample were included in the assay to ensure consistent measurements by the spectrophotometer. The spectrophotometer was set up to perform a kinetic assay to measure the OD 570nm absorbance every 15 minutes for a total of two hours set at 37°C incubation.

The clear flat bottomed 96-well plate was prepared with one column of the pyruvate standard spanning from 0 nM to 10 nM in increments of 2 nM. Then 20 µl of serum per sample and their duplicates were added to the plate. Next the reaction mix was prepared: 86 µl of ALT Assay Buffer, 2 µl of OxiRed Probe, 2 µl of ALT Enzyme Mix, and 10 µl of ALT Substrate for each well of samples and standards. After addition of the reaction mix, the plate is placed into the spectrophotometer, incubated at 37 °C, and the assay begins. The first reading of OD 570 nm (A1) was taken at 15-30 minutes after incubation at time (T1). The following read (A2) was read later at time (T2) after 60 minutes of incubation.

After exporting the data, I plotted the OD 570 nm for each of the pyruvate standard samples at time, T1 to generate the Pyruvate Standard Curve. The line fitted to the Pyruvate Standard Curve was later used to relate the amount of pyruvate generated to the corresponding OD 570 nm fluorescence generated. The ΔA_{570} nm was calculated for each experimental sample as the difference between the reading A2 and A1. The corresponding nM value on the Pyruvate Standard Curve for each ΔA_{570} nm value equaled the value B. This B value was then calculated for each sample within the experiment. In order to calculate the final ALT Activity in nM/min/ml, I used the equation:

$$\frac{B}{(T2 - T1) * V} = \text{ALT Activity (nmol/min/ml)}$$

Where T2 and T1 are the second and first times of reading and where V is the original volume within the sample well before the addition of the reaction mix, 20 µl.

RNA Extraction and Reverse Transcription

In order to see if a certain gene was successfully expressed as a protein within cells and tissues, I performed RNA extraction followed by reverse transcription into a cDNA library that I could then screen for the presence of a gene/protein. This method was used to confirm the overexpression of Btbd11 in the hCD2-Btbd11 mouse line as well as measure quantitative levels of Btbd11 and PLZF expression in experimental mice.

After removal of the desired tissues from experimental and wild type mice, the sample was homogenized into a single-cell suspension with 1 mL TRIzol Reagent (Life Technologies) per 50–100 mg of tissue sample. Then I added 0.2 ml of chloroform per 1 ml of the volume of the homogenized tissue and mixed well. Following 3 minutes at room temperature, dark, I centrifuged the samples at $12,000 \times g$ for 15 minutes at 4°C . This spin separated the clear aqueous phase containing RNA from the DNA and protein/cellular debris. The next step was to precipitate the RNA using 0.5 volumes of 100% isopropanol, incubate at room temperature for 10 minutes, and then spin the samples at $12,000 \times g$ for 10 minutes at 4°C . Then I washed the RNA pellet with equal parts of 75% ethanol and centrifuges each sample at $7500 \times g$ for 5 minutes at 4°C . Lastly, I resuspended the air-dried RNA pellet in 30 μl of RNAase-free water and measured its purity and concentration using the absorbance measurement via the Nanodrop1000 (Thermo Scientific).

Reverse transcription was performed using the GoScript Reverse Transcription System (Promega) following the provided protocol. The first step is to anneal Oligo primers to 1 μg of sample RNA at 70°C for 5 minutes using a PCR thermocycler. Then the samples were placed on ice and the remaining reaction mix is added: 4.0 μl of GoScript™ 5X

Reaction Buffer, 3 µl of MgCl₂, 1 µl of PCR Nucleotide Mix, 0.2 µl of Recombinant RNasin® Ribonuclease Inhibitor, 1 µl of GoScript™ Reverse Transcriptase, and 3 µl of Nuclease-Free Water. Then the sample was placed back on the thermocycler at 25°C for 5 minutes, then 42°C for 1 hour, and lastly 70°C for 15 minutes. From the final sample reaction cDNA library, I performed PCR using primers for the Btbd11 and PLZF gene. Importantly, I designed these primers to span multiple exons in order to eliminate any amplification of genomic DNA and only amplification of cDNA derived from transcribed mRNA within the sample. The PCR primers and programs are listed in Table 3.

Quantitative, Real-Time Polymerase Chain Reaction (qRT-PCR)

Quantitative RT-PCR is as the name suggests, a method by which we can quantitatively measure the amount of DNA being amplified during a PCR, in real time. This is accomplished through the acquisition and measurement of a fluorescent dye, SYBR Green, which only fluoresces as it is being incorporated into an actively amplifying portion of double-stranded DNA. The amount of fluorescent produced by this fluorescent agent, which excites at 497 nm wavelength and emits at 520 nm wavelength, is thus proportional to the amount of amplification and relative expression of the gene of interest within the sample. The reaction of each of the samples within my experiments were as follows: 10 µl PowerUp SYBR Green Master Mix, 1.6 µl of the forward primer, 1.6 µl of the reverse primer, 1 µl of the input cDNA, and 5.8 µl of dH₂O. The primers used are listed in Table 3. The PCR program used consists of the same normal steps of a conventional PCR, but at significantly shorter time intervals due to the increased accuracy and power of the QuantStudio 6 Flex instrument used (Applied Biosystems by Life Technologies Inc.). Also, the qRT-PCR reagents used, PowerUp SYBR Green

Master Mix (Life Technologies Inc.), provide a highly optimized PCR program. The program used for my experiments are as follows:

- 1) Hold Stage
 - a. 50°C for 2 minutes
 - b. 95°C for 2 minutes
- 2) 40 Amplification Cycles
 - a. Denaturation at 95°C for 1 second
 - b. Annealing and Extension at 60°C for 30 seconds

Following the completion of the qRT-PCR program, the built in program within the instrument displays the amplification curves of each sample within the experiment. The image below shows an example of these sample amplification curves.

TABLE 3

Primer Name	Primer Sequence (5' to 3')	Product Size
PLZF_F	AATGCATTTACTGGCTCATTCA	95 base pairs
PLZF_R	CAGGGCATCCTCCTTTGAG	
GAPDH_F	TTCTGGTGCTTGTCTCACTGA	121 base pairs
GAPDH_R	CAGTATGTTTCGGCTTCCCATTTC	
Btbd11_F	GCTGGCGTGTTCTGAGATG	145 base pairs
Btbd11_R	CACTGTGAAAGTCGTCCTTGAG	

Primer pairs used to shown mRNA transcript of the three genes above. These primers were also used for the qRT-PCR experiment described above. The GAPDH primers serve to amplify the housekeeping gene while the PLZF and Btbd11 primers will amplify our experimental genes of interest. Additionally, the Btbd11_F and Btbd11_R were used to determine the loss of Btbd11 transcript in the Btbd11 GT mice.

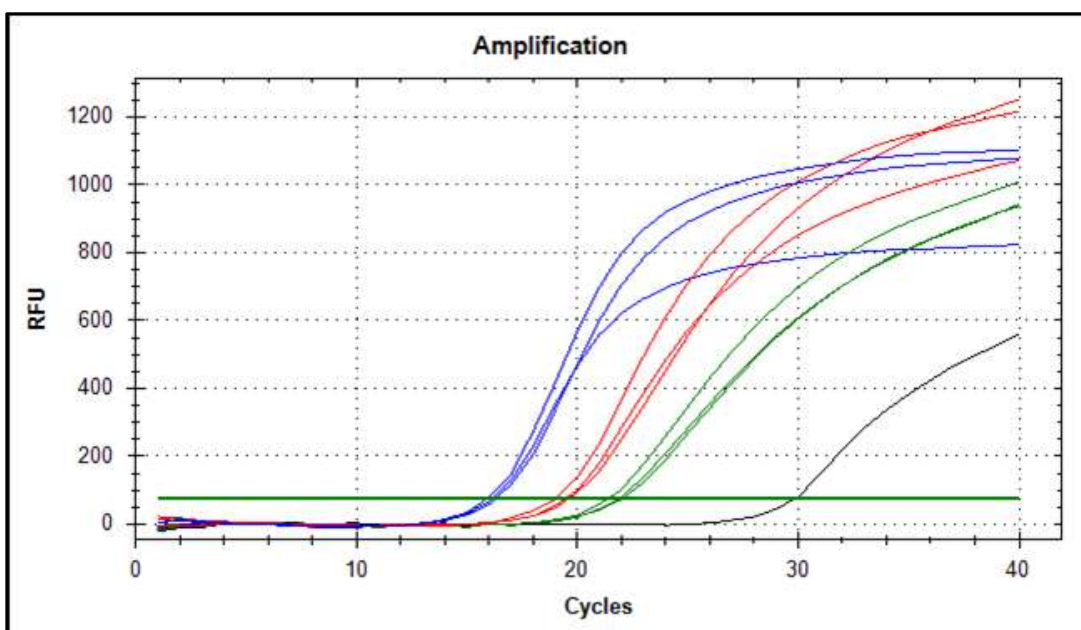


Figure 20. Sample qRT-PCR amplification plot with threshold value. RFU or relative fluorescent units are in the y-axis and represent the fluorescence of the probes generated by their inclusion within the amplifying DNA. The number of PCR amplification cycles is on the x-axis. The similarly colored curves represent technical replicates of the same sample. The horizontal green line is an arbitrary value chosen by the instrument, within the linear phase of amplification of each sample, is known as the threshold value and is used to define the Ct of each sample.

As seen in Figure 20, the various samples, grouped by color, are all amplifying at around the same rates. These repeated colors represent technical replicates of the same sample, which will be used to validate the experiment. The curves represent the amount of fluorescence produced by each sample (y-axis) during each cycle of the reaction (x-axis). The green horizontal line drawn on the plot represents the threshold value. This threshold value is defined as the threshold fluorescence, and is an arbitrary value chosen at a fluorescent value within the linear phase of all of the experimental amplification plots. Once this threshold value is chosen, the machine measures the number of cycles at which each sample took to reach the threshold value. This number of cycles is known as the cycle threshold or Ct value of each sample. Somewhat non-intuitively, the lower Ct values correspond to higher levels of gene expression measured within each sample because those sample are actually amplifying at earlier cycles. Following the definition of the Ct value for each sample, we can begin to compare the levels of gene expression between each sample.

Importantly, a housekeeping gene was also measured for each sample. This housekeeping gene, GAPDH, is used a normalizing measure because we assume that the expression of this housekeeping gene is expressed at similar levels within each sample of the experiment. For each sample the ΔCt value is defined at the Ct value of the experimental gene (Btbd11 or PLZF) sample minus the Ct value of the GAPDH gene for the same input sample. This ΔCt value was then normalized to the wild type sample of the experimental gene within each sample group. This was performed by subtracting the ΔCt value of the experimental gene of the wild type sample from the ΔCt value of the same experimental gene of the other experimental samples. This value is known as the $\Delta\text{-}\Delta\text{Ct}$

value. Lastly, the $\Delta\Delta$ Ct value of each experimental sample is used to calculate the fold-change over wild-type control, defined as $2^{(-1 \times [\Delta\Delta Ct])}$. This measurement allows us to compare the change in expression of each experimental gene (Btbd11 or PLZF) between the wild type and experimental mice (hCD2-Btbd11, lck-PLZF, dTG, and Btbd11 GT). Each of these calculations was performed in Microsoft Excel following exportation of the data from the qRT-PCR instrument.

Results

Generation of hCD2-Btbd11 Transgene

In order to study the role that Btbd11 plays in various T cell subsets as it interacts with PLZF, we created a transgenic mouse line with the ectopic overexpression of Btbd11 in all T cells through the hCD2 promoter. The vector design of the transgene is shown below in Figure 21. As illustrated, the transgene consists of four major components; the Btbd11 cDNA sequence, the hCD2 promotor sequence, the LCR promotor sequence, and the pBluescript SK(-) cloning vector backbone. Cloning the Btbd11 cDNA sequence into the hCD2 promotor vector was accomplished using the In-Fusion® HD Cloning Kit. Through high-fidelity PCR amplification and extension, complementary overhangs were added to the 5' and 3' ends of the Btbd11 cDNA. These overhangs were 22 bases long and complementary to the 3' and 5' end of the intended insert site within the linearized hCD2 vector backbone. The PCR product shown in lane 1 of the gel image in panel A of Figure 22 was excised from the agarose gel and purified. By comparing the size of the PCR product following the extension to the original Btbd11 cDNA sample, we can visually confirm that the extra base pairs had been added via the PCR extension as evidenced by the higher position of the PCR product in lane 1 of the gel.

The purified PCR product was then used along with the linearized hCD2 vector backbone in the In-Fusion® HD Cloning Kit. This kit used temperature activated recombinase enzymes to “flip” the Btbd11 cDNA insert into the hCD2 vector backbone via the interactions between the complementary overhangs and the backbone nucleotides. Following the In-Fusion® process, the resulting recombined DNA plasmid was transformed into competent bacterial cells. Various colonies of the competent bacterial cells were then screened via Miniprep and restriction enzyme digest. A restriction enzyme digest of EcoRI and SmaI should yield DNA fragments of size 13 kb, 2 kb, and 1 kb for samples that had undergone the In-Fusion® process successfully. Panel B of Figure 22 shows various samples resulting from an In-Fusion® reaction. Lane 2 shows successful insertion of the Btbd11 cDNA into the hCD2 vector backbone while lanes 1, 3, 4, and 5 do not.

The plasmid DNA sample with the correct restriction enzyme digest pattern was then sequenced to confirm the exact site of the insert as well as to check for point mutations that may have occurred during PCR amplification. Following confirmation that the sequence was correct, the transgene DNA was digested with NotI and SalI to remove the pBluescript SK(-) cloning vector backbone. Panel A of Figure 23 shows the digestion and separation of the 13.8 kb sized transgene construct and the 2.5 kb sized pBluescript SK(-) cloning vector backbone. The 13.8 kb transgene construct was then excised and purified from the gel and submitted to the Shared Transgenic/Knock-out Mouse Core Services (TG/KO) of the Cancer Institute of New Jersey and the Child Health Institute of New Jersey. Panel B of Figure 23 shows the final, purified transgene that was microinjected into the B6 oocytes.

Confirmation of hCD2-Btbd11 Transgene Expression

Following microinjection and maturation, mouse pups received from the Shared Transgenic/Knock-out Mouse Core Services (TG/KO) were screened or “genotyped” for the presence of the hCD2-Btbd11 transgene. Using primers specific for the overlapping region between the hCD2 promoter and the 3’ end of the Btbd11 cDNA, PCR was used to amplify the transgenic copy of Btbd11 while not amplifying the endogenous, non-transgenic, copy of Btbd11. Out of 40 pups that matured following microinjection, two female mice tested positive for the hCD2-btbd11 transgene, founders #18 and #30. Figure 24 shows PCR genotyping results for the two founder pups that were positive for the hCD2-Btbd11 construct. These two founder mice were bred independently of each other and gave rise to two separate mouse lines defined as line 1 and line 2 respectively.

Unfortunately, there does not yet exist an antibody that can be used to illustrate the forced overexpression of Btbd11 protein in the transgenic mice versus the wild-type control via flow cytometry. In order to circumvent this issue, we quantitatively evaluated the transcription levels of Btbd11 in the hCD2-Btbd11 transgenic mice versus wild-type mice in order to confirm that there are transgenic copies of Btbd11 capable of inducing higher levels of Btbd11 mRNA transcription through quantitative real-time PCR.

In order to perform qRT-PCR, RNA was extracted from the thymus, spleen, and liver of hCD2-btbd11 and wild type mouse. Reverse-transcription was then performed in-order to generate cDNA for each sample. PCR was performed on the cDNA samples utilizing primers defined in Table 3 of the methods section. As previously mentioned, these primers span multiple exons and the RNA sample are screened for the presence of genomic DNA contamination to ensure that the PCR is exclusively amplifying Btbd11

transcript. qRT-PCR allows us to quantitate the expression levels of a gene of interest by measuring the fluorescent signal generated during each PCR cycle as the product is amplified. By normalizing the expression of *Btbd11* to the expression level of a housekeeping gene, *GAPDH*, we can quantify the differences in expression of *Btbd11* and *PLZF* within each experimental sample. In panels A, B, and C of Figure 25 below we see the fold change of *Btbd11* expression in the hCD2-*Btbd11* mice compared to wild-type mice, within each tissue. A 5-8 fold increase in *Btbd11* expression in the hCD2-*Btbd11* transgenic mice confirms the successful ectopic overexpression of *Btbd11* through the hCD2 promotor in primary immune tissues.

Confirmation of *Btbd11* Gene-Trap (*Btbd11* GT) Transgene Expression

The *Btbd11* Gene-Trap (*Btbd11* GT) mice purchased were confirmed to have knocked down levels of *Btbd11* transcript. The *Btbd11* Gene-Trap mice possess a transgene, inserted within the endogenous copy of *Btbd11*, which induces preferential mRNA splicing to the splice acceptor site of a “gene trap” exon with a premature stop codon. This alternatively spliced mRNA is then most likely unstable and unable to translate into a functional *Btbd11* protein. Significantly, the splice acceptor site of the gene trap exon does not work 100% of the time; generally resulting in most but not all of the *Btbd11* mRNA transcripts in the *Btbd11* Gene-Trap mice becoming non-functional and unable to translate. Through RNA extraction, reverse-transcription to cDNA, and PCR with exon-spanning *Btbd11* primers, we show the knocked-down levels of *Btbd11* in the *Btbd11* GT versus wild-type mice in Figure 26. As seen in the figure, there is almost no *Btbd11* transcript in the *Btbd11* GT spleen sample versus the abundant expression of *Btbd11* in

the wild type spleen sample. Included are reverse-transcriptase negative controls to confirm that there was no genomic DNA contamination.

Btbd11 and PLZF are Differentially Expressed between lck-PLZF and dTG Mice

Expansion of the experimental mouse colonies led to the generation of mice expressing the Btbd11 transgene alone (hCD2-Btbd11 mice), mice expressing the PLZF transgene alone (lck-PLZF mice), mice expressing both the Btbd11 and PLZF transgenes (double-transgenic or dTG mice), mice expressing reduced levels of Btbd11 (Btbd11 GT mice) and mice expressing neither of the transgenes (wild-type control mice). In order to study the interactions between Btbd11 and PLZF, and the ramifications of augmenting their expression levels, we first quantified the expression of Btbd11 and PLZF within the experimental mice through qRT-PCR.

Before performing qRT-PCR, it was vital to test the samples and primers to ensure that each were fully optimized for the experiment. As seen in the six agarose gel pictures within Figure 27 the Btbd11, PLZF, and GAPDH primers were all able to correctly amplify the samples while not producing any noticeable primer-primer dimerization or unspecific amplification. Importantly the second row of each agarose gel included reverse-transcriptase negative controls or – RT samples. These samples serve to show that there is no DNA contamination within the samples, which would lead to unspecific amplification of genomic DNA instead of cDNA amplification. Following this validation, we could confidently proceed with the qRT-PCR and quantification of Btbd11 and PLZF within the various tissues of the experimental mice.

Below in Figure 28 are six bar graphs representing the fold change in Btbd11 and PLZF within the three experimental mice compared to the wild-type control. Panel A, B, and C

show the fold change in *Btbd11* expression from samples of the thymus, spleen, and liver respectively. Similarly, panel D, E, and F show the fold change in *PLZF* expression from samples of the thymus, spleen, and liver respectively. First, the delta-Ct values for each sample were calculated as the difference between the Ct of the experimental sample versus the Ct of the corresponding GAPDH control sample. Then, the delta-Ct values of each experimental sample were normalized to the corresponding delta-Ct values of the wild-type sample to calculate the fold change in expression over the WT. The error bars within each subplot represent the propagated error caused by the deviation between the two technical replicates of each sample.

As addressed earlier, we see a 5-7 fold increase in the expression of *Btbd11* within the hCD2-*Btbd11* and dTG mice when compared to wild-type levels of expression within each of the three different tissues. This confirms that the transgene is successful in inducing ectopic overexpression of *Btbd11* in all T cells through the hCD2 promotor. Interestingly, there is no increase in *Btbd11* expression within the lck-*PLZF* mice and no differential expression of *Btbd11* between the hCD2-*btbd11* and dTG tissue samples.

Also as expected, there is a large fold increase in the expression of *PLZF* within the lck-*PLZF* and dTG tissue when compared to wild type mouse tissues. This confirms that the lck-*PLZF* transgene is able to ectopically over express *PLZF* in all T cells. One striking difference is the differential expression of *PLZF* in the lck-*PLZF* and dTG liver samples as seen in Panel F of Figure 28. The 60-fold change over wild type expression of *PLZF* in the dTG sample is considerably lower than the 150-fold change over wild type expression of *PLZF* in the lck-*PLZF* sample. Significantly, this difference is consistent

with subsequent PLZF transcription factor staining by flow cytometry that will be presented in the next section.

CD4⁺, CD8⁺, and NKT Cell Populations Remained Unchanged between WT, hCD2-Btbd11, lck-PLZF, dTG, and Btbd11 GT Mice

Flow cytometry experiments were performed on experimental mice in order to study any induced phenotypic changes caused by the transgenic expression of Btbd11 and PLZF.

Three individually age-matched independent experiments were performed in order to determine if this transgenic expression led to differences in T cell populations within the thymus, spleen, liver, and lymph nodes. Specifically, using fluorescently labeled CD1d tetramer we can label NKT cells as all MHC-II negative and CD3 positive events as shown in row A of Figure 29. Numbers within each subplot represent the percentage of total T cells that the NKT cells comprise. Next we divided the NKT cell population into the stages of NKT cell development based upon their expression of NK1.1 and CD44 as described in the introduction. Stage 1 NKT cells (CD44⁻NK1.1⁻) are in the bottom left quadrant, Stage 2 NKT cells (CD44⁺NK1.1⁻) are in the bottom right quadrant, and Stage 3 NKT cells (CD44⁺NK1.1⁺) are in the top right quadrant of the subplots in row B. Numbers within each quadrant represent the percentage of total NKT cells that each stage subset comprises. Lastly, row C shows the percentages of all non-NKT, CD3 positive cells that are either CD4⁺ or CD8⁺ T cells. Figure 29 represent the above mentioned population subsets within the thymus tissue samples. T cell subset populations were also found unchanged in the spleen, liver, and lymph nodes of the experimental mice when compared to a wild type control mouse (data not shown).

PLZF and RORγt Expression in CD4⁺, CD8⁺, and NKT Cell Populations is Altered between WT, hCD2-Btbd11, lck-PLZF, dTG, and Btbd11 GT Mice

Intracellular staining of various transcription factors was performed via flow cytometry. PLZF, T-bet and ROR γ t expression was measured within various T cell subsets. As introduced earlier, these transcription factors have been implicated in the differentiation pathways that govern the unique and specific properties of NKT cells that we are studying. Through the quantification of these transcription factors we can begin to discover some of the molecular machinery affected by the altered expression of Btbd11 and PLZF within the different experimental mouse samples. Study of the spleen, thymus, and lymph nodes of the experimental mice did not generate any meaningful differences (data not shown).

However, within the liver of the experimental mice, there was a significant and interesting difference in the expression of both ROR γ t and PLZF. The histograms shown in Figure 30 display the ROR γ t expression within the CD8⁺ T cells of the wild type, lck-PLZF, and dTG mice. There is a significant appearance of ROR γ t expressing cells exclusively within the lck-PLZF and dTG samples as shown in right side of the red and blue histogram curves. Furthermore, there is also an increase in the overall expression of ROR γ t seen in the dTG sample when compared to the lck-PLZF sample as evidenced by the rightward shift of the blue curves compared to the red curves.

In regards to PLZF expression, as expected, both the lck-PLZF and dTG mice had significant overexpression of PLZF compared to the wild type control due to the presence of the lck-PLZF transgene as seen in Figure 31. But, as shown in panels A, B, and C of Figure 31, there is a surprising and different level of PLZF expression between the liver NKT, CD4⁺, and CD8⁺ T cell subsets of the lck-PLZF and dTG mice. In each of these subsets there is an apparent lower level of PLZF expression within the dTG samples

when compared to the lck-PLZF sample. The paired dot plots in Figure 31 compare the PLZF expression, as a function of the mean fluorescent intensity (MFI), between the two experimental mice alongside the wild type control within each of the 3 independently age-matched experiments. While this change is not statistically significant according to a paired Student's t tests, there is an apparent and consistent trend evidencing lower levels of PLZF expression within the dTG liver samples compared to lck-PLZF liver samples.

Cytokine Production by Splenic CD4⁺, CD8⁺, and NKT Cell Populations is Slightly Altered Following *in-vitro* Stimulation

In line with our hypothesis, we compared the cytokine production of wild type, hCD2-Btbd11, lck-PLZF, and dTG mice to determine if the ectopic expression of Btbd11 and PLZF in all T cells was able to induce a NKT cell-like phenotype in transgenic conventional T cells subsets. Spleens were extracted and processed from the experimental mice and then stimulated *in vitro* with PMA and ionomycin followed by Brefeldin A. This stimulation occurs independent of normal TCR signaling and is commonly used by our laboratory to stimulate whole tissue lymphocyte samples. Following the stimulation, the tissue samples are stained for extracellular surface markers and then intracellular cytokine production. Various experiments were performed to determine the production of IL-4, IFN- γ , IL-17a, GM-CSF, and IL-4 cytokines in order to study the activation profile of the various T cell subsets.

Figures 32, 33, and 34 are representative of two individually age-matched independent experiments that compare the cytokine production of splenic NKT cells, CD4⁺ T cells, and CD8⁺ T cells, respectively, following *in-vitro* stimulation. Row A of each figure is a dot plot of IFN- γ and IL-4 production. As seen in Figure 32 the NKT cells of each of the mice have similar, normal production of IFN- γ and IL-4 as evidenced by the equal

numbers of double producing population seen in each of the four mice. Interestingly, as shown within row B of Figure 32 NKT cells with overexpression of *Btbd11*, the second and fourth columns, have a slight skewing towards the production of IL-17a and away from the production of IL-4. Statistical analysis shows this skewing to be non-significant but within each individual experiment the same trend is apparent. Row C of Figure 32 displays the production of GMCSF and IL-2 by NKT cells. No obvious changes in these population percentages were discovered.

Figure 33 represents the same cytokine production comparisons between the experimental mice, but within the $CD4^{+}$ T cells. Importantly, these are all non-NKT cell, $CD4^{+}$ T cells so as to define any differences between cytokine production of the conventional T cells and the transgenic conventional T cells of the experimental mice. Row A of Figure 33 displays the IFN- γ and IL-4 production of the $CD4^{+}$ T cells. There was a consistent increase in the number of IFN- γ and IL-4 single-producing cells within the $CD4^{+}$ T cells of the lck-PZLF and dTG mice, but no change in IFN- γ and IL-4 double-producing $CD4^{+}$ T cells. Row B shows that there were no interesting changes in the production of IL-4 and IL-17a by the $CD4^{+}$ T cells. Row C shows that there is a small increase in the $CD4^{+}$ T cells of the lck-PZLF and dTG mice that can double-produce GMCSF and IL-2.

Lastly, Figure 34 shows the cytokine production by $CD8^{+}$ T cells within the experimental mice. Row A shows that there was an interesting decrease in the IFN- γ production by hCD2-Btbd11 $CD8^{+}$ T cells. Row B illustrates the emergence of a very interesting population of $CD8^{+}$ T cells that can produce IL-17a within the PLZF expressing $CD8^{+}$ T cells of the lck-PZLF and dTG mice. Importantly, the population sizes of IL-17a

producing CD8⁺ T cells are similar between the lck-PLZF and dTG mice. Row C also showed a small increase in the GMCSF production by the PLZF expressing CD8⁺ T cells of the lck-PZLF and dTG mice.

In a separate set of two individually age-matched independent experiments, we measured the cytokine production within splenic CD4⁺, CD8⁺, and NKT cell subsets between the wild type and Btbd11 GT mice. Figure 35 shows the cytokine production of IFN- γ , IL-4, and IL-17a within the NKT cells. As seen in row A of Figure 35, there is a slightly lower percentage of Btbd11 GT NKT cells that are able to co-produce IFN- γ and IL-4, while the percentage of IFN- γ and IL-4 individually producing cell populations remain the same. There is no change in the production of IL-17a as shown by row B of Figure 35. There is also no change in cytokine production seen between the CD4⁺ and CD8⁺ T cells of the wild type and Btbd11 GT mice (data not shown).

Cytokine Production by Liver CD4⁺, CD8⁺, and NKT Cell Populations is Significantly Altered Following *in-vitro* Stimulation

Upon determining that there were significant differences in the populations and effector functions of innate-like lymphocytes within the livers of the experimental mice, we investigated the cytokine profile of various T cell subsets within liver samples of the experimental mice. Liver samples were removed and stimulated *in-vitro* with PMA and ionomycin followed by Brefeldin A. The cytokine production profile of liver CD4⁺, CD8⁺, and NKT cells were found to be largely similar to the cytokine profile of the splenic T cell subsets with exception of a significant difference in IL-17a production by CD8⁺ T cells.

Row A of Figure 36 is representative data illustrating the varying IL-17a and IFN- γ production by liver CD8⁺ T cells of the experimental mice. As previously discovered by our laboratory, 2-5% of CD8⁺ T cells within lck-PLZF mice possess the ability to produce IL-17a. Notably, as shown in panel B of Figure 36, in addition to the significant increase in lck-PLZF CD8⁺ T cells that can produce IL-17a, 11% of CD8⁺ T cells within the dTG samples are shown to produce IL-17a upon activation. In fact, the IL-17a producing population of CD8⁺ T cells within the dTG liver sample was found to be significantly larger than the previously discovered population within lck-PLZF CD8⁺ T cells. Statistical significance was calculated from 3 individually age-matched independent experiments using multiple Student's t tests.

$\gamma\delta$ T Cell Populations are Significantly Altered between WT, hCD2-Btbd11, lck-PLZF, dTG, and Btbd11 GT Mice

Due to their similar classification as innate-like lymphocytes, and their proven expression of PLZF, we investigated the possible changes in $\gamma\delta$ T cells within our experimental mice. Of particular interest was the V γ 1.1⁺, V δ 6.3⁺ subset of $\gamma\delta$ T cells. This specific subset of $\gamma\delta$ T cells have been shown to co-produce IL-4 and IFN- γ and express high levels of PLZF, characteristics only shared with NKT cells [89]. Varying frequencies of $\gamma\delta$ T cells were seen between the experimental mice liver samples (Figure 37). Compared to 8% of all T cells in the wild type, the percentage of $\gamma\delta$ T cells was significantly decreased to 4% in the lck-PLZF and 3% in Btbd11 GT liver samples, while significantly increased to 13% in the dTG liver samples. There was also a significantly lower percentage of $\gamma\delta$ T cells within the lck-PLZF mice compared to hCD2-Btbd11 and dTG liver samples. Statistical significance was calculated from 3 individually age-matched independent experiments using multiple Student's t tests.

Figure 38 shows additional subsetting of the liver $\gamma\delta$ T cells. As seen in row A, V γ 1.1⁺, V δ 6.3⁺ cells or $\gamma\delta$ NKTs can be seen in the top right quadrant of each subplot.

Interestingly, the percentage of $\gamma\delta$ NKTs significantly increased to 32% within the lck-PLZF and dTG liver samples compared to 12% of total $\gamma\delta$ T cells seen in the wild type control (Figure 38B). There was also a significantly different percentage of $\gamma\delta$ NKTs within the lck-PLZF sample when compared to the hCD2-Btbd11 and dTG samples. Statistical significance was calculated from 3 individually age-matched independent experiments using multiple Student's t tests.

ALT Activity is Significantly Different between WT and Btbd11 GT Following Concanavalin A Injection

Concanavalin A is used to induce an experimental hepatitis model in mice. This ConA induced liver damage has been shown to be largely mediated by innate-like lymphocytes such as iNKT cells and $\gamma\delta$ T cells. As we are studying the role that Btbd11 plays in these specific T cell subsets, the ConA-induced hepatitis represents an appropriate and meaningful *in vivo* model of the effector function of NKT and $\gamma\delta$ T cells. Prior to ConA injections, a baseline serum sample is withdrawn to serve as an experimental control, as we do not expect to see any liver damage in the mice preceding injection. ConA injection dosages were consistent amongst the experimental mice at a concentration of 15 micrograms of ConA per gram of mouse weight. Following the intraocular ConA injections, the mice were bled for serum extraction at 6 hours and 24 hours post ConA injections.

Alanine aminotransferase (ALT) is the main liver enzyme that is released into the blood stream following the breaking down of liver hepatocytes caused by liver damage. Equal amounts of serum collected from the experimental mice at each time point were tested for

their ALT activity using the BioVision ALT Assay Kit described in the methods section. The ALT activity of three wild type and three Btbd11 GT mouse serum samples were measured following an injection of 15 μ g of ConA per gram of mouse weight. The standard curve for the ALT assay was generated from the absorbance readings of the pyruvate standards provided in the BioVision ALT Assay Kit (Figure 39A). The strict linear fitted line with an R^2 value close to 1.0 evidenced the precise ability of the assay to measure the pyruvate molecules generated by the ALT enzymes within the company-optimized standard samples. Panel B of Figure 39 shows the averages of three biological and two technical replicates of the wild type versus Btbd11 GT experimental mice. The baseline reading of ALT activity within each mouse was found to be very low as expected. Interestingly, the 6 hour post injection serum samples showed a large degree of variability, but with the Btbd11 GT samples reading at a lower average ALT activity, 9 mU/ml compared to 6 mU/ml of wild type. Significantly, at 24 hours post injection, the Btbd11 GT serum samples showed statistically significant lower levels of ALT activity than the wild type mice, 11 mU/ml compared to 3.5 mU/ml (Figure 39B). Statistical significance was determined within the 6 experimental mice using Student's t test.

T Cell Populations and PLZF Expression are Significantly Different within WT and Btbd11 GT Mice Following Concanavalin A Injections

Following the final bleeding and serum extraction for the ALT assay experiment described above, the livers of each experimental WT and Btbd11 GT mouse were extracted and processed for flow cytometry staining of various T cell subsets and intranuclear PLZF expression. Population percentages of T cell subsets such as NKT cells, CD4⁺ T cells, CD8⁺ T cells, and total $\gamma\delta$ T cells remained unchanged between the WT and Btbd11 GT mice (data not shown). Significantly, as shown in panel A of Figure

40, the 19% of V δ 6.3⁺ $\gamma\delta$ T cells seen in the Btbd11 GT samples was significantly lower than the 24% seen within the wild type samples. Statistical significance was calculated from 3 mice of each experimental group using an unpaired Student's t test.

Intranuclear flow cytometry staining for PLZF expression also found statistically significant differences within the V δ 6.3⁺, V γ 1.1⁺ $\gamma\delta$ T cells. Panel B of Figure 40 shows that these cells in the Btbd11 GT mice had significantly higher levels of PLZF expression, measured as the mean fluorescent intensity of the PLZF staining antibody. Similarly, PLZF expression was also found be significantly higher in total liver NKT cells of the Btbd11 GT mice compared to the WT samples, as seen in panel C of Figure 40. Statistical significance was calculated from 3 mice of each experimental group using an unpaired Student's t test.

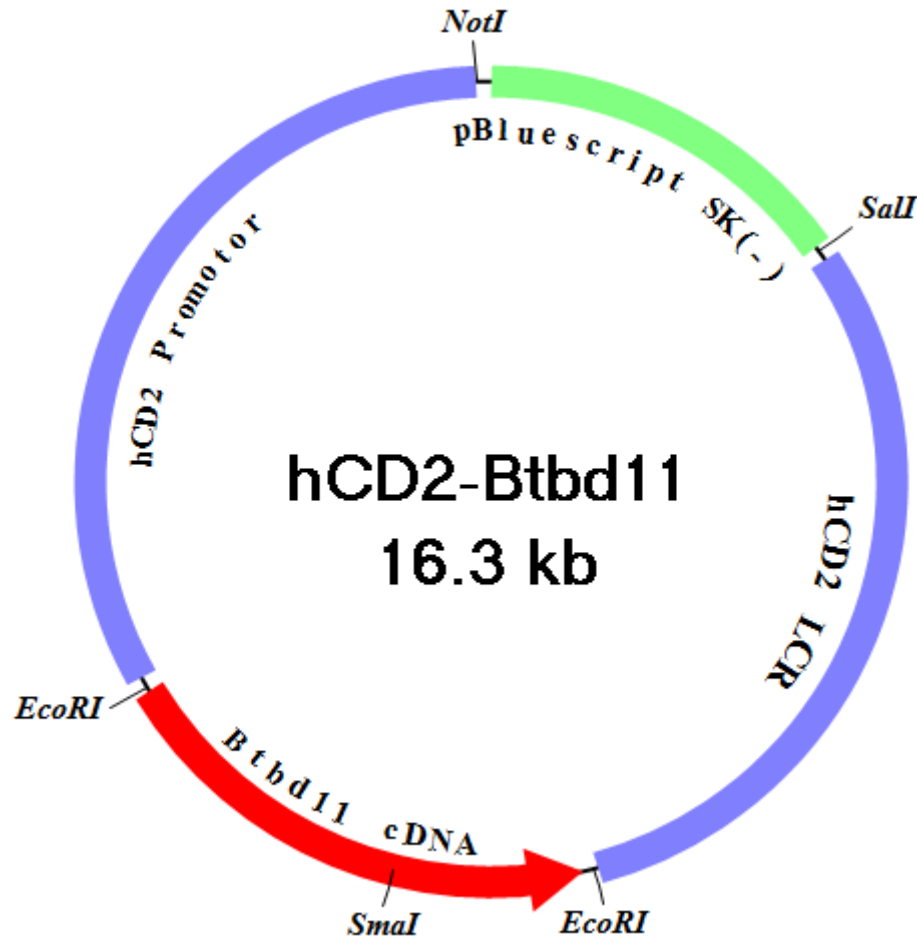


Figure 21. Graphical representation of hCD2-Btbd11 transgene vector. The Btbd11 cDNA of length 3.3 kb was inserted between the 5 kb long hCD2 promotor and 5.5 kb long hCD2 LCR region as shown above. The arrow represents the direction of the ORF of the Btbd11 cDNA. Also included within the construct is the 2.5 kb pBluescript SK(-) bacterial cloning component which includes the ampicillin resistant selection cassette shown in green. The sites of relevant restriction enzymes used throughout the transgene generation process are labeled as well.

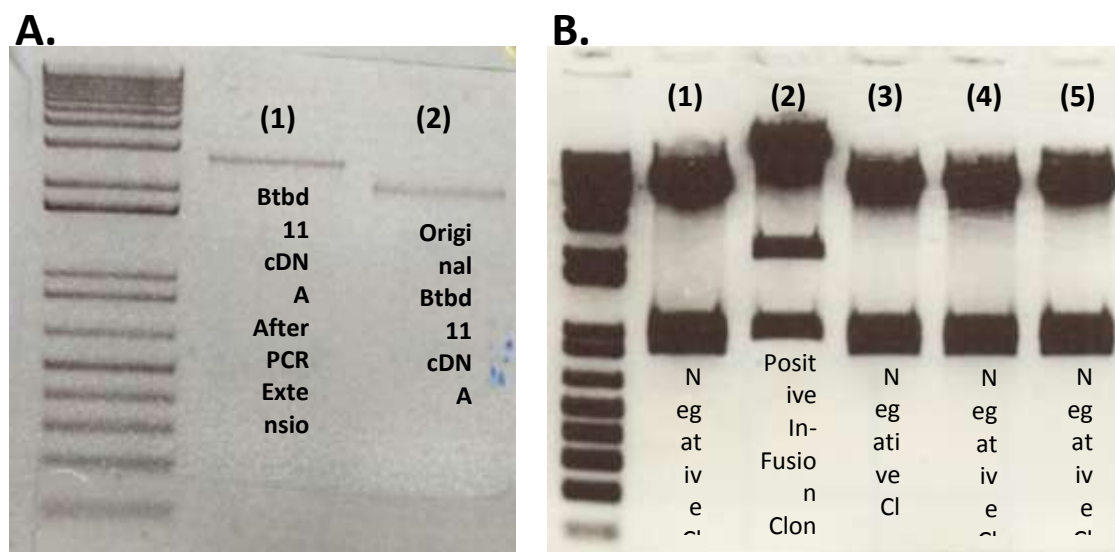


Figure 22. Successful hCD2-Btbd11 clone following PCR and In-Fusion Cloning. **(A).** Agarose gel of PCR extension of Btbd11 cDNA. Lane 1 is the output of the PCR extension that added the 22 nucleotide homologous arms to each end of the Btbd11 cDNA. These arms were designed to be complementary to each side of the insertion site of the hCD2 vector backbone. This PCR product is just under 3.5 kb, the correct size for the Btbd11 cDNA with both homologous arms added. Lane 2 shows the original cDNA clone of size 3.3 kb without the added homologous arms. **(B).** Agarose gel of restriction enzyme screening of In-Fusion bacterial clones. Lane 2 represents a positive candidate based upon the product sizes of the restriction enzyme digest. Digestion with SmaI and EcoRI produced 3 bands of size 13 kb, 2 kb, and 1 kb for the correct construct. Lanes 1, 3, 4, and 5 represent In-Fusion bacterial clones that did not generate the correct construct as evidenced by the incorrect digestion products.

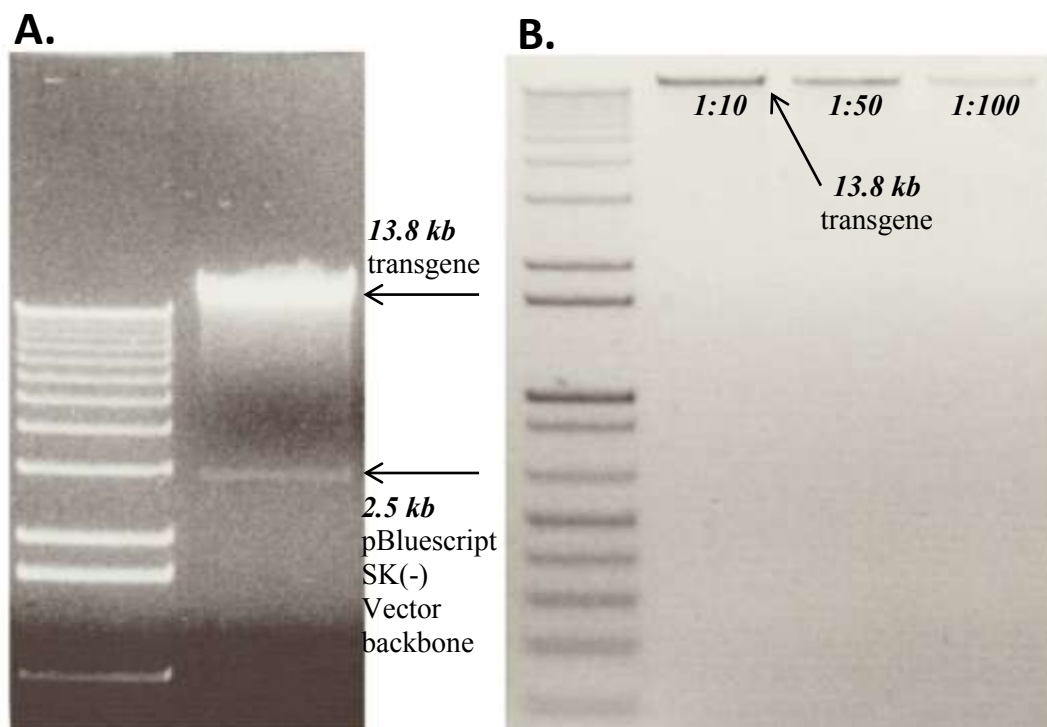


Figure 23. Isolation and purification of hCD2-Btbd11 construct prior to microinjection. **(A)**. Following verification that the construct has the correct sequence, it was digested with NotI and SalI restriction enzymes in order to separate the desired transgene from the unwanted pBluescript SK(-)Vector backbone. The transgene is then removed and purified from the agarose gel. **(B)**. Following gel purification of the transgene, the purity and concentration of the transgene are determined by loading a series of dilutions to ensure that there is no remaining pBluescript SK(-) Vector backbone in the sample before proceeding to microinjection.

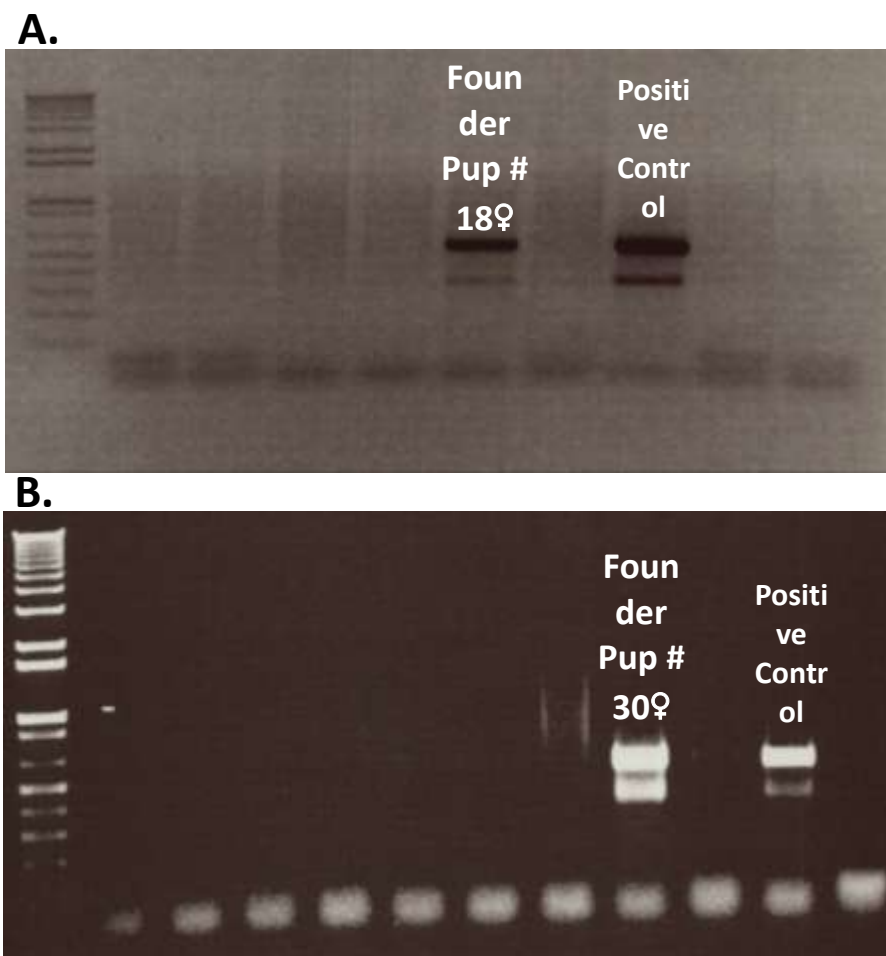


Figure 24. Genotyping results of the two hCD2-Btbd11 transgene positive founder pups. Agarose gel photo of PCR genotyping shows two mice positive for the hCD2-Btbd11 transgene.

(A). Compared to the positive control, DNA sample of the founder pup #18 shows the same amplification, confirming that founder pup #18 is positive for the transgene. **(B).** Compared to the positive control, DNA sample of the founder pup #30 shows the same amplification, confirming that founder pup #30 is positive for the transgene.

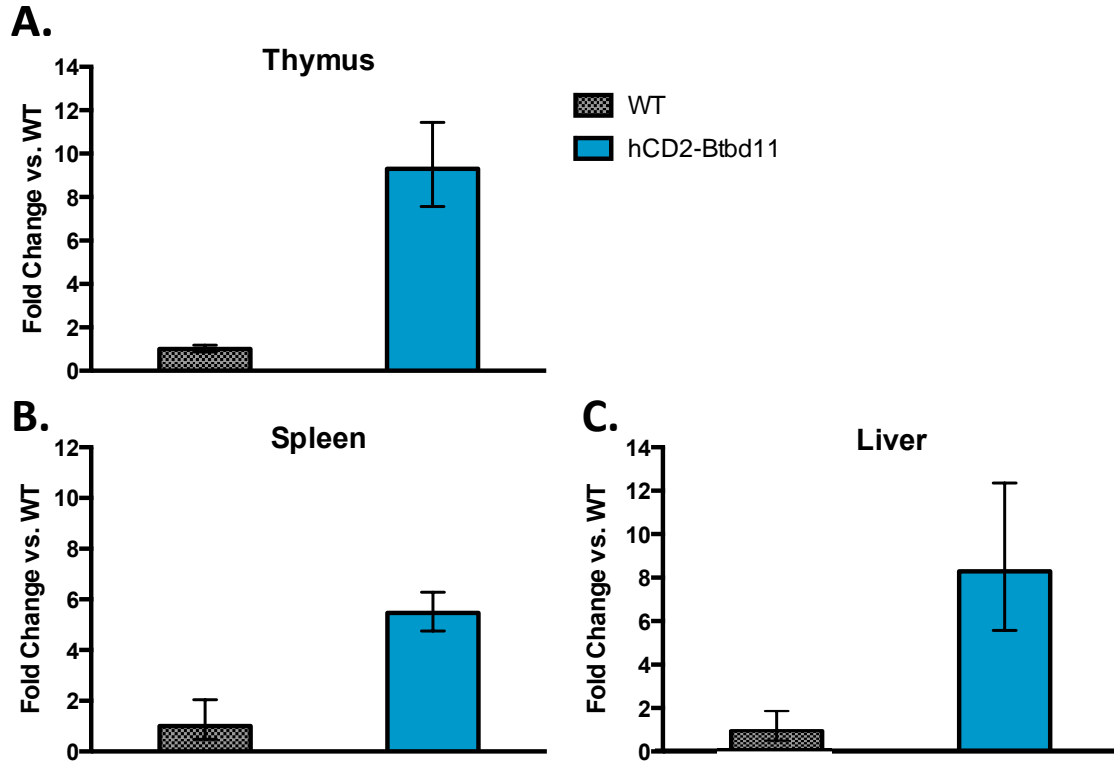


Figure 25. Overexpression of Btbd11 in hCD2-Btbd11 mice. Btbd11 overexpression was validated within the whole thymus, spleen, and liver of the WT and hCD2-btbd11 mice, via qRT-PCR following RNA isolation and reverse-transcription. (A) (B), and (C). Btbd11 expression was normalized to GAPDH control gene and then normalized to WT levels of Btbd11 expression to determine the fold-change in expression. Mean and S.E.M of the two technical replicates are displayed.

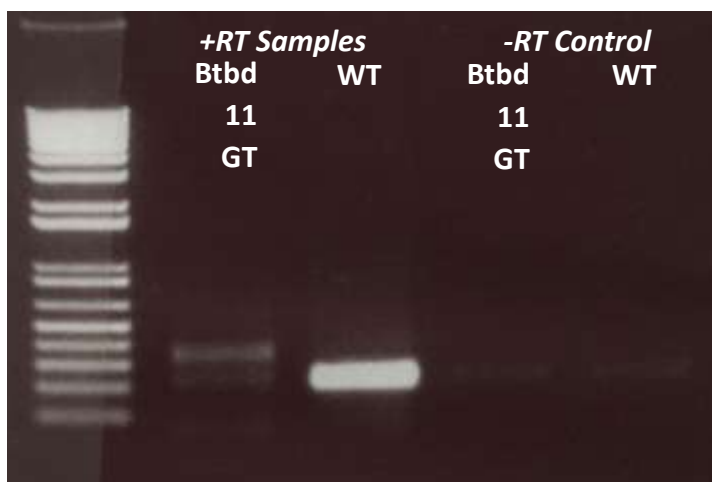


Figure 26. Reduction in Btbd11 mRNA transcript within Btbd11 GT mice. Confirmation of the significant knock down of Btbd11 expression in the Btbd11 GT mice compared to wild type control. Whole spleen samples were extracted and RNA was processed. Reverse transcriptase was then used to generate a cDNA library. PCR amplification with Btbd11 primers were used to qualitatively show the mRNA expression of the Btbd11 gene.

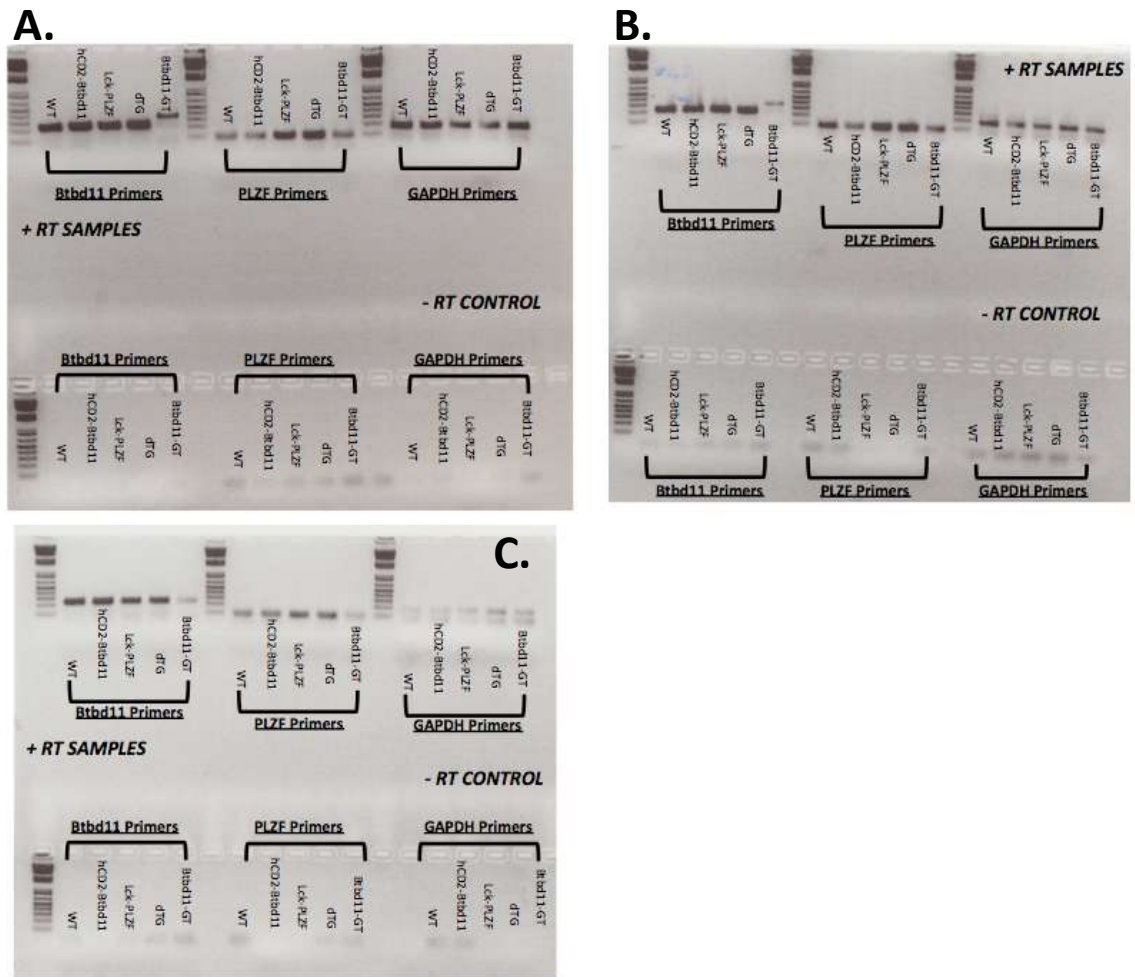


Figure 27. Validation of *Btbd11*, *PLZF*, and *GAPDH* qRT-PCR primers. **(A)**. Agarose gel photo of PCR amplification of whole thymus cDNA samples of the 5 experimental mice. Three sets of PCR were run on each sample, amplification of a *Btbd11* transcript, the *PLZF* transcript, and housekeeping gene, *GAPDH*. Bands on the gel represent mRNA expression and serve to validate the three primer sets for quantitative RT-PCR. **(B) and (C)**. Agarose gel photo of PCR amplification of whole spleen and liver cDNA samples of the 5 experimental mice. Each gel includes negative reverse-transcriptase controls for each sample in the bottom half of the panel.

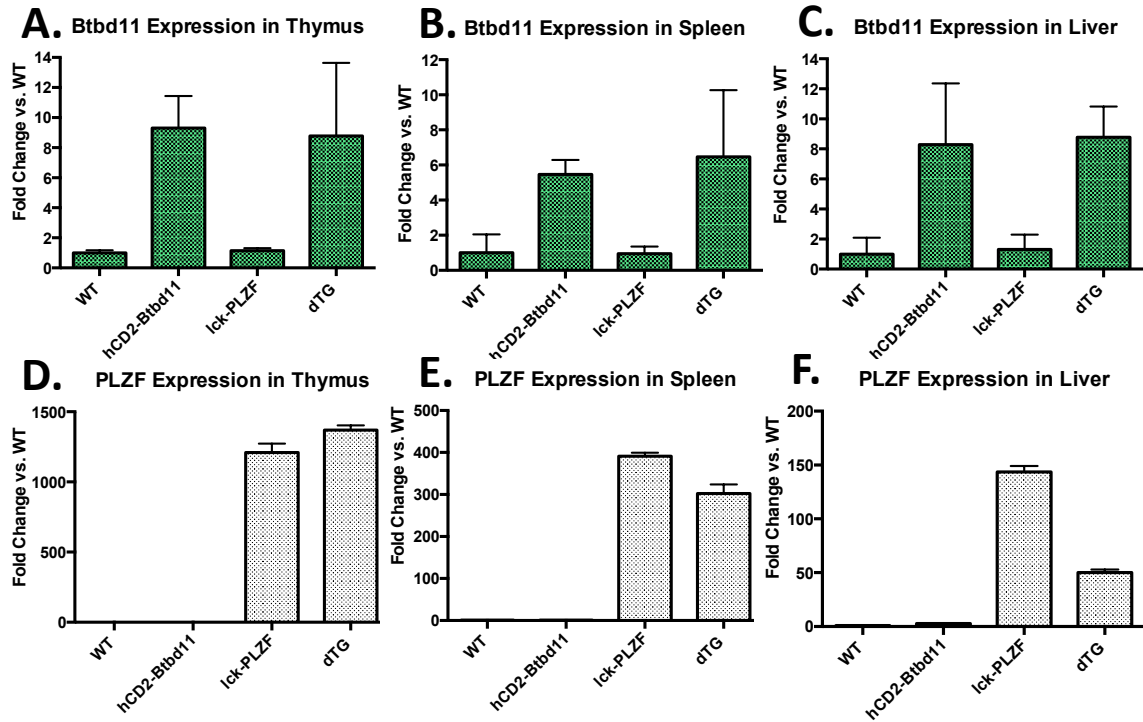


Figure 28. Altered PLZF gene expression between lck-PLZF and dTG mice.

(A), (B), and (C). Btbd11 expression is measured by real-time quantitative PCR of cDNA samples that have undergone reverse transcriptase from RNA samples extracted from whole thymus, spleen, and liver respectively. Analysis of RT-qPCR is performed by comparing the number of cycles that a sample requires to amplify to the threshold Ct value. The Ct value of each sample is then normalized to the Ct value of the housekeeping gene, GAPDH, to account for differing starting concentrations of input cDNA. Then each sample is normalized to the WT sample within each experimental group to calculate the fold change in expression versus the wild type displayed on the y-axis. (D), (E), and (F). PLZF expression is measured by real-time quantitative PCR of cDNA samples that have undergone reverse transcriptase from RNA samples extracted from the thymus, spleen, and liver respectively. Displayed is the mean value and S.E.M between the technical replicates of each sample.

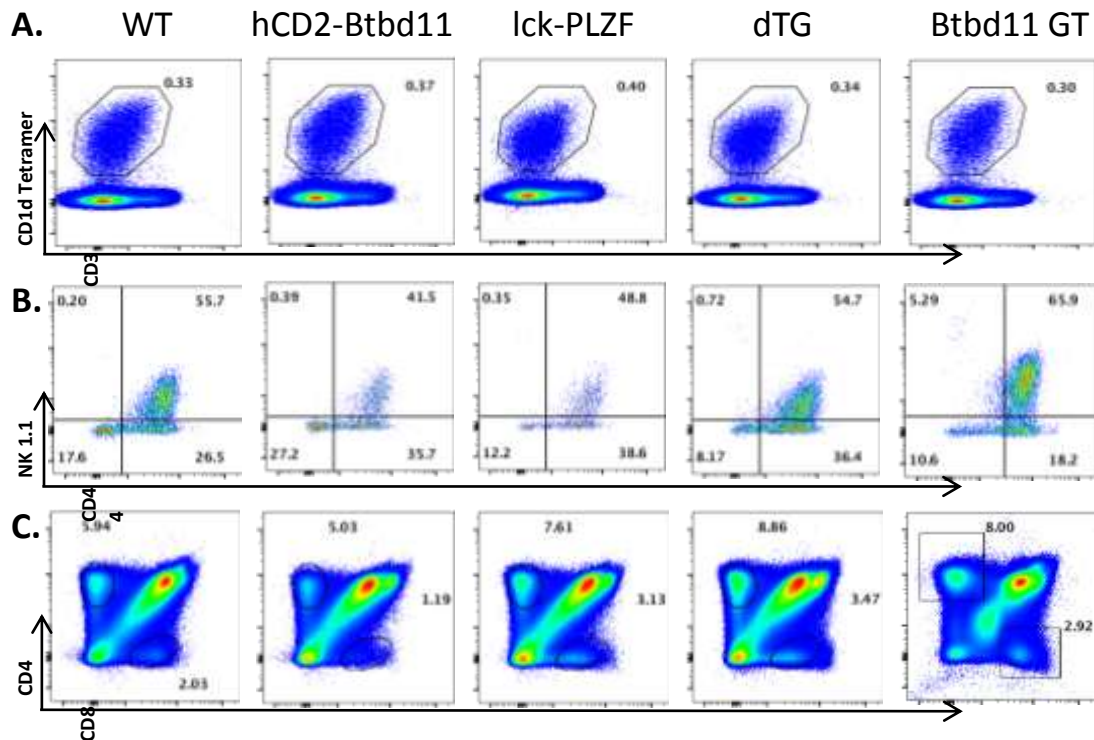


Figure 29. NKT and Conventional T Cell populations are not altered in experimental mice. Various NKT cell subsets were analyzed by flow cytometry within thymus tissues from the five experimental mice. This figure is representative of at least 3 individual age-matched experiments. **(A)**. Total NKT cell populations were stained for and gated upon all CD3⁺, CD1d tetramer⁺ cells. **(B)**. Upon gating upon all NKT cells within each sample, events are separated based upon the cell surface marker NK1.1 on the y-axis and the cell surface marker CD44 on the x-axis. Cells within the bottom left quadrant are Stage 0/1 NKT cells, cells within the bottom right quadrant are Stage 2 NKT cells, and cells within the top right quadrant are Stage 3 NKT cells. **(C)**. All CD3⁺ T cells are separated based upon CD4 on the y-axis and CD8 on the x-axis. Numbers within each subplot represent the percentage population of each T cell subset.

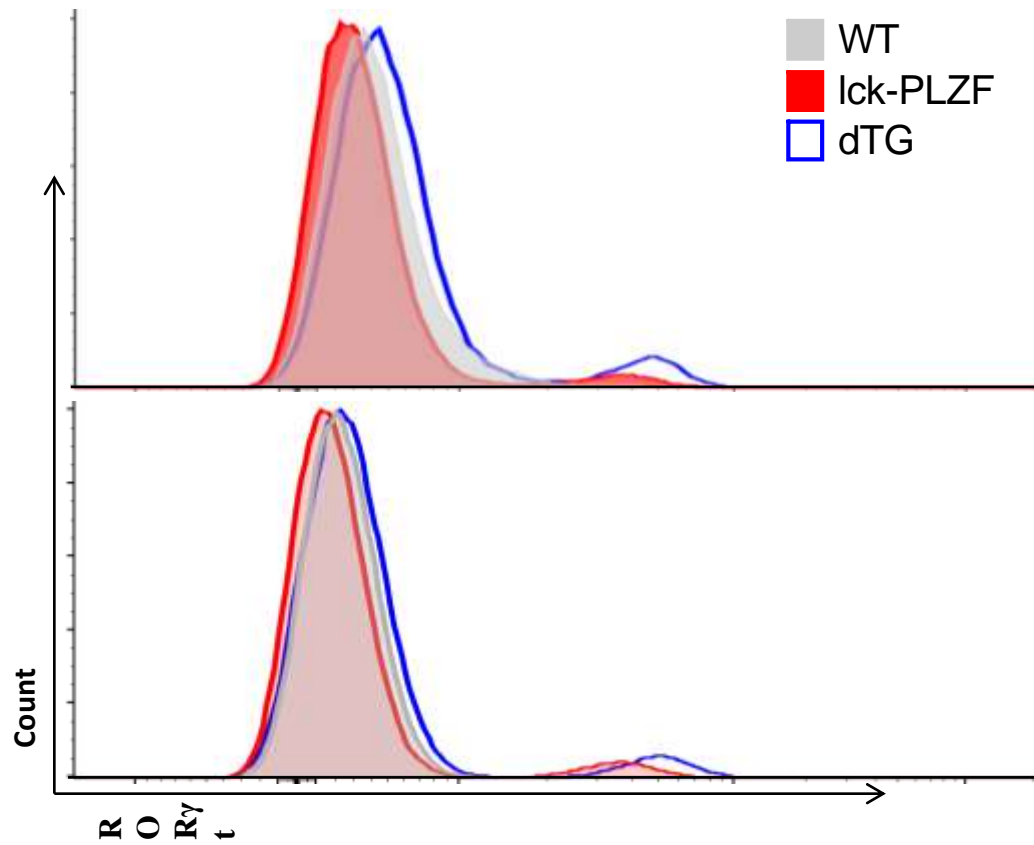


Figure 30. Flow cytometry was performed to show the different expression of ROR γ t transcription factor within liver CD8⁺ T cells of experimental mice. Expression of ROR γ t is compared to the expression within the wild type sample shown in gray. The red filled histogram curve represents the expression within the lck-PLZF sample and the blue histogram curve represents ROR γ t expression within the dTG sample. Each histogram represents repeated and separate experiments.

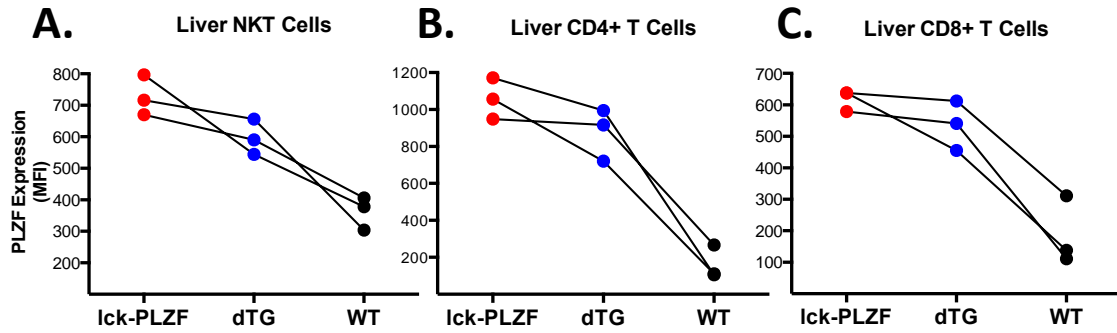


Figure 31. ROR γ t protein expression is increased in dTG and lck-PLZF mice. Flow cytometry was performed to determine that there is differential expression of PLZF within various T cell subsets of the liver. **(A)**. PLZF expression within liver NKT cells was measured as a function of the mean fluorescence intensity (MFI) of the PLZF antibody and compared between the lck-PLZF, dTG, and wild type samples. **(B) and (C)**. PLZF expression within liver non-NKT, CD4⁺ and CD8⁺ T cells, respectively, was measured as a function of the mean fluorescence intensity (MFI) of the PLZF antibody and compared between the lck-PLZF, dTG, and wild type samples.

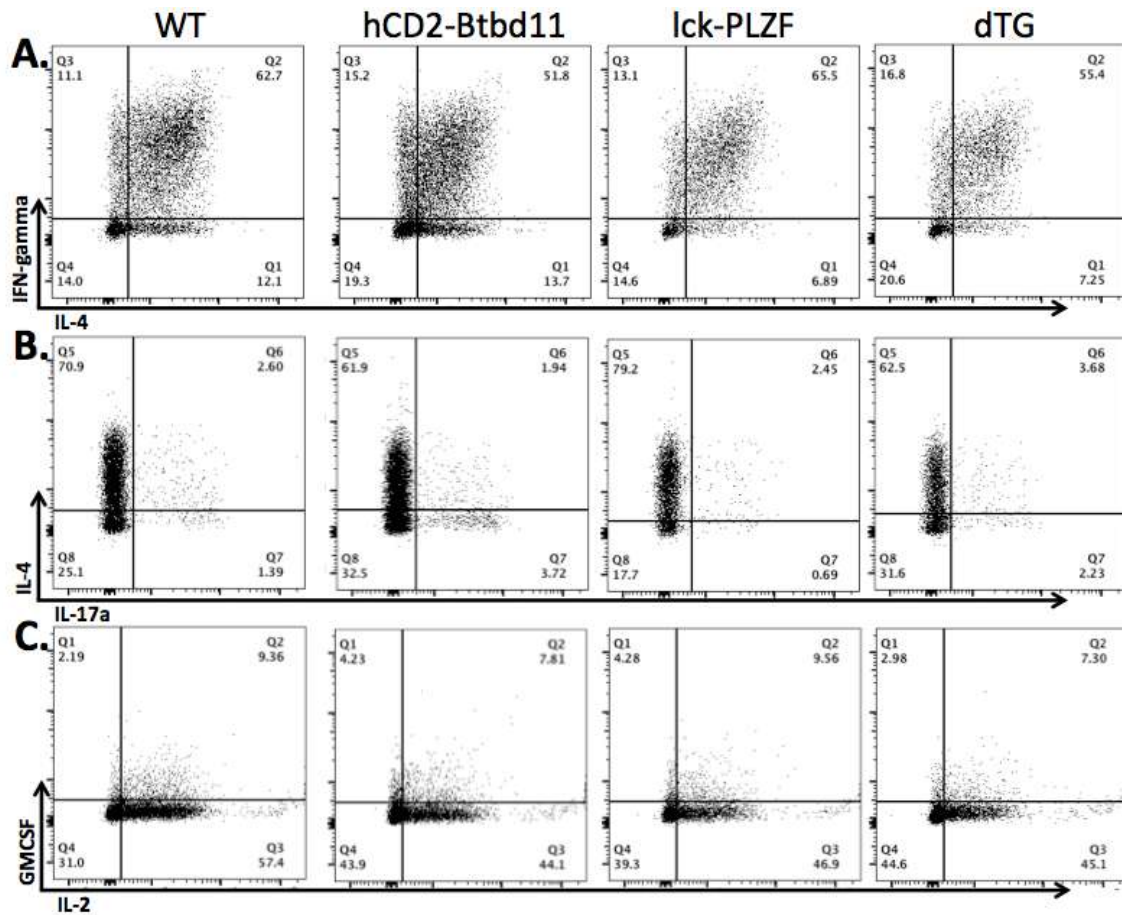


Figure 32. Splenic NKT cells do not exhibit altered cytokine production. Total splenic NKT cells of the experimental mice were stained for cytokine production after in vitro activation by PMA and Ionomycin followed by Brefeldin A. **(A)**. NKT cells are stained for their intracellular production of IFN- γ on the y-axis and IL-4 on the x-axis. **(B)**. NKT cells are stained for their intracellular production of IL-4 on the y-axis and IL-17a on the x-axis. **(C)**. NKT cells are stained for their intracellular production of GM-CSF on the y-axis and IL-2 on the x-axis.

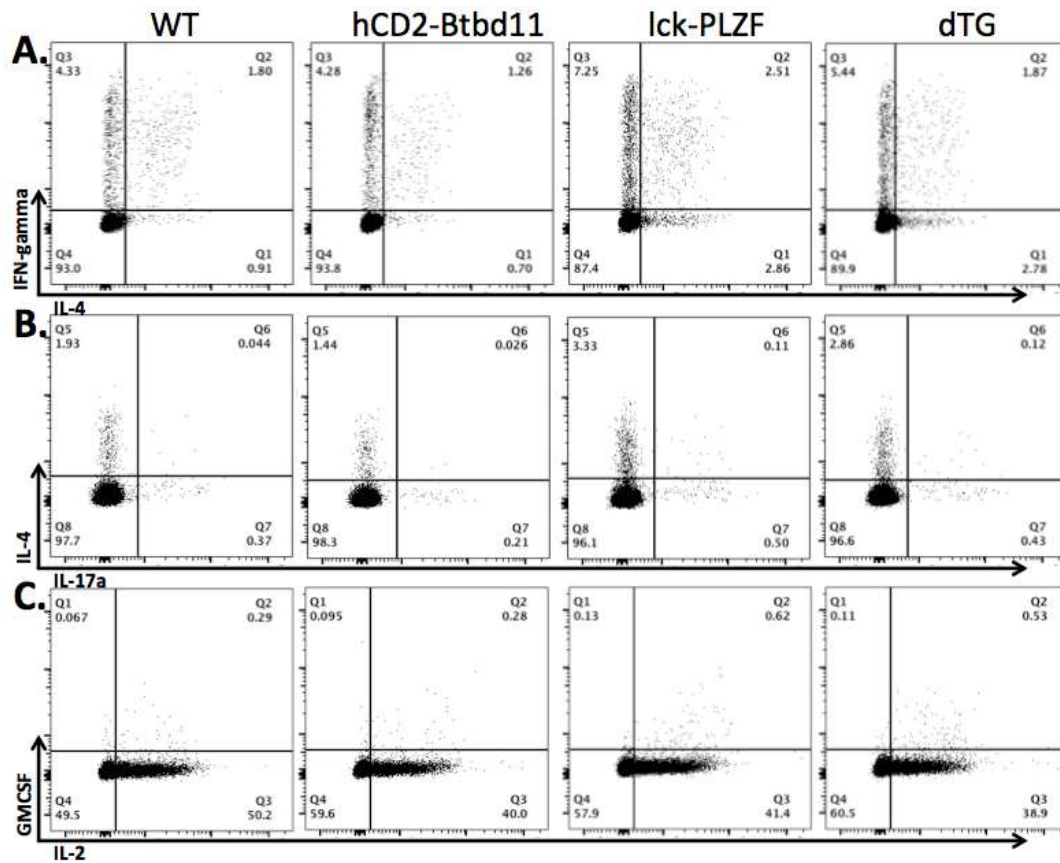


Figure 33. Splenic $CD4^+$ T cells do not exhibit altered cytokine production. Total splenic $CD4^+$ T cells of the experimental mice were stained for cytokine production after in vitro activation by PMA and Ionomycin followed by Brefeldin A. (A). $CD4^+$ T cells are stained for their intracellular production of IFN- γ on the y-axis and IL-4 on the x-axis. (B). $CD4^+$ T cells are stained for their intracellular production of IL-4 on the y-axis and IL-17a on the x-axis. (C). $CD4^+$ cells are stained for their intracellular production of GMCSF on the y-axis and IL-2 on the x-axis.

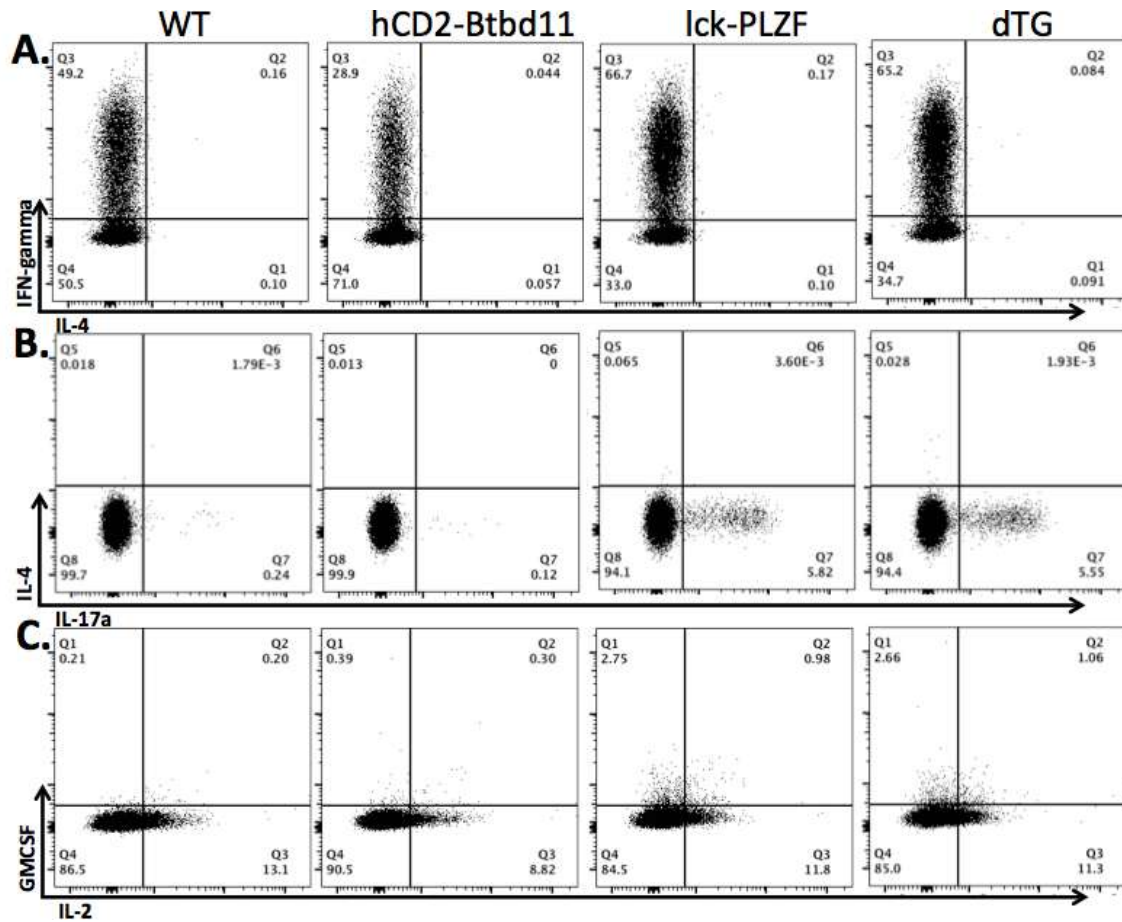


Figure 34. Splenic CD8⁺ T cells do not exhibit altered cytokine production. Total splenic CD8⁺ T cells of experimental mice were stained for cytokine production after in vitro activation by PMA and Ionomycin followed by Brefeldin A. **(A)**. CD8⁺ T cells are stained for their intracellular production of IFN- γ on the y-axis and IL-4 on the x-axis. **(B)**. CD8⁺ T cells are stained for their intracellular production of IL-4 on the y-axis and IL-17a on the x-axis. **(C)**. CD8⁺ T cells are stained for their intracellular production of GM-CSF on the y-axis and IL-2 on the x-axis.

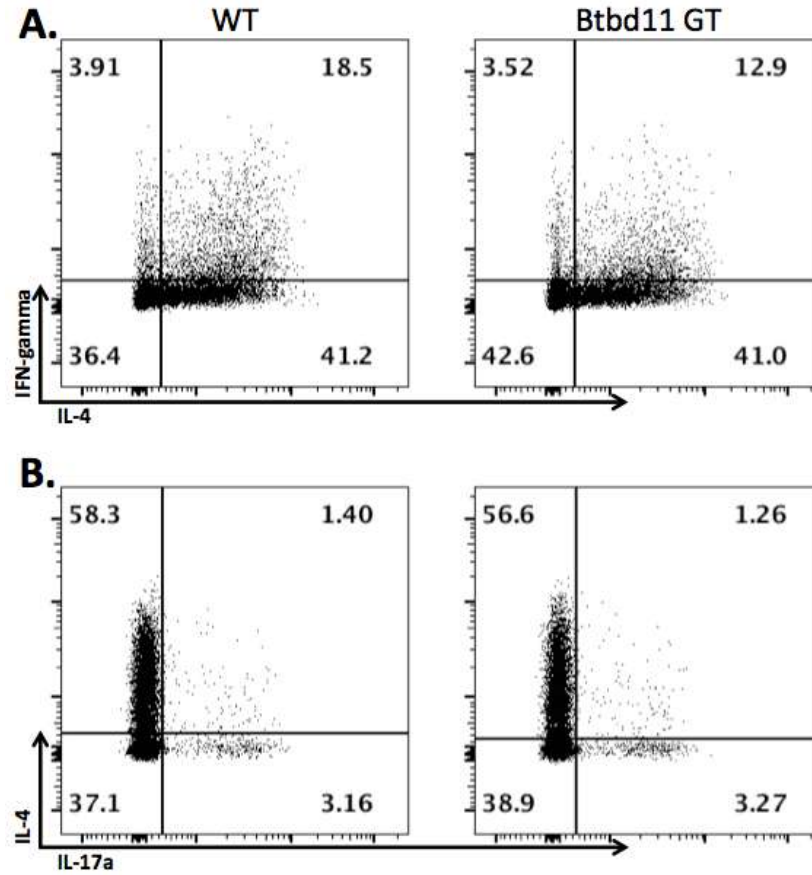


Figure 35. Btbd11 GT NKT cells do not exhibit altered cytokine production. Total splenic NKT cells were stained for cytokine production following in vitro activation by PMA and Ionomycin followed by Brefeldin A. **(A)**. NKT cells are stained for their intracellular production of IFN- γ on the y-axis and IL-4 on the x-axis. **(B)**. NKT cells are stained for their intracellular production of IL-4 on the y-axis and IL-17a on the x-axis.

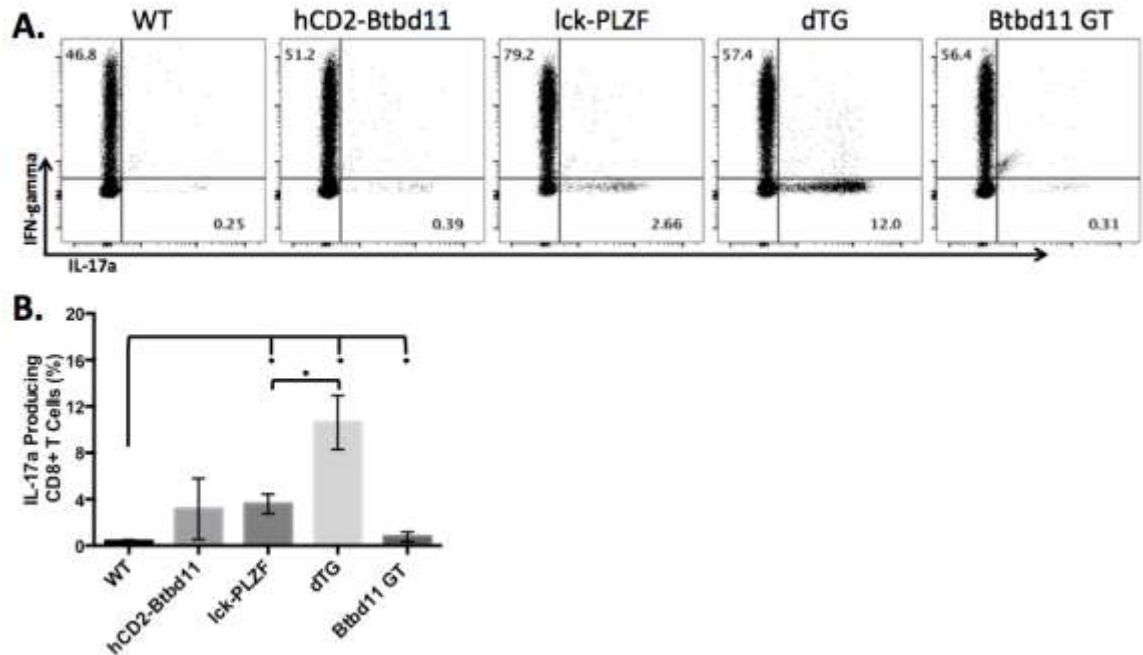


Figure 36. Significant expansion of IL-17a producing liver CD8⁺ T cells in dTG mice. Total liver CD8⁺ T cells were stained for cytokine production following in vitro activation by PMA and Ionomycin followed by Brefeldin A. **(A)**. CD8⁺ T cells were stained for their intracellular production of IFN- γ on the y-axis and IL-17a on the x-axis. Numbers within each quadrant represent the percentage of CD8⁺ T cells that produce either IL-17a or IFN- γ . These plots are representative of 3 independent age-matched experiments. **(B)**. The mean and S.E.M of CD8⁺ T cells that produce IL-17a are graphed for the 3 individual age-matched experiments. Significantly different percentages of IL-17a producing CD8⁺ T cells are labeled as * for $p < 0.05$. Statistical significance was determined by multiple Student's t tests.

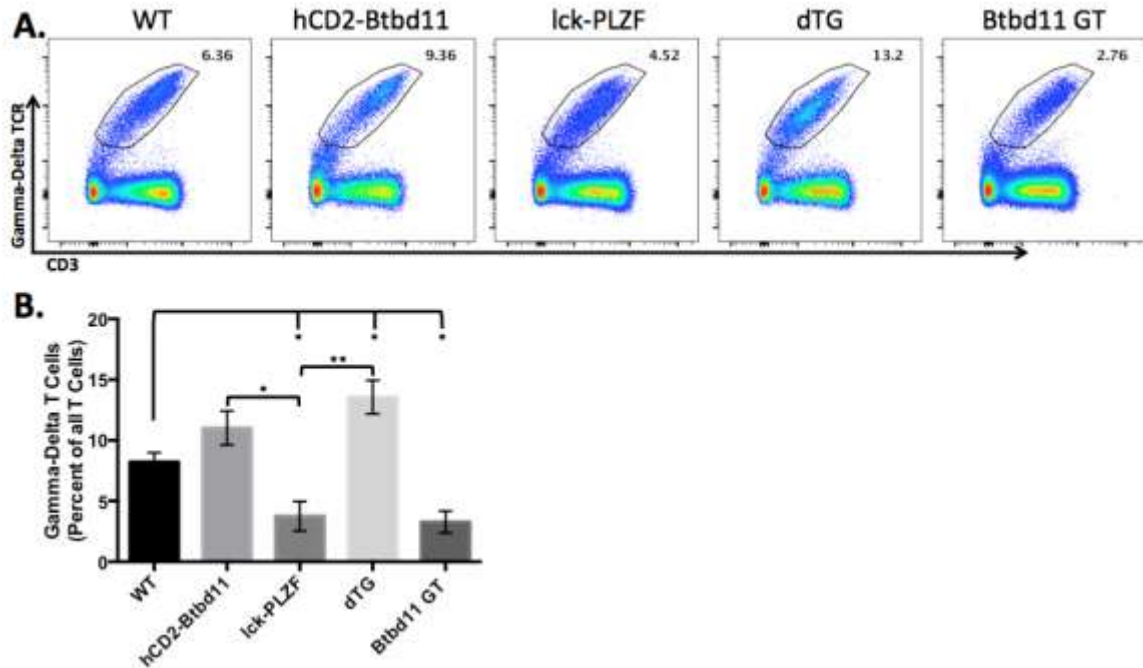


Figure 37. Total percentages of $\gamma\delta$ T cells are significantly different in experimental mice. Liver $\gamma\delta$ T cell populations were found to differ between the five experimental mice. This figure is representative of at least 3 individual age-matched experiments. (A). Total $\gamma\delta$ T cell populations were stained for and gated upon all $CD3^+$, $\gamma\delta$ TCR $^+$ cells. (B). Mean and S.E.M are graphed for the 3 individual age-matched experiments. Significantly different percentages of $\gamma\delta$ T cells are labeled as * for $p<0.05$, and ** for $p<0.01$. Statistical significance was determined by multiple Student's t tests.

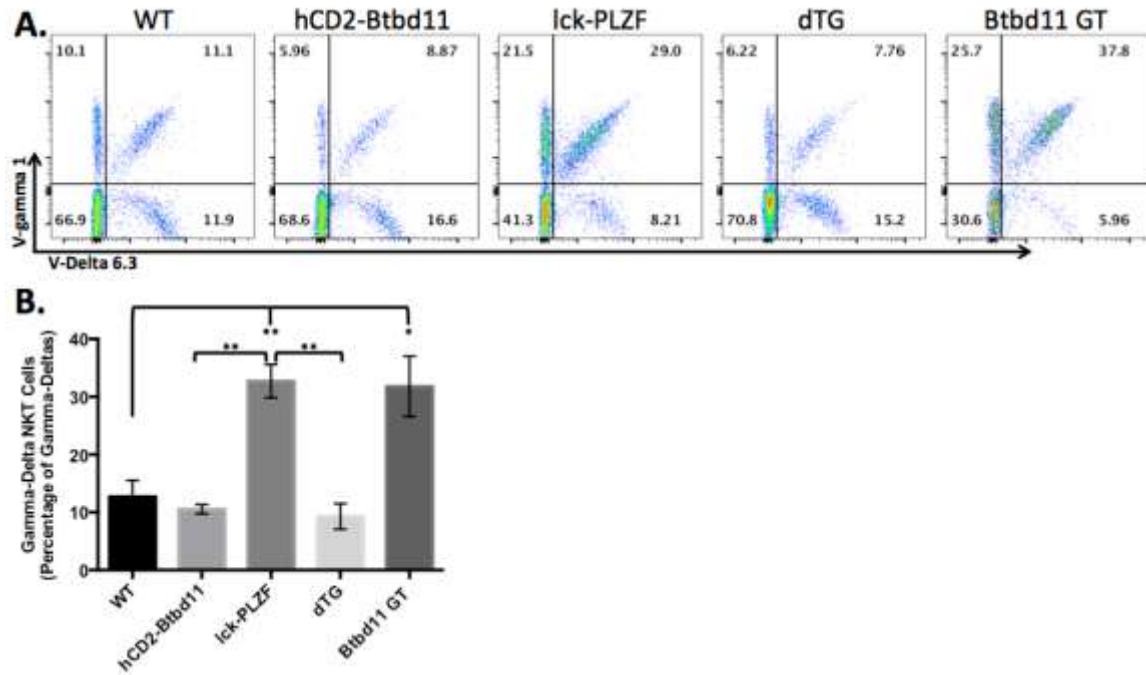


Figure 38. Percentages of $\gamma\delta$ NKT cells are significantly different in experimental mice. This figure is representative of at least 3 individual age-matched experiments. **(A)**. Upon gating upon all $\gamma\delta$ T cells within each liver sample, the cells were further separated based upon expression of the V γ 1.1 TCR subunit on the y-axis and the V δ 6.3 TCR subunit on the x-axis. Cells that are V γ 1.1⁺, V δ 6.3⁺, in the upper right quadrant, are classified as $\gamma\delta$ NKT cells. **(B)**. Mean and S.E.M are graphed for the 3 individual age-matched experiments. Significantly different percentages of $\gamma\delta$ NKT cells are labeled as * for p<0.05, and ** for p<0.01. Statistical significance was determined by multiple Student's t tests.

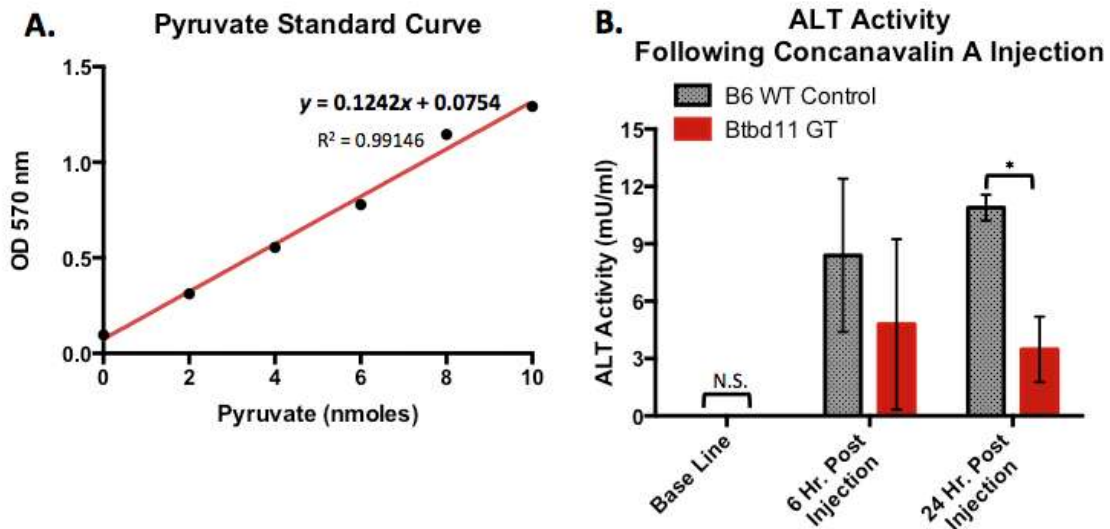


Figure 39. Btbd11 GT mice exhibited lower ALT activity following Con A dosage. Analysis of the ALT assay shows significant differences within the serum of WT and Btbd11 GT samples. **(A)**. The Pyruvate Standard Curve is calculated by plotting the maximum OD 570 nm value for each of the 5 standards, shown as points along the curve, included within the experimental assay. The linear trend line is then used to convert the measured OD 570 nm of each sample to the corresponding nmoles of pyruvate generated. **(B)**. Following the calculation of nmoles of pyruvate generated by each sample, the total ALT Activity of each sample is calculated as the amount of ALT which generates 1.0 μ mol of pyruvate per minute at 37°C. Statistical significance is calculated using multiple Student's t tests to compare the ALT Activity between the WT (n=3) versus the Btbd11 GT (n=3) serum samples independently at each of the three time points. Mean and S.E.M are graphed for the 3 samples for each time point. Significantly different ALT levels are labeled as * for $p < 0.05$. Statistical significance was determined by Student's t test.

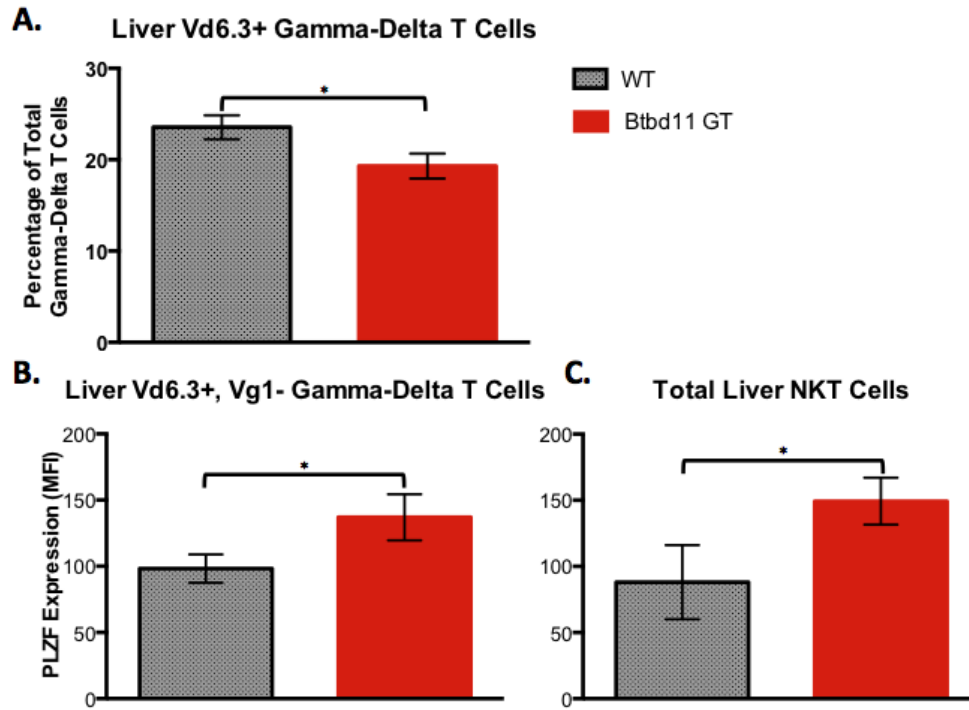


Figure 40. Btbd11 GT liver samples had altered effector cell populations and PLZF expression following Con A dosage. 24 hours post Concanavalin A injection, wild type and Btbd11 GT experimental mice were sacrificed and flow cytometry was performed to determine a significant change in cell populations and PLZF expression within the liver. **(A)**. Following gating upon all $\gamma\delta$ TCR⁺ T cells, V δ 6.3⁺ $\gamma\delta$ T cell populations are measured as a percentage of all $\gamma\delta$ T cells. **(B)**. PLZF expression within V δ 6.3⁺, V γ 1.1⁻ $\gamma\delta$ T cells is measured as a histogram function via mean fluorescent intensity. **(C)**. Following gating upon the CD1d tetramer⁺, CD3⁺ NKT cells, PLZF expression is measured as a histogram function via mean fluorescent intensity. Mean and S.E.M are graphed for the 3 mice per experimental group. Significantly different percentages of gamma-delta NKT cells are labeled as * for p<0.05. Statistical significance was determined by Student's t tests.

Discussion

My Master's thesis research sought to outline and define the role in which Btbd11 affects the transcriptional control of various aspects of the immune system. These studies define the substantial impact that this protein has on potent immune cells such as Natural Killer T cells and $\gamma\delta$ T cells. The function of Btbd11 has not been previously studied in this cell type, and we have succeeded in answering some questions while also unearthing many more questions that will hopefully be answered in the near future. The impact that this future research may have on the field of immunology and cellular therapies cannot be understated. The evidence presented suggests that Btbd11 plays a role in modulating the effector functionality of cells known to play a role in cancer surveillance, front-of-the-line pathogen clearance, liver regeneration, and various other diseases. Exploratory research in this field can only serve to improve, expand, and support the existing body of work relating to immunotherapies targeting diseases that plague human society.

Btbd11 originally became an interesting target for our lab to research due to its linked expression with PLZF within NKT cells. Our lab has previously discovered the role that the transcription factor PLZF plays in controlling the effector functionality of NKT cells, including their ability to quickly activate and release many different types of cytokines in response to infection. In PLZF knock out mice, microarray data showed that Btbd11 expression was significantly decreased in NKT cells. Supporting information from ImmGen databases and mass spectroscopy data confirmed the association and direct interactions between Btbd11 and PLZF, possibly through their shared BTB protein interaction domains, specifically within NKT cells [73]. Due to these findings, it was

reasonable to hypothesize that Btbd11 interacts with and modulates certain features of PLZF's ability to control transcription in NKT cells and other innate-like lymphocytes.

This research pursues the idea that forced ectopic expression of PLZF and Btbd11 in conventional T cells could induce NKT cell-like effector functionality within conventional T cells. A portion of this project consisted of creating the mouse line, hCD2-Btbd11 mice, in which we induce overexpression of Btbd11 in all T cells through the hCD2 promotor region. The steps taken to accomplish the successful generation of this transgenic mouse line are discussed in the methods section as well as Figures 20-22 in the results section. This process of genetic engineering allowed us to study the function and effect of Btbd11 and PLZF within an *in vivo* and biologically relevant system, rather than studying its expression in *in vitro* models such as cell lines. Concurrently, we utilized a Btbd11 Gene Trap (Btbd11 GT) transgenic mouse line to study the same systems in a mouse immune setting where Btbd11 expression was significantly knocked down as shown in Figure 26.

Following the expansion of the hCD2-Btbd11 transgenic mice, and subsequent breeding with existing lck-PLZF mice to generate double-transgenic or dTG mice, we had finished preparing the intended system of ectopic overexpression of Btbd11 and PLZF in conventional T cell subsets. Initial studies of these mice consisted of defining the expression profile of Btbd11 and PLZF. Using qRT-PCR and flow cytometry, we were able to quantify the gene expression and protein expression of Btbd11 and PLZF. We found that overexpression of PLZF alone did not lead to a considerable overexpression of Btbd11, as seen in Figure 28. Due to previous microarray data stating that Btbd11 was downregulated within PLZF KO mice, we hypothesized that PLZF was controlling the

expression of *Btbd11*, as without PLZF there was decreased expression of *Btbd11*. However, if this were the case, there would be overexpression of *Btbd11* in the lck-PLZF mice compared to the wild type expression levels. This is proven incorrect by Figure 28a-c where there is equal gene expression of *Btbd11* in the wild type and lck-PLZF tissue samples. PLZF gene and protein expression studies also generated interesting and puzzling results. Figure 28d-f displays a differential level of PLZF gene expression between various tissues of lck-PLZF and dTG mice. Specifically, PLZF expression within the dTG liver sample was shown to be meaningfully decreased compared to the lck-PLZF liver sample. Significantly, this difference in PLZF gene expression was found to be in agreement with differing levels of PLZF protein expression. Intranuclear staining of PLZF protein and flow cytometry was performed to quantify the consistent lower levels of PLZF expression in dTG liver lymphocytes when compared to lck-PLZF samples, as shown in Figure 31. These interesting findings support the notion that *Btbd11* and PLZF are somehow influencing the expression and presence of each other within various T cell subsets.

Previous work in our laboratory has concluded that ectopic expression of PLZF in all T cells alone can induce some of the NKT-like effector functionality [67]. It remains clear, following these findings, that there are other transcription factors and co-factors required to fully induce the NKT-like phenotype within conventional $\alpha\beta$ T cells. As part of this research, I tested the hypothesis that over expression of *Btbd11* in conjunction with PLZF in all T cells would result in the acquisition of NKT-like effector functionality within a significant portion of conventional $\alpha\beta$ T cells. The hallmark of an activated NKT cell is their ability to co-produce large quantities of various cytokines, most notable IL-4 and

IFN- γ almost instantaneously upon becoming activated by pathogens. Within the lab setting, in vitro stimulation of lymphocytes by PMA and Ionomycin followed by Brefeldin A represents the most effective way of activating lymphocytes and analyzing their cytokine production abilities. Following activation, intracellular staining for IL-4, IFN- γ , IL-17a, GM-CSF, and IL-2 cytokines and flow cytometry was performed in order to quantify the cytokine production capabilities of various T cell subsets. We found that there was no substantial change in the IL-4, IFN- γ , GM-CSF, and IL-2 production of CD4⁺, CD8⁺, $\gamma\delta$, and NKT cells within spleen samples of dTG and lck-PLZF mice as seen in Figures 32-34. From these experiments we can conclude that the overexpression of Btbd11 in conjunction with PLZF in all T cells did not lead to the significant acquisition of NKT-like cytokine production capabilities, with the exception of IL-17a production levels. Similarly, as shown in Figure 35, there was no significant change in the cytokine production profile between the Btbd11 GT and wild type samples.

IL-17a is a pro-inflammatory cytokine responsible for autoimmune inflammation and neutrophil recruitment to infected organs. Normal production of IL-17a in the skin is important for the clearance of various extracellular bacterium while dysregulation of IL-17a production has been implicated in autoimmune diseases such as rheumatoid arthritis, multiple sclerosis, psoriasis, and inflammatory bowel disease [103]. Intriguingly, previous studies performed by our lab showed that 2-5% of CD8⁺ T cells within lck-PLZF mice possess the ability to produce IL-17a, as shown in Figure 12 [37]. As less than 0.5% of wild type CD8⁺ T cells produce IL-17a, the emergence of this population is significant and perplexing. We can conclude from this that ectopic expression of PLZF in CD8⁺ T cells is responsible for the activation of IL-17a specific cytokine production

machinery. In vitro activation of liver lymphocytes of hCD2-Btbd11, lck-PLZF, and dTG mice unveiled a surprising phenotype of mice overexpression Btbd11 in all T cells. As shown in Figure 36, overexpression of Btbd11 alone leads to a small increase in the percentage of liver CD8⁺ T cells that are capable of producing IL-17a, while overexpression of both Btbd11 and PLZF in the dTG mice leads to a large and significant increase of IL-17a producing CD8⁺ T cells. The addition of Btbd11 and PLZF into CD8⁺ T cells leads to a three-fold increase in the percentage of CD8⁺ T cells that are capable of producing IL-17a when compared to CD8⁺ T cells from mice ectopically expressing PLZF alone. This significant difference evidences the role that Btbd11 plays in further inducing an IL-17a production profile within CD8⁺ T cells already ectopically expressing PLZF. Decreased Btbd11 expression in the Btbd11 GT samples does not affect IL-17a production, as this process seems to be initially dependent on PLZF and is further modulated by overexpression of Btbd11.

Transcription factors are often utilized to define certain subsets of immune cells. Due to their ability to regulate a vast network of genes responsible for inducing a cell's phenotype, it is not unreasonable for certain transcription factors to be deemed the “master regulator” of a cell subset, just as PLZF has been for NKT cells. Similarly, ROR γ t has been defined as the master regulator of cells that produce IL-17a. Expression of ROR γ t ensures that the effector cell possess the correct machinery to produce IL-17a upon activation. Significantly, certain subsets of IL-17a producing Th17 cells are dependent on both PLZF in conjunction with ROR γ t [103, 104]. There also is proof that PLZF is able to directly interact with and regulate ROR γ t in order to control Th17 differentiation in human lymphocytes [106]. We hypothesized that, due to the proposed

interactions between PLZF and ROR γ t and the emergence of IL-17a producing CD8⁺T cells in the lck-PLZF and dTG mice, ROR γ t expression levels would be altered in CD8⁺ T cells of the wild type, lck-PLZF, and dTG mice. As shown in the two histograms of Figure 30, both the lck-PLZF and dTG liver CD8⁺ T cell samples contain a small population of cells expressing high levels of ROR γ t. Upon closer inspection, the dTG sample has more cells expressing higher levels of ROR γ t than the lck-PLZF sample as supported by the increased height and rightward shift of the blue curve versus the red curve. This endogenous induction of ROR γ t expression correlates perfectly with the induction of a population of CD8⁺ T cells capable of producing IL-17a upon activation. Future work within our laboratory will utilize a ROR γ t reporter mouse line crossed to both lck-PLZF and dTG mice to further study the spontaneous generation of these IL-17a producing CD8⁺ T cells. Studies will include chromatin immunoprecipitation (ChIP) experiments to determine if and where PLZF is able to directly bind to and regulate expression of the ROR γ t and IL-17a gene loci.

Other innate-like lymphocytes such as $\gamma\delta$ T cells have been proven by our lab to rely upon PLZF for development and effector functionality. In line with this, we also sought to determine if Btbd11 modulates and interacts with PLZF within $\gamma\delta$ T cells. As shown in Figure 37, flow cytometry staining of $\gamma\delta$ T cells was performed and found that hCD2-Btbd11 liver samples contained moderately higher percentages of total $\gamma\delta$ T cells than wild type while lck-PLZF liver samples contained significantly lower percentages of total $\gamma\delta$ T cells than wild type. Interestingly, dTG liver samples consisted of significantly higher percentages of total $\gamma\delta$ T cells than wild type while Btbd11 GT liver samples consisted of significantly lower percentages of total $\gamma\delta$ cells than wild type. This data

supports the concept that *Btbd11* controls certain aspects of the balance between $\alpha\beta$ versus $\gamma\delta$ T cell lineage. Perplexingly, PLZF overexpression alone leads to a drop in total $\gamma\delta$ T cell population, but when overexpressed alongside *Btbd11*, we see an almost two-fold increase in total $\gamma\delta$ T cell population size over wild type as seen in the dTG sample. While PLZF expression in total $\gamma\delta$ T cells is relatively low, a specific subset of $V\gamma 1.1^+$, $V\delta 6.3^+$ $\gamma\delta$ T cells have been discovered by our laboratory to express high levels of PLZF [69, 86]. Due to their significant expression of PLZF and their ability to co-produce IL-4 and IFN- γ , we have coined these $\gamma\delta$ T cells as $\gamma\delta$ NKT cells, because of their similar phenotypic properties to $\alpha\beta$ iNKT cells. Flow cytometry analysis of these specific subsets of $\gamma\delta$ T cells lead to the interesting finding that lck-PLZF and *Btbd11* GT liver samples consisted of significantly greater percentages of $V\gamma 1.1^+$, $V\delta 6.3^+$ $\gamma\delta$ NKT cells as shown in Figure 38. Compiling this information with the findings that lck-PLZF liver samples contained fewer total $\gamma\delta$ T cells, leads to the conclusion that overexpression of PLZF leads to a skewing away from all $\gamma\delta$ T cells towards the $\alpha\beta$ T cell lineages with the exception of the $V\gamma 1.1^+$, $V\delta 6.3^+$ $\gamma\delta$ NKT cells. Similarly, the diminished *Btbd11* expression in *Btbd11* GT samples leads to the strong skewing away from the $\gamma\delta$ cell lineage, but does not seem to affect the $V\gamma 1.1^+$, $V\delta 6.3^+$ $\gamma\delta$ NKT subset. Further experiments must be performed to conclude whether or not these percentage population changes are due to a loss in absolute cell number.

As we have continued to characterize these transgenic mice, an obvious phenotype has emerged specifically within the liver. The liver houses the highest percentage of NKT cells per body tissue while also housing large populations of $\gamma\delta$ T cells and other innate-like lymphocytes. The liver performs the important role of filtering antigen-rich blood

from the intestinal tract. Due to this function, hepatocytes may become infected by the pathogens within the blood. Lymphocytes within the liver serve to quickly eliminate infected host cells and prevent infections from spreading and infecting other portions of the liver. These liver lymphocytes play a role in recruiting other immune cells to infected sites via the release of pro-inflammatory cytokines. It is these cytokines that can also lead to damage of the liver. The obvious balance between cytokine activity necessary for eliminating foreign pathogens versus injuring the host tissue has become a highly studied field of immunology. Embroiled within this balance are innate-like lymphocytes such as NKT cells and $\gamma\delta$ T cells, which are able to quickly release vast amounts of various effector cytokines. The dysregulation of cytokine production within the liver have been implicated in hepatocyte destruction, liver fibrosis/cirrhosis, liver-specific autoimmune diseases, and toxic/metabolic liver disease [62, 63]. A murine liver damage is the injection of Concanavalin A. Con A is a lectin that specifically activates immune cells via interactions with Toll-like receptors (TLRs) leading to activation of innate cells and innate-like lymphocytes such as NKT cells and $\gamma\delta$ T cells possessing the compatible TLRs [105]. Cell activation following interaction with the Con A antigen generates an endogenous response resulting in cytokine release and immune cell recruitment mimicking short term liver damage [64, 65]. The extent of this liver damage is determined by the release of various liver enzymes into the blood stream. One such liver enzyme, ALT, was measured within serum samples using a colorimetric assay. Each of the three mice within two groups of experimental mice, wild type and Btbd11 GT, were injected with 15 μ g of Con A per gram of mouse weight. Serum extracted at 6 and 24 hours post injection was compared to baseline serum readings taken prior to the Con A

injection. Figure 39 shows the difference in ALT activity within each experimental group. At 6 hours post injection there is substantial and varying ALT activity within both the wild type and Btbd11 GT groups. Significantly, at 24 hours following injection, the wild type group continues to exhibit increasing ALT activity when compared to the 6 hour time point while the Btbd11 GT group has begun to exhibit lower levels of ALT activity when compared to the 6 hour time point. The difference in ALT activity, and thus liver damage, seen in this in vivo model allows us to conclude that the lack of Btbd11 expression in the Btbd11 GT mice served to protect those mice from Con A induced liver damage. Due to the known role that pro-inflammatory cytokines play in mediating liver damage, we can infer that the cytokine profile of the innate and innate-like lymphocytes within the Btbd11 GT livers was augmented enough to prevent liver damage along the same scale seen in the wild type samples.

In order to determine what was mediating the different levels of liver damage seen in the wild type and Btbd11 GT mice following Con A injections, we performed flow cytometry of the experimental mice livers at 24 hours post injection. Analysis of both NKT and $\gamma\delta$ T cells subsets exposed significant differences between the two experimental groups of mice. Figure 40a illustrates the significantly lower percentages of V δ 6.3⁺ $\gamma\delta$ T cells within the Btbd11 GT mice samples when compared to wild type mice.

Additionally, the subset of V γ 1.1⁺, V δ 6.3⁺ $\gamma\delta$ T cells within the Btbd11 GT experimental group were found to have higher levels of PLZF expression than the wild type mice as seen in Figure 40b. Similarly within the NKT cells, Figure 40c shows that Btbd11 GT samples had significantly greater PLZF expression than the wild type samples. While the increased expression of PLZF in the Btbd11 GT mice seems counter-intuitive, as these

mice exhibited lower levels of ALT release and liver damage, this is actually consistent with previous data generated by our lab showing that upon stimulation NKT cells will actually downregulate PLZF expression (data not shown). Following this line of logic, we can conclude that the NKT and $V\gamma 1.1^+$, $V\delta 6.3^+$ $\gamma\delta$ T cells within the *Btbd11* GT samples exhibit suppressed activation and thus fail to downregulate PLZF to the extent normally seen in wild type, possibly explaining why the *Btbd11* mice experienced significantly lower levels of liver damage. Another explanation for the lower levels of liver damage seen in the *Btbd11* GT mice is the significant reduction in $V\delta 6.3^+$ $\gamma\delta$ T cells at 24 hours following Con A injections. As we know $\gamma\delta$ T cells are at least partially responsible for Con A specific liver damage [64, 65, 105]. From this, we can conclude that the lower presence of $V\delta 6.3^+$ $\gamma\delta$ T cells within *Btbd11* GT mice could explain the lower levels of liver damage seen. Further studies must be performed to determine whether *Btbd11* recruits immune cells that mediate liver damage following Con A injections, or if *Btbd11* modulates the levels to which existing liver immune cells activate to induce liver damage following Con A injections. Although not performed, we would also hypothesize that dTG mice would have an increased level of ALT activity and liver damage due to the data previously mentioned concluding that innate cells within these mice tend to exhibit a more pro-inflammatory phenotype than wild type mice. The significant differences seen in these in vivo studies are supported by previous data showing increased IL-17a production in the *Btbd11* and PLZF transgenic mice. Yan et al. recently defined the IL-17a cytokine-signaling axis as critical in the progression of Con A induced hepatitis [107-109]. The significant levels of liver damage seemingly dependent on *Btbd11* expression combined with the significant generation of IL-17a producing $CD8^+$ T cells in *lck*-PLZF

and dTG mice support the claim that Btbd11 modulates PLZF's transcriptional control of the effector functions of various innate and conventional T cell subsets.

The method by which Btbd11 modulates PLZF is unknown. As previously mentioned, Bcl-6, another BTB-ZF transcription factor, has been proved to rely upon interaction with vital co-factors via the BTB protein-interaction domain in order to function properly [91]. While these co-factors cannot directly interact with DNA, they are obviously playing a meaningful role in modulating the ability of each transcription factor to repress or activate transcription of a target gene. Our studies on Btbd11, one such co-factor, have shown the significant role that it plays via direct interaction with PLZF. Overexpression and underexpression of Btbd11 in mouse models have led to noteworthy phenotypic changes in various subsets of T cells. The ability for BTB domain containing co-factors to modulate highly important molecular processes is not a newly discovered phenomenon. Svendsen et al. found that Btbd12, a fellow member of the BTB-domain containing protein family with Btbd11, plays a critical role in the generation of multi-protein complexes responsible for assembling Holliday junction resolvases that occur during double-stranded DNA break repairs [110]. These researchers claim that Btbd12 is responsible for creating a protein "scaffold" that recruits various DNA repair enzymes to sites of double-stranded DNA damage [110, 111]. While Btbd12 operates in a completely different context and with completely different proteins to Btbd11, we can hypothesize that Btbd11 may be responsible for generating a similar "scaffold" required for transcription factors to localize to and modulate transcription of genes relevant to immune system cell subsets. The exact combination of proteins that this Btbd11 "scaffold" interacts with would be highly dependent on the cell type, further supported by

the fact that we see a significant role played by Btbd11 in the many different T cell subsets studied throughout this project.

In conclusion, our exploratory research of Btbd11 has shown that it is an important transcriptional co-factor that directly interacts with PLZF and modulates PLZF's ability to transcriptionally control the effector function and phenotype of potent innate T cell populations. These innate T cells are a rare but powerful subset of our immune system responsible for responding almost instantaneously to foreign antigens and recruiting adaptive immune cells. Understanding the processes by which these innate T cells recognize antigens, activate and produce effector cytokines, and influence the following steps of the immune response remains a goal of many immunology laboratories. The specific focus of our laboratory is to study and unearth the complex transcriptional machinery that controls these processes. While PLZF is known as the master regulator of the effector function of NKT and $\gamma\delta$ NKT cells, we are constantly investigating new proteins that interact and impact PLZF's ability to do its important job. My research on Btbd11 has begun to reveal the impact that it has upon these innate T cells and has provided us with thought-provoking findings, further expanding our field of knowledge on transcription machinery responsible for the effector function of immune cells.

References

1. Hemmi, H., Takeuchi, O., Kawai, T., Kaisho, T., Sato, S., Sanjo, H., ... & Akira, S. (2000). A Toll-like receptor recognizes bacterial DNA. *Nature*, 408(6813), 740-745.
2. Kawai, T., & Akira, S. (2010). The role of pattern-recognition receptors in innate immunity: update on Toll-like receptors. *Nature immunology*, 11(5), 373-384.
3. Fraser, I. P., Koziel, H., & Ezekowitz, R. A. B. (1998). The serum mannose-binding protein and the macrophage mannose receptor are pattern recognition molecules that link innate and adaptive immunity. *Seminars in immunology* 10(5), 363-372. Academic Press.
4. Litman, G. W., Cannon, J. P., & Dishaw, L. J. (2005). Reconstructing immune phylogeny: new perspectives. *Nature Reviews Immunology*, 5(11), 866-879.
5. Boehm, T. (2011). Design principles of adaptive immune systems. *Nature Reviews Immunology*, 11(5), 307-317.
6. Tonegawa, S. (1983). Somatic generation of antibody diversity. *Nature*, 302(5909), 575-581.
7. Dreyer, W. J., & Bennett, J. C. (1965). The molecular basis of antibody formation. *Proc. Natl. Acad. Sci. USA*, 54, 864-869.
8. Hozumi, N., & Tonegawa, S. (1976). Evidence for somatic rearrangement of immunoglobulin genes coding for variable and constant regions. *Proceedings of the National Academy of Sciences*, 73(10), 3628-3632.
9. Reizis, B., & Leder, P. (2002). Direct induction of T lymphocyte-specific gene expression by the mammalian Notch signaling pathway. *Genes & development*, 16(3), 295-300.
10. Sambandam, A., Maillard, I., Zediak, V. P., Xu, L., Gerstein, R. M., Aster, J. C., ... & Bhandoola, A. (2005). Notch signaling controls the generation and differentiation of early T lineage progenitors. *Nature immunology*, 6(7), 663-670.
11. Godfrey, D. I., Kennedy, J., Suda, T., & Zlotnik, A. (1993). A developmental pathway involving four phenotypically and functionally distinct subsets of CD3-CD4-CD8-triple-negative adult mouse thymocytes defined by CD44 and CD25 expression. *The Journal of Immunology*, 150(10), 4244-4252.
12. Rothenberg, E. V., Moore, J. E., & Yui, M. A. (2008). Launching the T-cell-lineage developmental programme. *Nature Reviews Immunology*, 8(1), 9-21.
13. Porritt, H. E., Rumfelt, L. L., Tabrizifard, S., Schmitt, T. M., Zúñiga-Pflücker, J. C., & Petrie, H. T. (2004). Heterogeneity among DN1 prothymocytes reveals multiple progenitors with different capacities to generate T cell and non-T cell lineages. *Immunity*, 20(6), 735-745.
14. Porritt, H. E., Rumfelt, L. L., Tabrizifard, S., Schmitt, T. M., Zúñiga-Pflücker, J. C., & Petrie, H. T. (2004). Heterogeneity among DN1 prothymocytes reveals multiple progenitors with different capacities to generate T cell and non-T cell lineages. *Immunity*, 20(6), 735-745.
15. Aifantis, I., Azogui, O., Feinberg, J., Saint-Ruf, C., Buer, J., & von Boehmer, H. (1998). On the Role of the Pre-T Cell Receptor in $\alpha\beta$ versus $\gamma\delta$ T Lineage Commitment. *Immunity*, 9(5), 649-655.

16. Hogquist, K. A., Jameson, S. C., & Bevan, M. J. (1994). The ligand for positive selection of T lymphocytes in the thymus. *Current opinion in immunology*, 6(2), 273-278.
17. Jameson, S. C., Hogquist, K. A., & Bevan, M. J. (1995). Positive selection of thymocytes. *Annual review of immunology*, 13(1), 93-126.
18. Ashton-Rickardt, P. G., Bandeira, A., Delaney, J. R., Van Kaer, L., Pircher, H. P., Zinkernagel, R. M., & Tonegawa, S. (1994). Evidence for a differential avidity model of T cell selection in the thymus. *Cell*, 76(4), 651-663.
19. Marrack, P., & Kappler, J. (1987). The T cell receptor. *Science*, 238(4830), 1073-1079.
20. Bonomo, A., & Matzinger, P. (1993). Thymus epithelium induces tissue-specific tolerance. *The Journal of experimental medicine*, 177(4), 1153-1164.
21. Croft, M., & Dubey, C. (1997). Accessory molecule and costimulation requirements for CD4 T cell response. *Critical Reviews in Immunology*, 17(1).
22. Johnson, J. G., & Jenkins, M. K. (1993). Accessory cell-derived signals required for T cell activation. *Immunologic research*, 12(1), 48-64.
23. Nelson, B. H., & Willerford, D. M. (1997). Biology of the interleukin-2 receptor. *Advances in immunology*, 70, 1-81.
24. Antov, A., Yang, L., Vig, M., Baltimore, D., & Van Parijs, L. (2003). Essential role for STAT5 signaling in CD25⁺ CD4⁺ regulatory T cell homeostasis and the maintenance of self-tolerance. *The Journal of Immunology*, 171(7), 3435-3441.
25. Lancki, D. W., Kaper, B. P., & Fitch, F. W. (1989). The requirements for triggering of lysis by cytolytic T lymphocyte clones. II. Cyclosporin A inhibits TCR-mediated exocytosis by only selectively inhibits TCR-mediated lytic activity by cloned CTL. *The Journal of Immunology*, 142(2), 416-424.
26. Lancki, D. W., Kaper, B. P., & Fitch, F. W. (1989). The requirements for triggering of lysis by cytolytic T lymphocyte clones. II. Cyclosporin A inhibits TCR-mediated exocytosis by only selectively inhibits TCR-mediated lytic activity by cloned CTL. *The Journal of Immunology*, 142(2), 416-424.
27. Jerne, N. K. (1955). The natural-selection theory of antibody formation. *Proceedings of the National Academy of Sciences of the United States of America*, 41(11), 849.
28. Burnet, F. M. (1976). A modification of Jerne's theory of antibody production using the concept of clonal selection. *CA: a cancer journal for clinicians*, 26(2), 119-121.
29. Parker, D. C. (1993). T cell-dependent B cell activation. *Annual review of immunology*, 11(1), 331-360.
30. Coutinho, A., Pobor, G., Pettersson, S., Leandersson, T., Forsgren, S., Pereira, P., & Bandeira, A. (1984). T Cell-Dependent B Cell Activation. *Immunological reviews*, 78(1), 211-224.
31. Murakami, J., Shimizu, Y., Kashii, Y., Kato, T., Minemura, M., Okada, K. et al. (1999). Functional B cell response in intrahepatic lymphoid follicles in chronic hepatitis C. *Hepatology*, 30:143-150.
32. Gerberick GF, Cruse LW, Miller CM, Sikorski EE, Ridder GM. (1997.) Selective modulation of T cell memory markers CD62L and CD44 on murine

- draining lymph node cells following allergen and irritant treatment. *Toxicology Applied Pharmacology*, 146(1):1-10.
33. Bendelac, A., Savage, P.B. & Teyton, L. (2007). The biology of NKT cells. *Annual review of immunology*, 25:297-336.
 34. Bonneville, M., O'Brien, R.L. & Born, W.K. (2010). Gammadelta T cell effector functions: a blend of innate programming and acquired plasticity. *Nature reviews. Immunology*, 10:467-78.
 35. Haas, W., Pereira, P. & Tonegawa, S. (1993). Gamma/delta cells. *Annual review of immunology*, 11:637-85.
 36. Bendelac, A. (1995). Positive selection of mouse NK1+ T cells by CD1-expressing cortical thymocytes. *The Journal of experimental medicine*, 182:2091-6.
 37. Lantz, O., and A. Bendelac. (1994). An invariant T cell receptor alpha chain is used by a unique subset of MHC class I-specific CD4+ and CD4- 8- T cells in mice and humans. *J. Exp. Med.*, 180:1097-1106.
 38. Franck RW. (2012). C-Galactosylceramide: Synthesis and Immunology. *Comptes rendus Chimie (Print)*. 15(1):46-56.
 39. Cowan, J. E., Jenkinson, W. E. and Anderson, G. (2015), Thymus medulla fosters generation of natural Treg cells, invariant $\gamma\delta$ T cells, and invariant NKT cells: What we learn from intrathymic migration. *Eur. J. Immunol.*, 45: 652–660.
 40. Berzins, S. P., F. W. McNab, C. M. Jones, M. J. Smyth, D. I. Godfrey. (2006). Long-term retention of mature NK1.1+ NKT cells in the thymus. *J. Immunol.* 176: 4059–4065.
 41. Henry Lin, Mie Nieda, Vladislav Rozenkov, Andrew J. Nicol, (2006) Analysis of the effect of different NKT cell subpopulations on the activation of CD4 and CD8 T cells, NK cells, and B cells. *Experimental Hematology*, 34(3):289-295.
 42. Benlagha, K., Wei, D. G., Veiga, J., Teyton, L., & Bendelac, A. (2005). Characterization of the early stages of thymic NKT cell development. *The Journal of Experimental Medicine*, 202(4), 485–492.
 43. Gapin, L., Matsuda, J. L., Surh, C. D., & Kronenberg, M. (2001). NKT cells derive from double-positive thymocytes that are positively selected by CD1d. *Nature immunology*, 2(10), 971-978.
 44. Kronenberg M, Engel I. (2007). On the road: progress in finding the unique pathway of invariant NKT cell differentiation. *Curr Opin Immunol.*, 19(2):186-93.
 45. Gapin, L. (2008). The making of NKT cells. *Nature immunology*, 9(9):1009-1011.
 46. Kovalovsky, D., Uche, O. U., Eladad, S., Hobbs, R. M., Yi, W., Alonzo E., Sant'Angelo, D. B. (2008). The BTB–zinc finger transcriptional regulator PLZF controls the development of invariant natural killer T cell effector functions. *Nature immunology*, 9(9): 1055-1064.
 47. Das, R., Sant'Angelo, D. B., & Nichols, K. E. (2010). Transcriptional control of invariant NKT cell development. *Immunological Reviews*, 238(1): 195–215.

48. Savage, A. K., Constantinides, M. G., Han, J., Picard, D., Martin, E., Li, B., Bendelac, A. (2008). The transcription factor PLZF (Zbtb16) directs the effector program of the NKT cell lineage. *Immunity*, 29(3): 391–403.
49. Bezbradica, J. S., Hill, T., Stanic, A. K., Van Kaer, L., & Joyce, S. (2005). Commitment toward the natural T (iNKT) cell lineage occurs at the CD4+8+ stage of thymic ontogeny. *Proceedings of the National Academy of Sciences of the United States of America*, 102(14): 5114–5119.
50. Michel, M.-L., Mendes-da-Cruz, D., Keller, A. C., Lochner, M., Schneider, E., Dy, M., Leite-de-Moraes, M. C. (2008). Critical role of ROR- γ t in a new thymic pathway leading to IL-17-producing invariant NKT cell differentiation. *Proceedings of the National Academy of Sciences of the United States of America*, 105(50): 19845–19850.
51. Lazarevic, V., Glimcher, L. H., & Lord, G. M. (2013). T-bet: a bridge between innate and adaptive immunity. *Nature Reviews Immunology*, 13(11): 777–789.
52. Matsuda, J. L., Zhang, Q., Ndonye, R., Richardson, S. K., Howell, A. R., & Gapin, L. (2006). T-bet concomitantly controls migration, survival, and effector functions during the development of V α 14i NKT cells. *Blood*, 107(7): 2797–2805.
53. Tomura M, Yu WG, Ahn HJ, Yamashita M, Yang YF, et al. (1999). A novel function of V α 14+CD4+NKT cells: stimulation of IL-12 production by antigen-presenting cells in the innate immune system. *J. Immunol.*, 163:93–101.
54. Kitamura H, Iwakabe K, Yahata T, Nishimura S, Ohta A, et al. (1999). The natural killer T (NKT) cell ligand α -galactosylceramide demonstrates its immunopotentiating effect by inducing interleukin (IL)-12 production by dendritic cells and IL-12 receptor expression on NKT cells. *J. Exp. Med.*, 189:1121–28.
55. Stetson, D. B., Mohrs, M., Reinhardt, R. L., Baron, J. L., Wang, Z.-E., Gapin, L., Locksley, R. M. (2003). Constitutive Cytokine mRNAs Mark Natural Killer (NK) and NK T Cells Poised for Rapid Effector Function. *The Journal of Experimental Medicine*, 198(7): 1069–1076.
56. Nagaleekar, V. K., Sabio, G., Aktan, I., Chant, A., Howe, I. W., Thornton, T. M., Boyson, J. E. (2011). Translational control of NKT cell cytokine production by p38 MAP kinase. *Journal of Immunology (Baltimore, Md. : 1950)*, 186(7): 4140–4146.
57. Eberl G, MacDonald HR. (1998). Rapid death and regeneration of NKT cells in anti- CD3epsilon- or IL-12-treated mice: a major role for bone marrow in NKT cell homeostasis. *Immunity*, 9:345–53.
58. Uldrich AP, Crowe NY, Kyparissoudis K, Pellicci DG, Zhan Y, et al. (2005). NKT cell stimulation with glycolipid antigen in vivo: costimulation-dependent expansion, Bim-dependent contraction, and hyporesponsiveness to further antigenic challenge. *J. Immunol.*, 175:3092–101.
59. Parekh VV, Wilson MT, Olivares-Villagomez D, Singh AK, Wu L, et al. (2005). Glycolipid antigen induces long-term natural killer T cell anergy in mice. *J. Clin. Invest.*, 115:2572–83.

60. Smyth, M. J., Thia, K. Y., Street, S. E., Cretney, E., Trapani, J. A., Taniguchi, M., & Godfrey, D. I. (2000). Differential tumor surveillance by natural killer (NK) and NKT cells. *The Journal of experimental medicine*, 191(4): 661-668.
61. Pilonis, K. A., Aryankalayil, J., & Demaria, S. (2012). Invariant NKT cells as novel targets for immunotherapy in solid tumors. *Clinical and Developmental Immunology*.
62. Swain, M. (2008). Hepatic NKT cells: friend or foe?. *Clinical science*, 114: 457-466.
63. De Lalla, C., Galli, G., Aldrichetti, L. et al. (2004). Production of profibrotic cytokines by invariant NKT cells characterizes cirrhosis progression in chronic viral hepatitis. *J. Immunol.*, 173: 1417-1425.
64. Racanelli, V., & Rehermann, B. (2006). The liver as an immunological organ. *Hepatology*, 43(S1): S54-S62.
65. Dwyer, J. M.; Johnson, C (1981). The use of concanavalin A to study the immunoregulation of human T cells. *Clinical and experimental immunology*, 46 (2): 237-49.
66. Beaulieu AM, Sant'Angelo DB. (2011). The BTB-ZF family of transcription factors: key regulators of lineage commitment and effector function development in the immune system. *Journal of Immunology*, 187:2841-2847.
67. Kovalovsky D, Alonzo E, Uche OU, Eidson M, Nichols KE, Sant'Angelo DB. (2010). PLZF Induces the Spontaneous Acquisition of Memory/ Effector Functions in T Cells Independently of NKT Cell-Related Signals. *J Immunol.*, 184:6746-6755.
68. Uche, O. U., & Sant'Angelo, D. B. (2007). PLZF is essential for iNKT cell development. *The Journal of Immunology*, 178(Meeting Abstracts), S110.
69. Alonzo, E. S., & Sant'Angelo, D. B. (2011). Development of PLZF-expressing innate T cells. *Current Opinion in Immunology*, 23(2): 220-227.
70. Ahmad, K. F., Engel, C. K., & Privé, G. G. (1998). Crystal structure of the BTB domain from PLZF. *Proceedings of the National Academy of Sciences of the United States of America*, 95(21): 12123-12128.
71. Zelent, A., Guidez, F., Melnick, A., Waxman, S., & Licht, J. D. (2001). Translocations of the RARalpha gene in acute promyelocytic leukemia. *Oncogene*, 20(49): 7186-7203.
72. Simoni, Y., Diana, J., Ghazarian, L., Beaudoin, L. and Lehuen, A. (2013). Therapeutic manipulation of natural killer (NK) T cells in autoimmunity: are we close to reality?. *Clinical & Experimental Immunology*, 171: 8-19.
73. Mathew, R., Seiler, M. P., Scanlon, S. T., Mao, A., Constantinides, M. G., Bertozzi-Villa, C., Bendelac, A. (2012). BTB-ZF factors recruit the E3 ligase cullin 3 to regulate lymphoid effector programs. *Nature*, 491(7425): 618-621.
74. Vantourout, P., & Hayday, A. (2013). Six-of-the-best: unique contributions of $\gamma\delta$ T cells to immunology. *Nature Reviews Immunology*, 13(2): 88-100.
75. Hayday, A. C. (2000). $\gamma\delta$ cells: a right time and a right place for a conserved third way of protection. *Annual review of immunology*, 18(1): 975-1026.
76. O'Brien, R. L., & Born, W. K. (2010). $\gamma\delta$ T cell subsets: A link between TCR and function?. *Seminars in immunology*, 22(4):193-198. Academic Press.

77. Pai, S. Y., Truitt, M. L., Ting, C. N., Leiden, J. M., Glimcher, L. H., & Ho, I. C. (2003). Critical roles for transcription factor GATA-3 in thymocyte development. *Immunity*, 19(6): 863-875.
78. Carding, S. R., & Egan, P. J. (2002). $\gamma\delta$ T cells: functional plasticity and heterogeneity. *Nature reviews immunology*, 2(5): 336-345.
79. Schweighoffer, E., & Fowlkes, B. J. (1996). Positive selection is not required for thymic maturation of transgenic gamma delta T cells. *The Journal of experimental medicine*, 183(5): 2033-2041.
80. Lewis, J. M., Girardi, M., Roberts, S. J., Barbee, S. D., Hayday, A. C., & Tigelaar, R. E. (2006). Selection of the cutaneous intraepithelial $\gamma\delta^+$ T cell repertoire by a thymic stromal determinant. *Nature immunology*, 7(8): 843-850.
81. Xiong, N., & Raulet, D. H. (2007). Development and selection of $\gamma\delta$ T cells. *Immunological reviews*, 215(1): 15-31.
82. Bonneville, M. (2012). Thymic signatures of tailored peripheral functions. *Nature immunology*, 13(5): 431-433.
83. Jameson, J., & Havran, W. L. (2007). Skin $\gamma\delta$ T-cell functions in homeostasis and wound healing. *Immunological reviews*, 215(1): 114-122.
84. Gerber, D. J., Azuara, V., Levraud, J. P., Huang, S. Y., Lembezat, M. P., & Pereira, P. (1999). IL-4-producing $\gamma\delta$ T cells that express a very restricted TCR repertoire are preferentially localized in liver and spleen. *The Journal of Immunology*, 163(6): 3076-3082.
85. Kreslavsky, T., Savage, A. K., Hobbs, R., Gounari, F., Bronson, R., Pereira, P., ... & Von Boehmer, H. (2009). TCR-inducible PLZF transcription factor required for innate phenotype of a subset of $\gamma\delta$ T cells with restricted TCR diversity. *Proceedings of the National Academy of Sciences*, 106(30): 12453-12458.
86. Alonzo, E. S., Gottschalk, R. A., Das, J., Egawa, T., Hobbs, R. M., Pandolfi, P. P., ... & Sant'Angelo, D. B. (2010). Development of promyelocytic zinc finger and ThPOK-expressing innate $\gamma\delta$ T cells is controlled by strength of TCR signaling and Id3. *The journal of immunology*, 184(3): 1268-1279.
87. Agrati, C., D'Offizi, G., Gougeon, M. L., Malkovsky, M., Sacchi, A., Casetti, R., ... & Martini, F. (2011). Innate gamma/delta T-cells during HIV infection: Terra relatively Incognita in novel vaccination strategies. *AIDs Rev*, 13(1): 3-12.
88. Nicol, A. J., Tokuyama, H., Mattarollo, S. R., Hagi, T., Suzuki, K., Yokokawa, K., & Nieda, M. (2011). Clinical evaluation of autologous gamma delta T cell-based immunotherapy for metastatic solid tumours. *British journal of cancer*, 105(6):778-786.
89. Girardi, M., Oppenheim, D. E., Steele, C. R., Lewis, J. M., Glusac, E., Filler, R., ... & Hayday, A. C. (2001). Regulation of cutaneous malignancy by $\gamma\delta$ T cells. *Science*, 294(5542): 605-609.
90. Ferrick, D. A., Schrenzel, M. D., Mulvania, T., Hsieh, B., Ferlin, W. G., & Lepper, H. (1995). Differential production of interferon- γ and interleukin-4 in response to Th1-and Th2-stimulating pathogens by $\gamma\delta$ T cells in vivo. *Nature*, 375:255-257.

91. Nance, J. P., Bélanger, S., Johnston, R. J., Takemori, T., & Crotty, S. (2015). Cutting Edge: T Follicular Helper Cell Differentiation Is Defective in the Absence of Bcl6 BTB Repressor Domain Function. *The Journal of Immunology*, 1500200.
92. Borowski, C., & Bendelac, A. (2005). Signaling for NKT cell development the SAP–FynT connection. *The Journal of experimental medicine*, 201(6): 833-836.
93. Cerundolo, V., Silk, J. D., Masri, S. H., & Salio, M. (2009). Harnessing invariant NKT cells in vaccination strategies. *Nature Reviews Immunology*, 9(1): 28-38.
94. Imhof, B. A., & Aurrand-Lions, M. (2004). Adhesion mechanisms regulating the migration of monocytes. *Nature Reviews Immunology*, 4(6): 432-444.
95. Waterston, R. H., K. Lindblad-Toh, E. Birney, J. Rogers, J. F. Abril, P. Agarwal, R. Agarwala, R. Ainscough, M. Alexandersson, P. An, et al. (2002). Initial sequencing and comparative analysis of the mouse genome. *Nature*, 420:520.
96. Haley PJ. (2003). Species differences in the structure and function of the immune system. *Toxicology*, 188:49.
97. Gordon, J.W., Scangos, G.A, Plotkin, D.J., Barbosa, J.A. and Ruddle F.H. (1980). Genetic transformation of mouse embryos by microinjection of purified DNA. *Proc. Natl. Acad. Sci. USA*, 77(12): 7380–7384.
98. Zhumabekov, T., Corbella, P., Tolaini, M., & Kioussis, D. (1995). Improved version of a human CD2 minigene based vector for T cell-specific expression in transgenic mice. *Journal of immunological methods*, 185(1): 133-140.
99. Garvin AM, Pawar S, Marth JD, Perlmutter RM. (1988). Structure of the murine lck gene and its rearrangement in a murine lymphoma cell line. *Mol. Cell. Biol.*, 8:3058
100. Kowolik CM, Hu J, Yee JK. (2001). Locus Control Region of the Human CD2 Gene in a Lentivirus Vector Confers Position-Independent Transgene Expression. *Journal of Virology*, 75(10):4641–4648.
101. Smirnikhina, S. A., Lavrov, A. V., & Bochkov, N. P. (2011). Dynamics of Elimination of Plasmids and Expression of VEGF121 Gene Transfected into Human Mesenchymal Stem Cells by Different Methods. *Bulletin of experimental biology and medicine*, 151(1): 121-125.
102. Chatila, T. A. L. A. L., Silverman, L., Miller, R., & Geha, R. (1989). Mechanisms of T cell activation by the calcium ionophore ionomycin. *The Journal of Immunology*, 143(4):1283-1289.
103. Jin, W., & Dong, C. (2013). IL-17 cytokines in immunity and inflammation. *Emerging Microbes & Infections*, 2(9): e60.
104. Massot, B., Michel, M. L., Diem, S., Ohnmacht, C., Latour, S., Dy, & Leite-de-Moraes, M. C. (2014). TLR-induced cytokines promote effective proinflammatory natural Th17 cell responses. *The Journal of Immunology*, 192(12): 5635-5642.
105. Cao, Qing-yi et al. (2010). A Microarray Analysis of Early Activated Pathways in Concanavalin A-Induced Hepatitis. *Journal of Zhejiang University. Science*, 11(5): 366–377.

106. Singh, S., Zhang, H., Tsang, H., Gardina, P., Myers, T., & Farber, J. (2014). PLZF supports the acquisition and maintenance of the Th17 phenotype in human cells (CCR5P. 250). *The Journal of Immunology*, 192(1 Supplement): 181-4.
107. Yan, S., Wang, L., Liu, N., Wang, Y., & Chu, Y. (2012). Critical role of interleukin-17/interleukin-17 receptor axis in mediating Con A-induced hepatitis. *Immunology and cell biology*, 90(4), 421-428.
108. Xu, M., Morishima, N., Mizoguchi, I., Chiba, Y., Fujita, K., Kuroda, M., ... & Yoshimoto, T. (2011). Regulation of the development of acute hepatitis by IL- 23 through IL- 22 and IL- 17 production. *European journal of immunology*, 41(10), 2828-2839.
109. Crispe, I. N. (2012). IL-17 in liver injury: an inflammatory issue? *Immunology and cell biology*, 90(4), 369-370.
110. Svendsen, J. M., Smogorzewska, A., Sowa, M. E., O'Connell, B. C., Gygi, S. P., Elledge, S. J., & Harper, J. W. (2009). Mammalian BTBD12/SLX4 assembles a Holliday junction resolvase and is required for DNA repair. *Cell*, 138(1), 63-77.
111. Fekairi, S., Scaglione, S., Chahwan, C., Taylor, E. R., Tissier, A., Coulon, S., ... & Gaillard, P. H. L. (2009). Human SLX4 is a Holliday junction resolvase subunit that binds multiple DNA repair/recombination endonucleases. *Cell*, 138(1), 78-89.